NASA Contractor Report 178243

Evaluation of the ERBE Scene Identification Algorithm

S.K. Vemury

Science and Technology Corporation

101 Research Drive, Hampton, Virginia 23666-1340

Contract NAS1-18166

March 1987

National Aeronautics and Space Administration

Langley Research Center
Hampton, Virginia 23665

FOREWORD

The Science and Technology Corporation (STC) is pleased to submit this report entitled "Evaluation of the ERBE Scene Identification Algorithm," as the final report on NASA Contract NAS1-18166. We would like to acknowledge the assistance of Dr. J. T. Suttles and Dr. Bruce Wielicki of NASA Langley Research Center who provided useful discussion on the various aspects of this work; Dr. Richard Green of NASA Langley Research Center, for providing the angular models; and Dr. H. Lee Kyle of NASA Goddard Space Flight Center, for providing the Nimbus-7 ERB data.

TABLE OF CONTENTS

LIST OF FIGURES

LIST OF TABLES

SECTION 1

INTRODUCTION

Scanning instruments on orbiting satellites make measurements of the reflected or emitted radiance coming from the top of the atmosphere into a narrow solid angle. The measured radiances are highly sensitive to the underlying surface type and to the viewing and solar zenith angle conditions. Presence of cloud and the amount of cloud in the path of measured radiance has to be determined before the radiance could be converted to flux value. This operation is performed in the ERBE algorithm by the maximum likelihood estimation (MLE) procedure using satellite measured radiances from the scanner using the shortwave and longwave channels. An earlier study (Vemury et al., 1985; Vemury 1985) indicated that the MLE algorithm when applied to the Nimbus-7 ERB Scanner observations, led to an improvement in scene identification. It also improved the radiation budget parameters when compared with the results from the Sorting into Angular Bins (SAB) method. However, some of the data used in that study had several deficiencies. The input datasets in the present study are considerably improved. Some changes in the algorithms are also implemented and some computer related problems removed.

This report deals with several tasks relating to an evaluation of the MLE method for scene identification by examining several aspects of the scene identification process, and of the computed radiation budget parameters at different spatial and temporal scales. Effect of changes in the input

datasets, use of other scene identification methods like the perpendicular bisector algorithm, sensitivity to the parameters of the MLE method, etc. are also investigated and reported here. An analysis of the sampling adequacies at different temporal intervals using the SAB method is also presented. This is an important aspect of the validation process since the SAB method provides the necessary datasets against which the results with the MLE method are compared. A good understanding of the sampling situation in the SAB method is necessary to make any assertions as to the accuracy of the results obtained with the MLE method.

The results are presented in the following sections. Each of the studies performed is discussed in a separate section and the elements of the study are shown as subsections.

SECTION 2

IMPROVED BASELINE RESULTS

A set of baseline results was developed with an earlier algorithm and the results were presented in Vemury (1985). The analysis in this section and most of the following sections is for the month of June 1979. The scanner observations were from the Nimbus-7 Earth Radiation Budget (ERB) instrument narrow field of view (NFOV) channels. The CLE angular models were used in this study. This study will, therefore, be referred to as the CLE study.

(a) Longwave flux field

The input datasets for the study mentioned above contained the clear sky longwave flux field which corresponded to the November period. The study is for the month of June and this required a longwave flux field corresponding to the summer season. Correct flux fields are obtained in the folowing way. The latitude dependent and surface dependent longwave flux values are taken from "ERBE" Angular Models" (unpublished blue book from the ERBE team) for the summer season. Based upon the latitude band and upon the underlying surface category, viz., ocean, land, snow, desert and mixed ocean/land, the longwave flux values are computed for each 2.5^{o} x 2.5^{o} region of the globe.

Due to differences between the Nimbus-7 ERB and the ERBE instruments, an adjustment to the longwave flux values was made when recorded in the ERBE blue book. Since the present application is for the ERB instrument data, that adjustment had to be removed by subtracting 8 W/m^2 from

each of the flux values for each lat-lon grid. This new set of longwave flux values constitutes the appropriate clear sky longwave flux field for the month of June.

(b) Snow fields

The distribution of snow in the geography field is also modified. The earlier study used a snow field for the southern hemisphere, but none was used in the northern hemisphere. This has resulted in extremely large cloud identifications in the northern hemisphere. This result became apparent only when the cloud fields derived using the MLE method were compared with the THIR cloud fields for the same month. New snow fields on our spatial grid are therefore generated. The snow field from HIRS2/MSU for June is interpolated to the $2.5^{o} \times 2.5^{o}$ grid. This new snow field is overlaid on the previous geopraphy field and those regions which contained snow in the previous geography field and no snow in the new field were replaced with the appropriate geographical category, primarily land, ocean or land/ocean mix.

(c) Compiler errors

Another modification made was in the albedo field. Clear sky albedo values for nadir sun for ocean, land, desert, etc. are specified. Depending on the surface category in the geography field, clear sky nadir albedo is picked. Compiler problems with the computer tended to round off this number to a smaller value. The effect of this was to enhance the cloud condition cases in the scene identification process. Necessary changes were made to the code so that the compiler provided the correct albedo field to the algorithms.

(d) MLE software modifications

A modified software for scene selection was supplied by NASA/Langley Research Center which was incorporated into the ERB processing algorithms. The primary modification was in the use of an interpolation scheme for the clear sky longwave flux values between latitude bands. The earlier procedure made use of one longwave flux value for a latitude band and suddenly jumped to a different value for the next band. This caused strong discontinuities in the cloud identification and the cloud amount. A linear interpolation scheme in the values smoothed out the field and thus the cloud field selected was smoother. Additional modifications in the code were provided subsequently at the time when the NCLE models were supplied. These modifications were incorporated into the NCLE model runs, to be discussed in a later section.

2.1 COMPARISON OF ERB PARAMETERS BETWEEN MLE AND SAB METHODS

The primary objective of this study is validation of the derived parameters using MLE with those from the SAB method. Due to sampling limitations, values with the SAB method were derived for the entire month of June 1979 and were provided by the Nimbus-7 ERB team (Dr. H.L. Kyle, GSFC, personal communication). The results with the MLE method were derived for each day using the scene identification and the CLE angular models. The daily means were used to compute the monthly mean parameters. Thus the monthly mean MLE results were compared with the monthly mean SAB results.

This section deals with this comparison at the target area (TA), zonal and global mean levels. To eliminate the scene identification deficiencies at very large zenith angles, the radiation budget parameters were divided into two categories. The first category consisted of the results where all the available observations were kept, and in the second category, observations with the satellite zenith angle greater than 70° were not included in the computation. These are referred to as CLE-90 and CLE-70 cases in the following. References to computed albedo values always mean instantaneous albedo.

2.1.1 Target Area Comparisons

Comparison of the radiation budget parameters between the MLE and SAB methods are shown in Figures 2.1, 2.2, 2.3 and 2.4. CLE on the ordinate implies results with the MLE method using CLE models. Figure 2.1,a,b shows the MLE results for instantaneous albedo with satellite zenith angle cutoff value of 90° and 70° respectively compared with the SAB method. In both figures, the parameters of linear correlation are shown on the figure along with the rms difference between the MLE and SAB values.

The longwave flux values are compared in Figure 2.2a,b for daytime longwave flux; Figure 2.3a,b for nighttime longwave flux; and Figure 2.4a,b for total (day, night average) longwave flux, respectively. The subtle differences between the 90° amd 70° cutoff cases are not apparent at this level. In general, RMS differences are smaller in the 70° cutoff case. The correlation coefficient R is larger than 0.99 in all cases, indicating that the CLE-90 and CLE-70 results are very highly correlated with the SAB

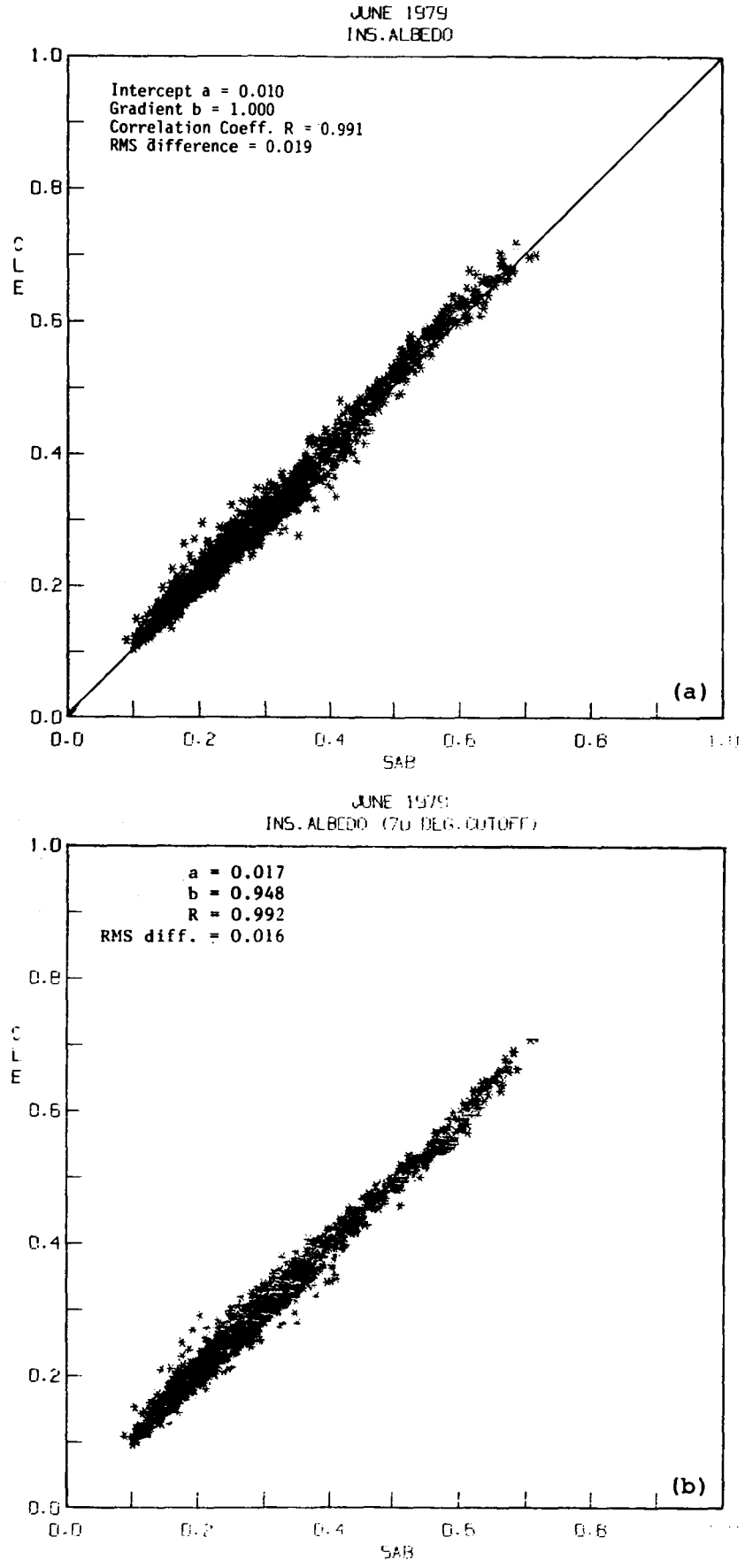

FIGURE 2.1. Regression plot of monthly mean instantaneous albedo using CLE models on the ordinate and SAB method on the abscissa. Parameters of linear regression, correlation coefficient, and RMS differences between the TA means are also shown. (a) 90° cutoff in satellite zenith angle; (b) 70° cutoff in satellite zenith angle both for CLE. Results are for the month of June 1979.

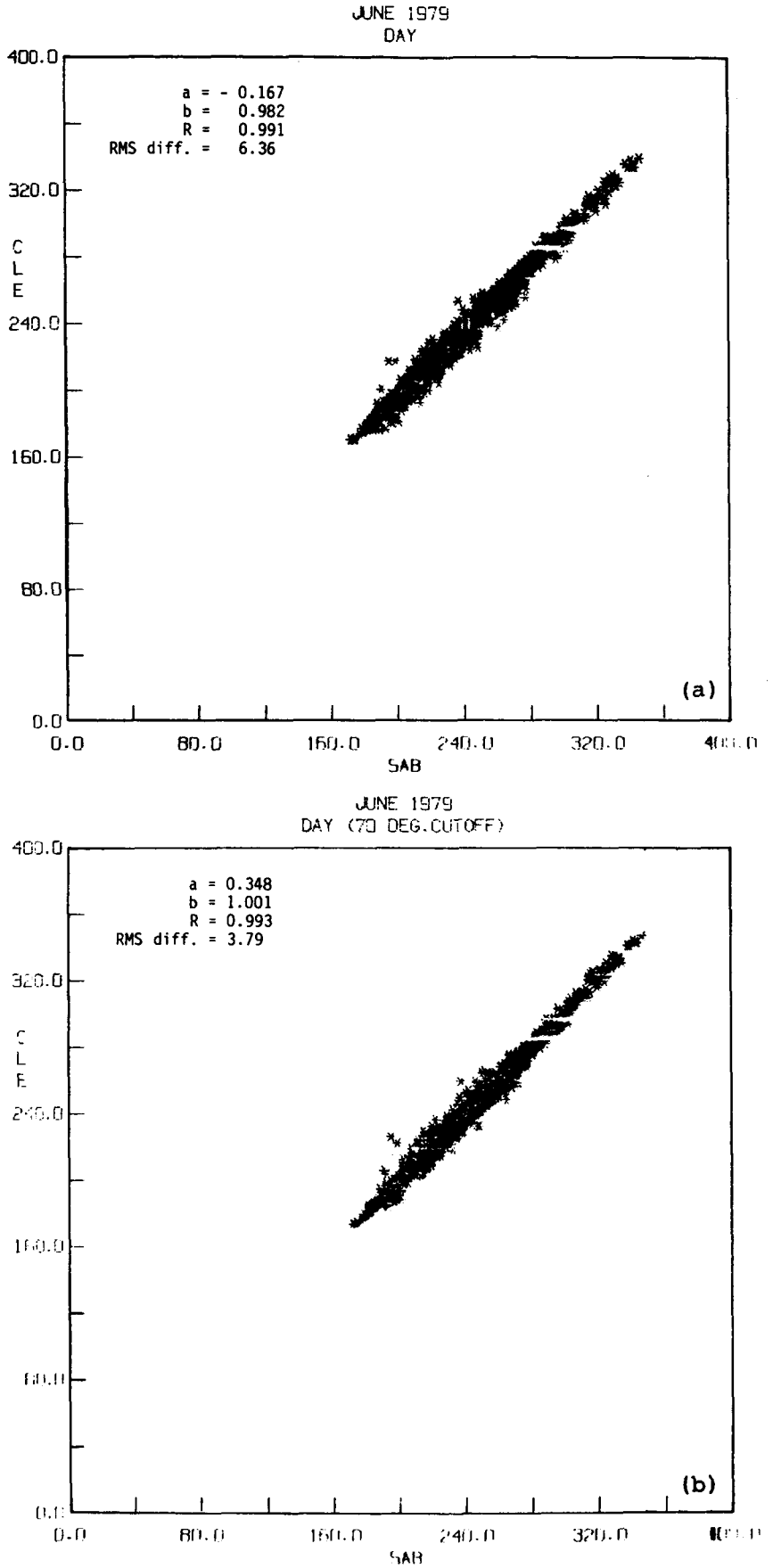

FIGURE 2.2 Regression plot of monthly mean daytime longwave flux (W/m^2) using CLE models on the ordinate and SAB method on the abscissa. Parameters of linear regression, correlation coefficient, and RMS differences between the IA means are also shown. (a) 90° cutoff in satellite zenith angle; (b) 70° cutoff in satellite zenith angle both for CLE. Results are for the month of June 1979.

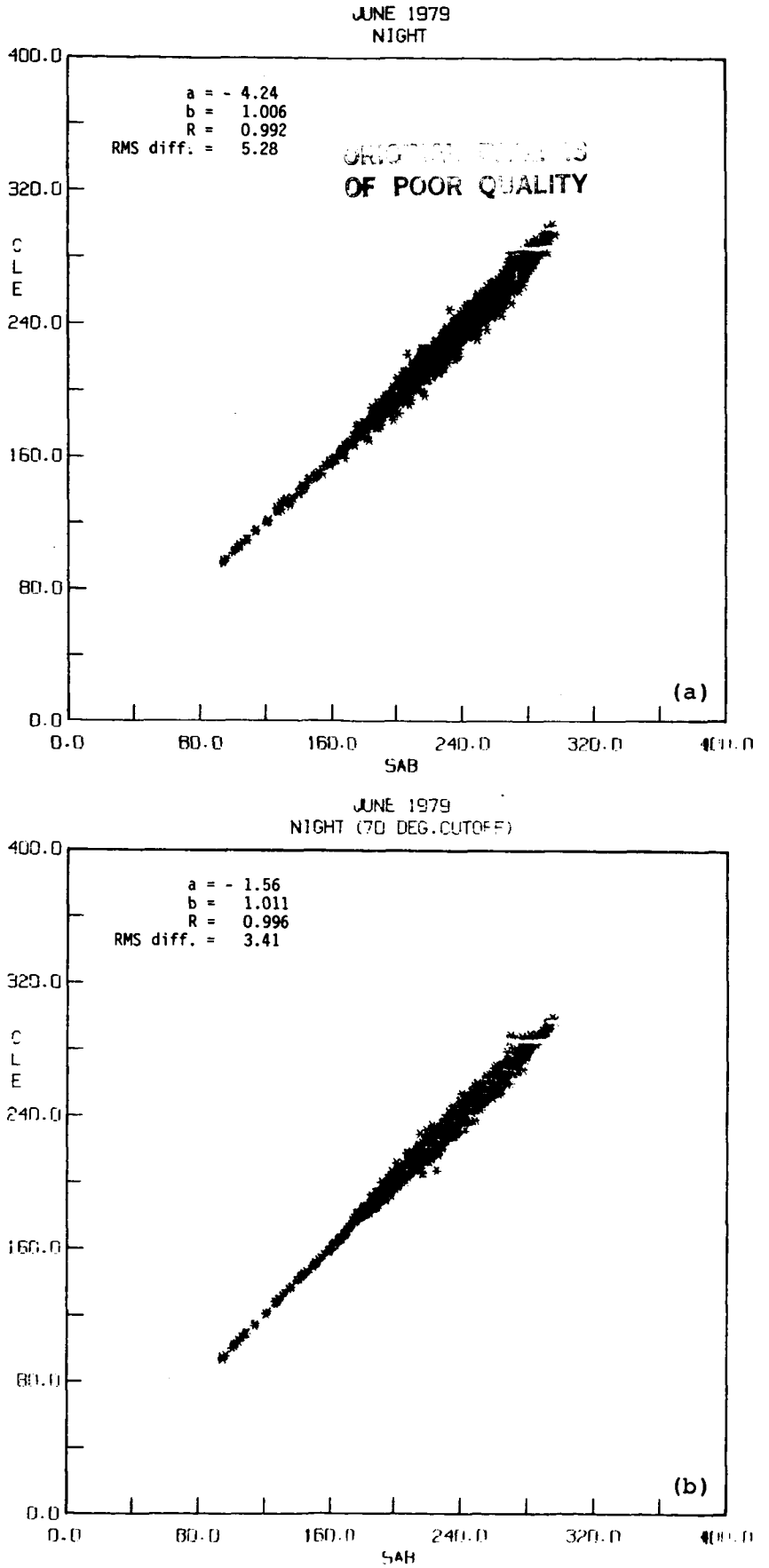

FIGURE 2.3 Regression plot of monthly mean nighttime longwave flux (W/m^2) using CLE models on the ordinate and SAB method on the abscissa. Parameters of linear regression, correlation coefficient, and RMS differences between the TA means are also shown. (a) 90° cutoff in satellite zenith angle; (b) 70° cutoff in satellite zenith angle both for CLE. Results are for the month of June 1979.

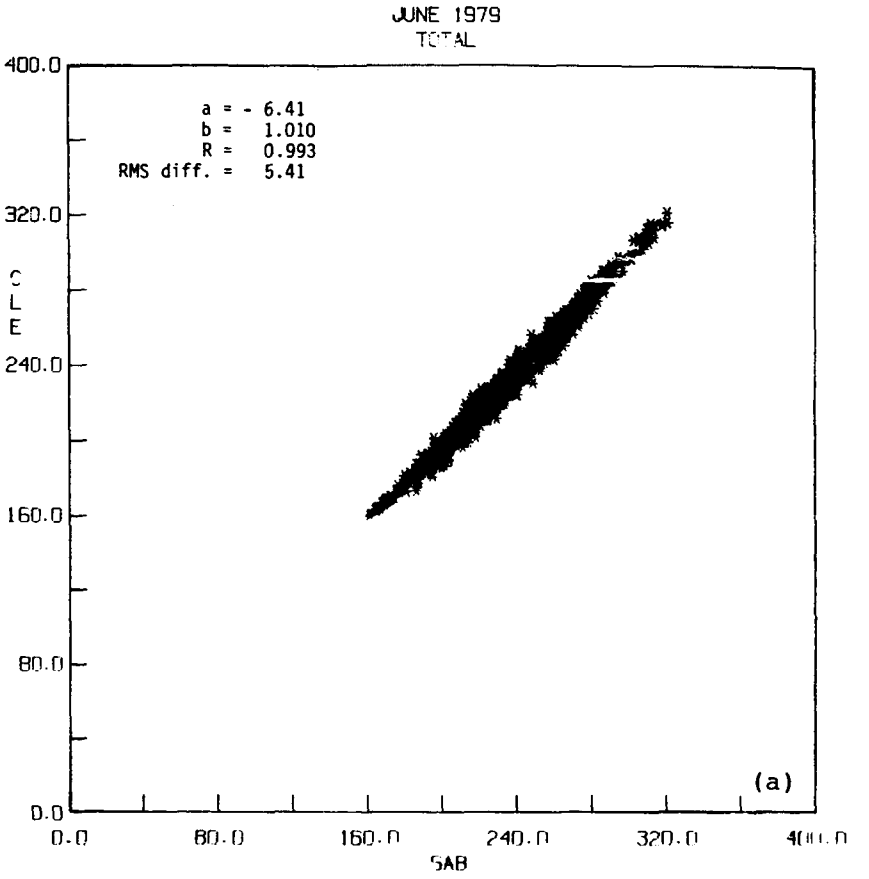

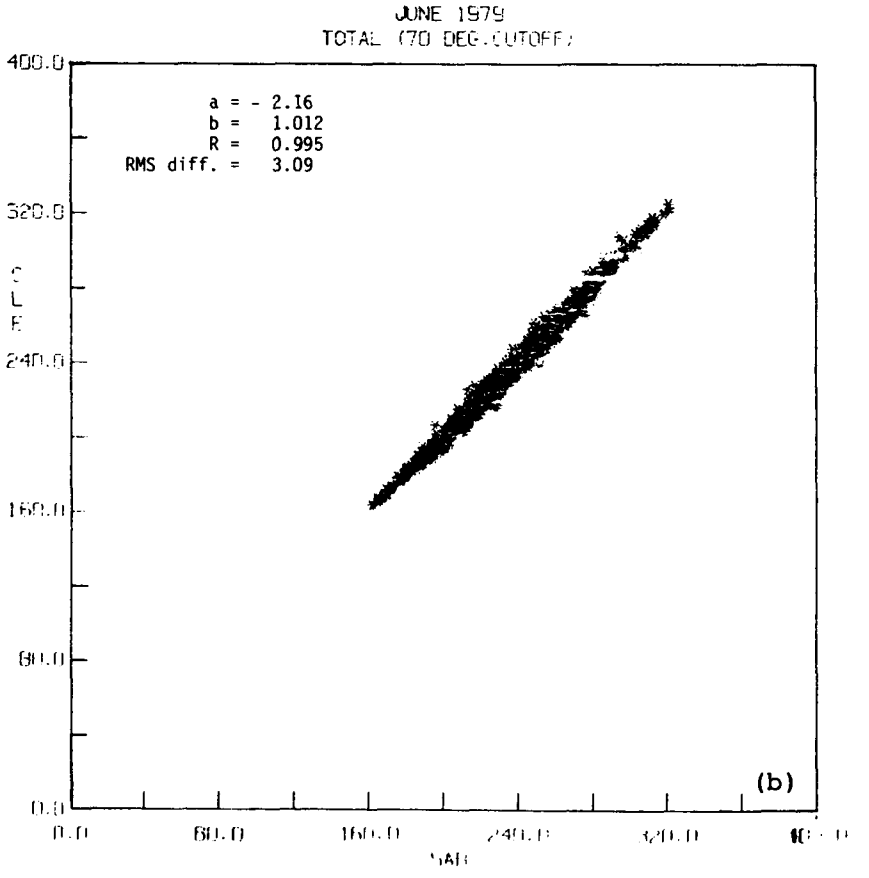

FIGURE 2.4 Regression plot of monthly mean day, night averaged longwave flux (W/m^2) using CLE models on the ordinate and SAB method on the abscissa. Parameters of linear regression, correlation coefficient, and RMS differences between the TA means are also shown. (a) 90° cutoff in satellite zenith angle; (b) 70° cutoff in satellite zenith angle both for CLE. Results are for the month of June 1979.

values. A complete list of the parameters of linear regression and the values of the RMS differences for the 90^{o} and 70^{o} cutoff cases, is given in Table 2.1.

Mercator maps of the albedo and the longwave flux differences are shown in Figures 2.5-2.7 for the CLE-70 case. Albedo differences are shown in percentages in Figure 2.5 while the longwave flux cases are in W/m^2. Albedo differences typically are 2% or less over most of the globe. The exception is over the east Pacific where values as large as 6% seem to appear. The longwave flux differences for the daytime (Fig. 2.6) show that the regional values of the flux could be different up to nearly 5 W/m^2 and do not ever reach 10 W/m^2 differences. Nighttime flux differences (Fig. 2.7) are higher over the land masses in North and South America and over the South Pacific regions. Similar structure exists in the total flux differences. With the cutoff at 70^{o}, therefore, there is general agreement between the reflected and emitted fluxes except over isolated regions. The nighttime difference is larger because of the use of daytime emission models for correcting the radiances at night.

2.1.2 Zonal Mean Comparisons

Differences in zonally averaged instantaneous albedo values are plotted in Figures 2.8a,b for the 90^{o} and 70^{o} satellite zenith angle cutoff cases respectively. At the 90^{o} cutoff angle, CLE 90, which uses MLE, slightly overestimates (relative to SAB) the instantaneous albedo over several latitude bands. The largest difference is over the snow covered regions of the oceans in the southern hemisphere. For other latitudes, the differences

TABLE 2.1 SAB, MLE Parameter Regression Relationships

Param	Data Sample Size	Intercept	Gradient	Corr. Coeff.	RMS diff.
90° Case					
Inst. Albedo	1909	0.010	1.000	0.991	0.019
LW flux (day)	1912	-0.167	0.982	0.991	6.36
LW flux (night)	1930	-4.24	1.006	0.992	5.28
LW flux (Total)	1844	-6.41	1.010	0.993	5.41
70° Case					
Inst. Albedo	1909	0.017	0.948	0.992	0.016
LW flux (day)	1912	0.348	1.001	0.993	3.79
LW flux (night)	1930	-1.561	1.011	0.996	3.41
LW flux (Total)	1844	-2.158	1.012	0.995	3.09

ORIGINAL PAGE IS
OF POOR QUALITY

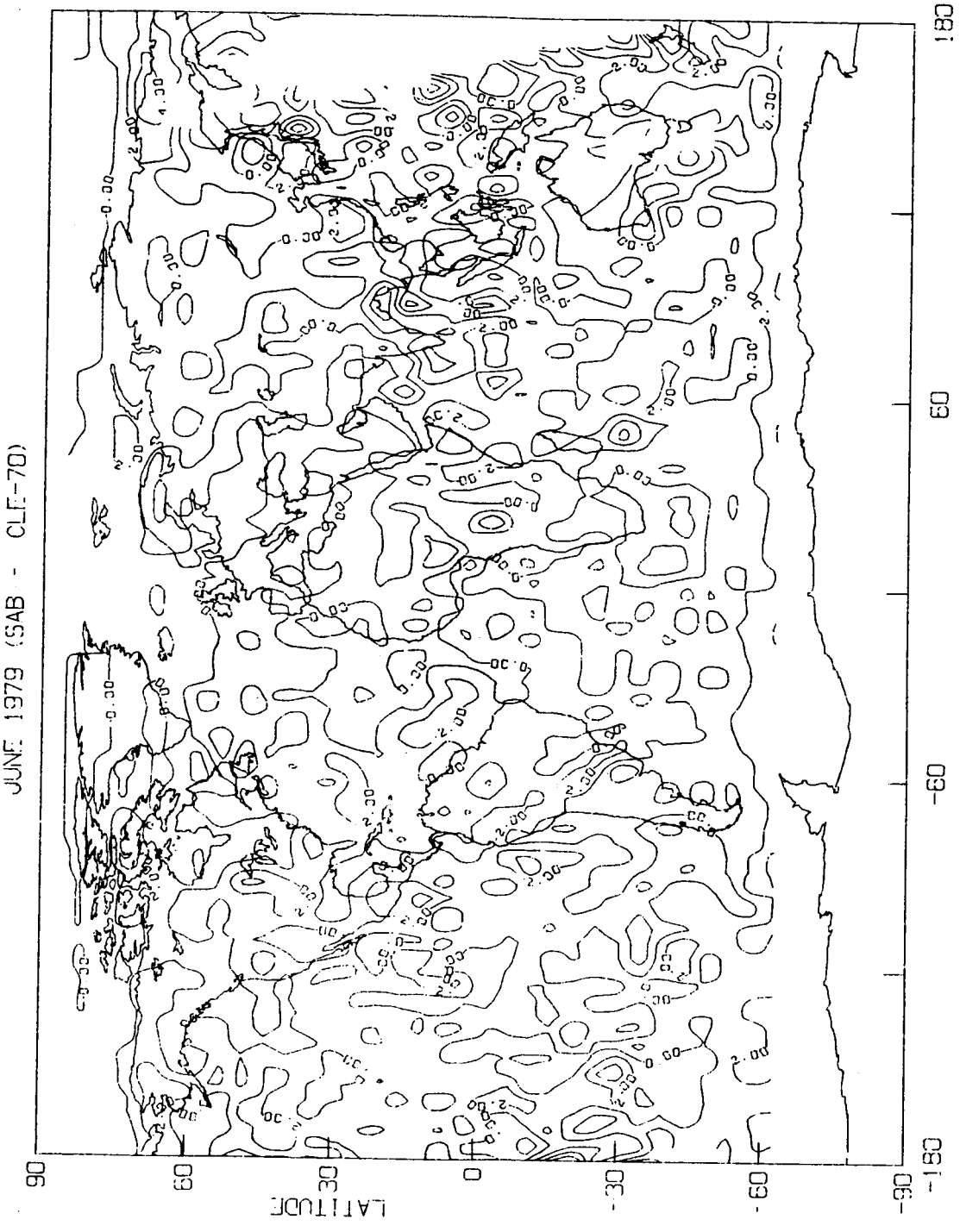

FIGURE 2.5 Mercator map of monthly mean instantaneous albedo (as percentages) differences between the SAB and MLE methods. CLE angular models are used with the MLE method. The case shown is for 70° satellite zenith angle cutoff (CLE-70 case).

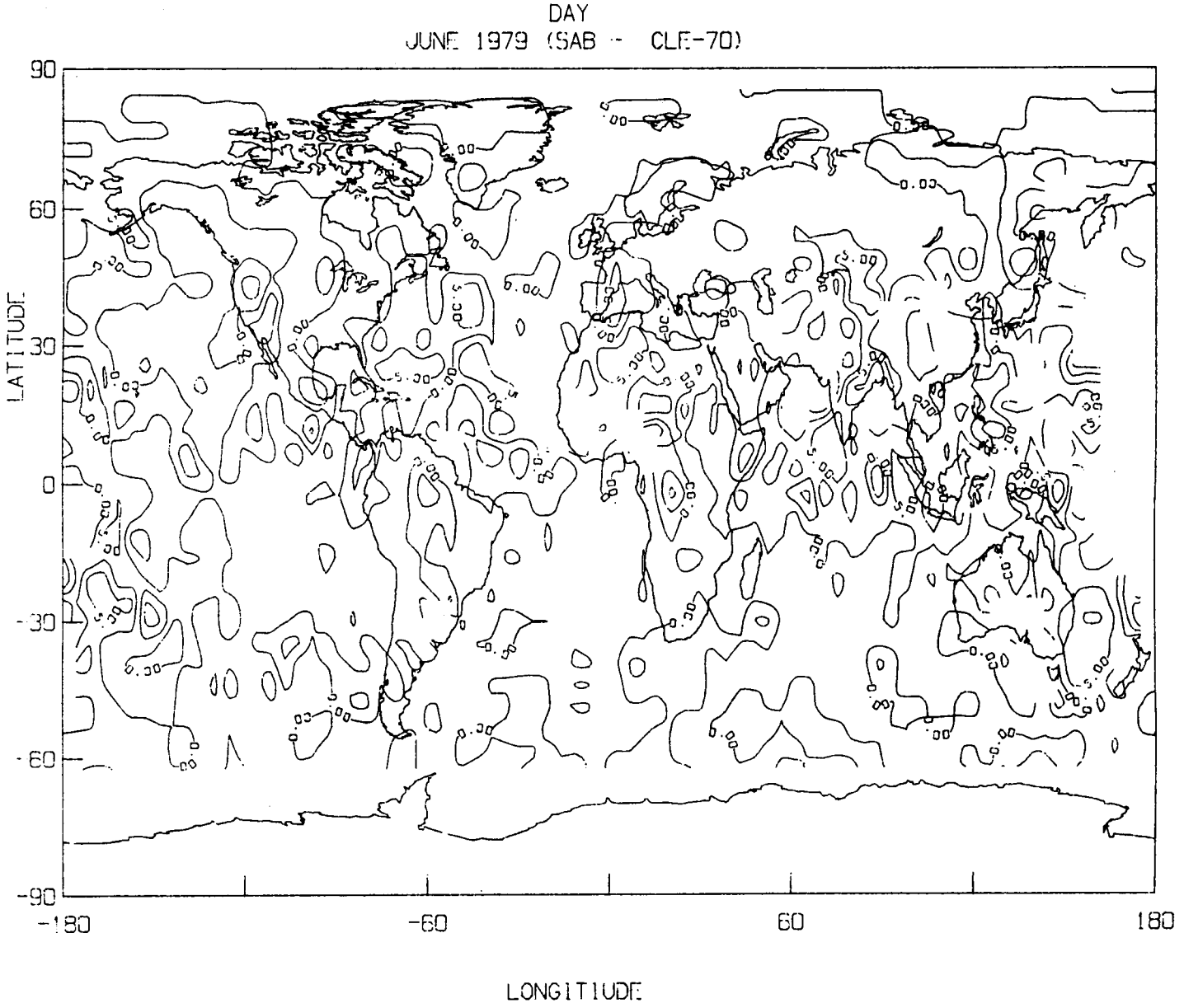

FIGURE 2.6 Mercator map of monthly mean daytime longwave flux differences (W/m^2) between SAB and MLE methods. CLE angular models are used with the MLE method. The case shown is for 70° satellite zenith angle cutoff (CLE-70 case).

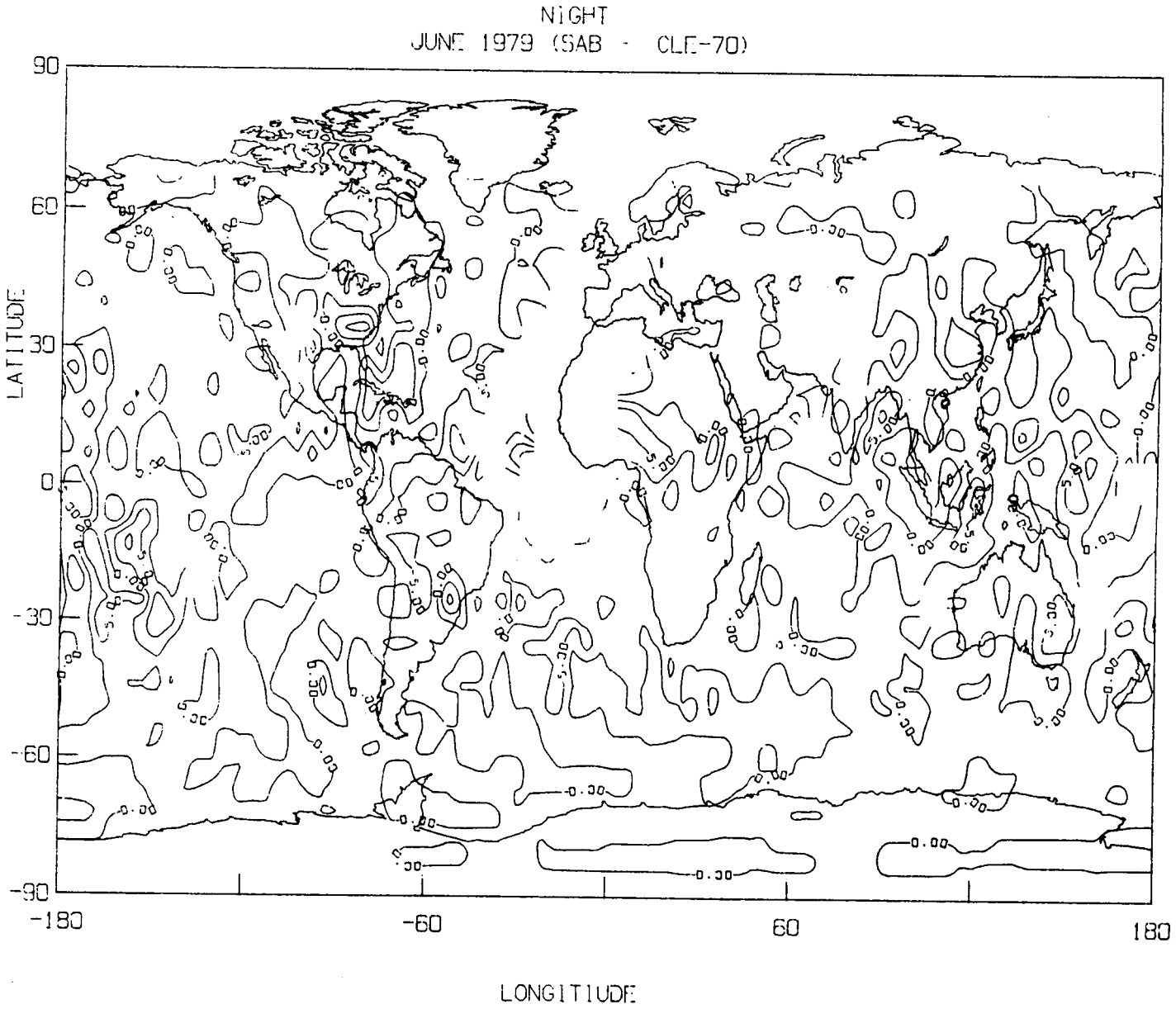

FIGURE 2.7 Mercator map of monthly mean nighttime longwave flux (W/m^2) differences between SAB and MLE methods. CLE angular models are used with the MLE method. The case shown is for 70° satellite zenith angle cutoff (CLE-70 case).

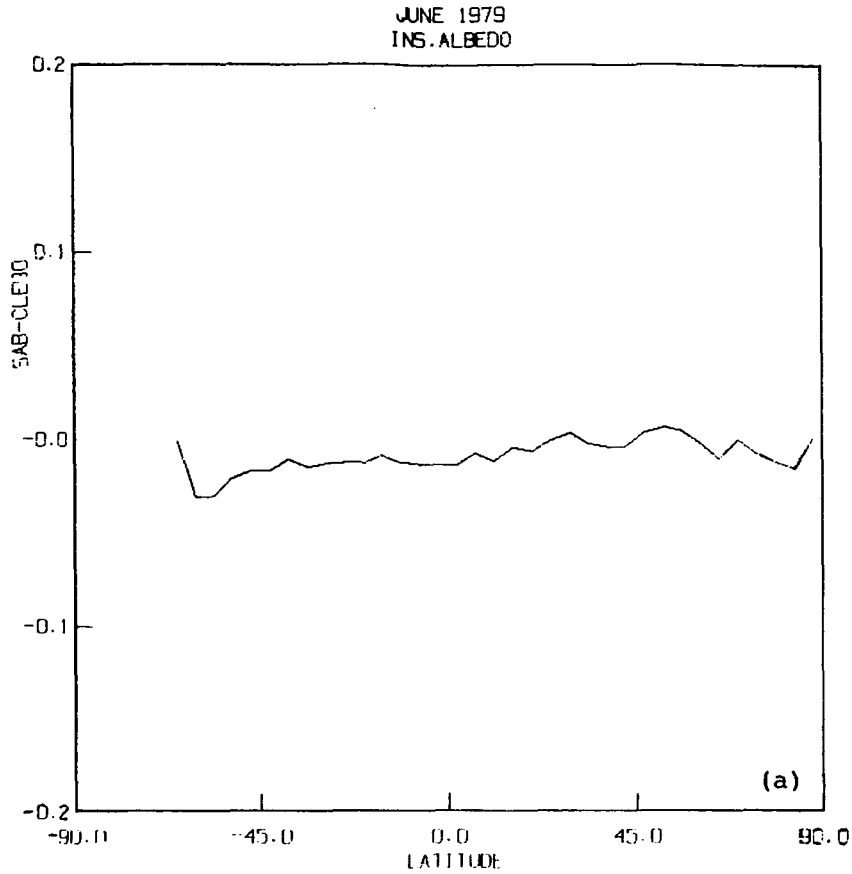

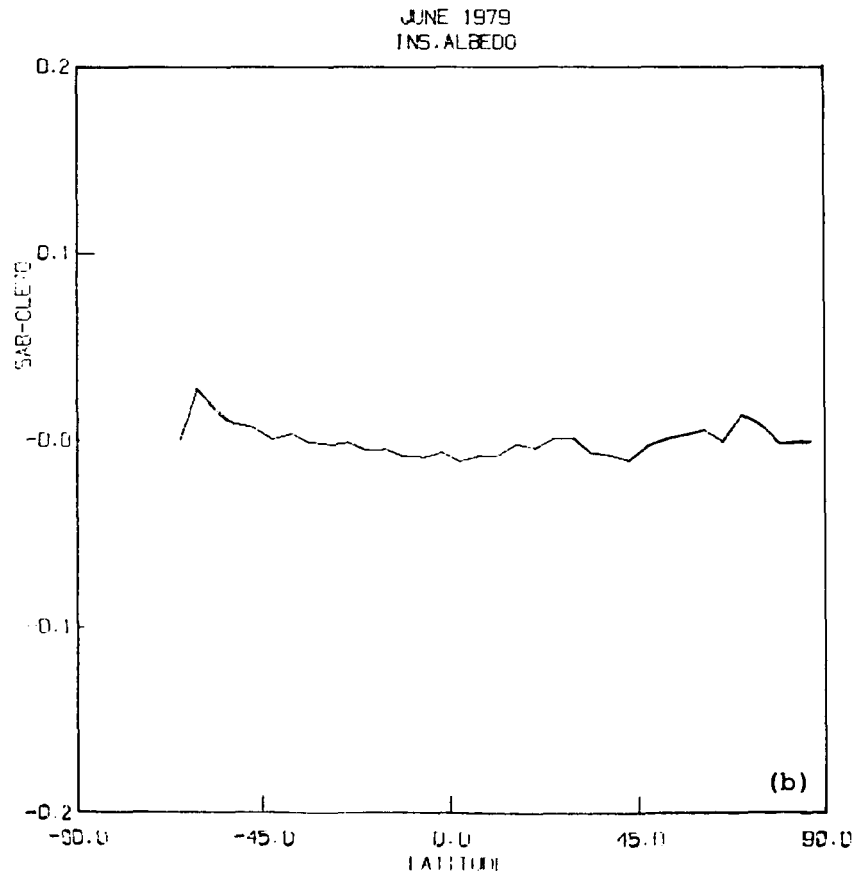

FIGURE 2.8 Zonally averaged monthly mean instantaneous albedo differences (as fractions) between SAB and CLE. CLE90 and CLE70 refer to cutoff at 90° and 70° cases with the MLE method. (a) CLE 90° case; (b) CLE 70° case.

are about 0.01 or less in albedo. At the 70^{o} cutoff, the MLE method underestimates (relative to SAB) the albedo. Over most latitude zones, the differences are close to zero and generally tend to be of opposite sign to the SAB, CLE 90 differences.

The longwave flux differences are shown in Figures 2.9a,b; 2.10a,b; and 2.11a,b, for daytime, nighttime and day-night average cases respectively. Daytime flux averages at the zonal level tend to be generally smaller with cutoff angle at 90^{o} relative to the SAB method (Fig. 2.9a). In the case of cutoff at 70^{o}, the differences (Fig. 2.9b) are smaller and are of the order of 1 to 1.5 W/m^2 compared with a mean value of 5 W/m^2 for the MLE 90^{o} case. The implication of the differences between the 90^{o} and 70^{o} cases is that, between 70^{o} and 90^{o}, the limb correction is smaller, tending to reduce the longwave flux values when all the observations up to 90^{o} are included. The case of 70^{o} cutoff (CLE 70) shows a better agreement with the SAB zonal means. The nighttime (Fig. 2.10a,b) and total longwave (Fig. 2.11a,b) flux differences show similarly large values at 90^{o} cutoff, while 70^{o} cutoff cases show better agreement with the SAB method. Since the SAB method includes all radiance means up to 90^{o} and its agreement with MLE 70 implies that the limb correction being applied at large zenith angles is not corect. The largest difference in both the nighttime and total longwave flux for the 90^{o} case occurs in the region of the ITCZ. This might mean that the cloud emission models could be in some error.

2.1.3 Global Means

The zonal mean values are used to compute the global means which are shown in Table 2.2. The global means with the standard deviations for the 90^{o}

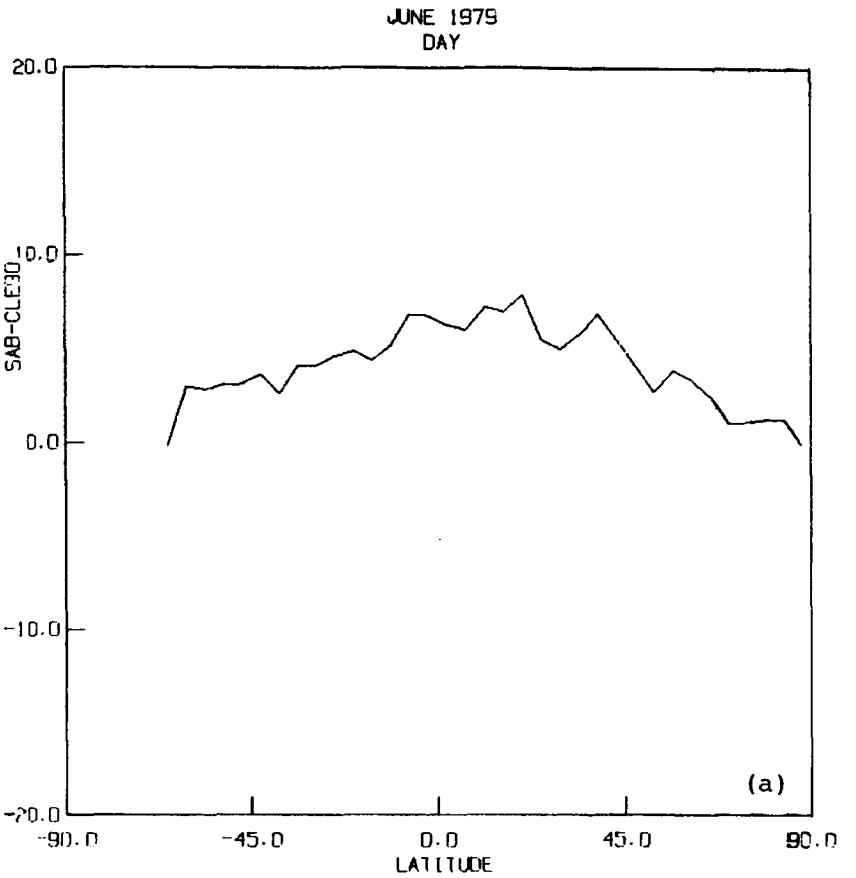

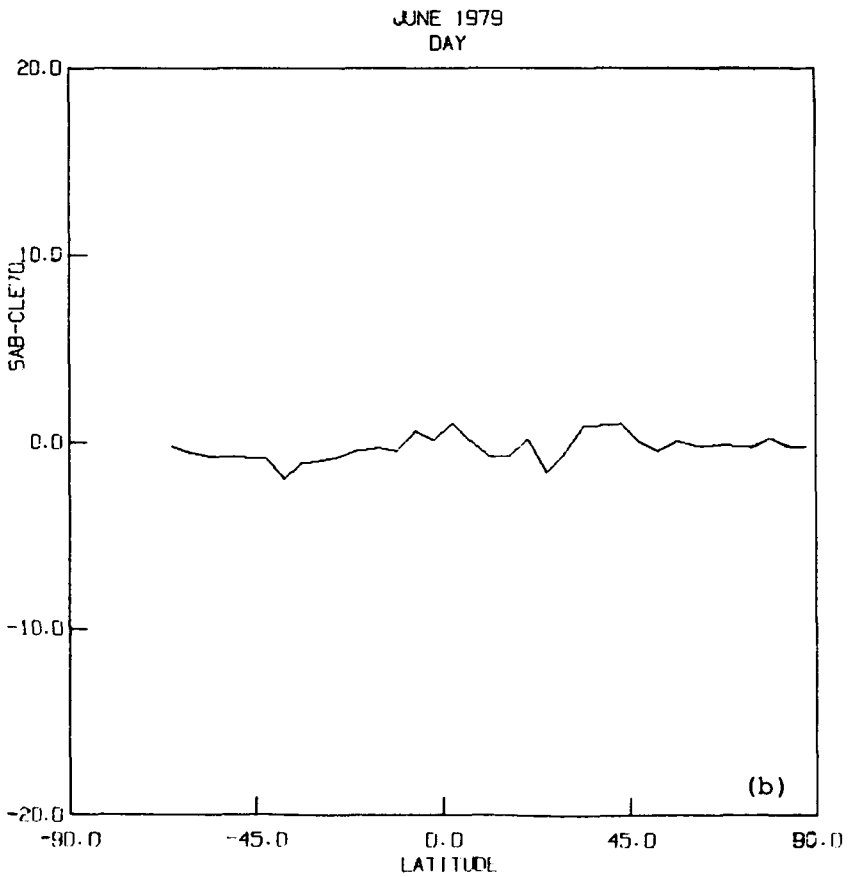

FIGURE 2.9 Zonally averaged monthly mean daytime longwave flux differences (W/m^2) between SAB and CLE. CLE90 and CLE70 refer to cutoff at 90° and 70° cases with the MLE method. (a) CLE 90° case; (b) CLE 70° case.

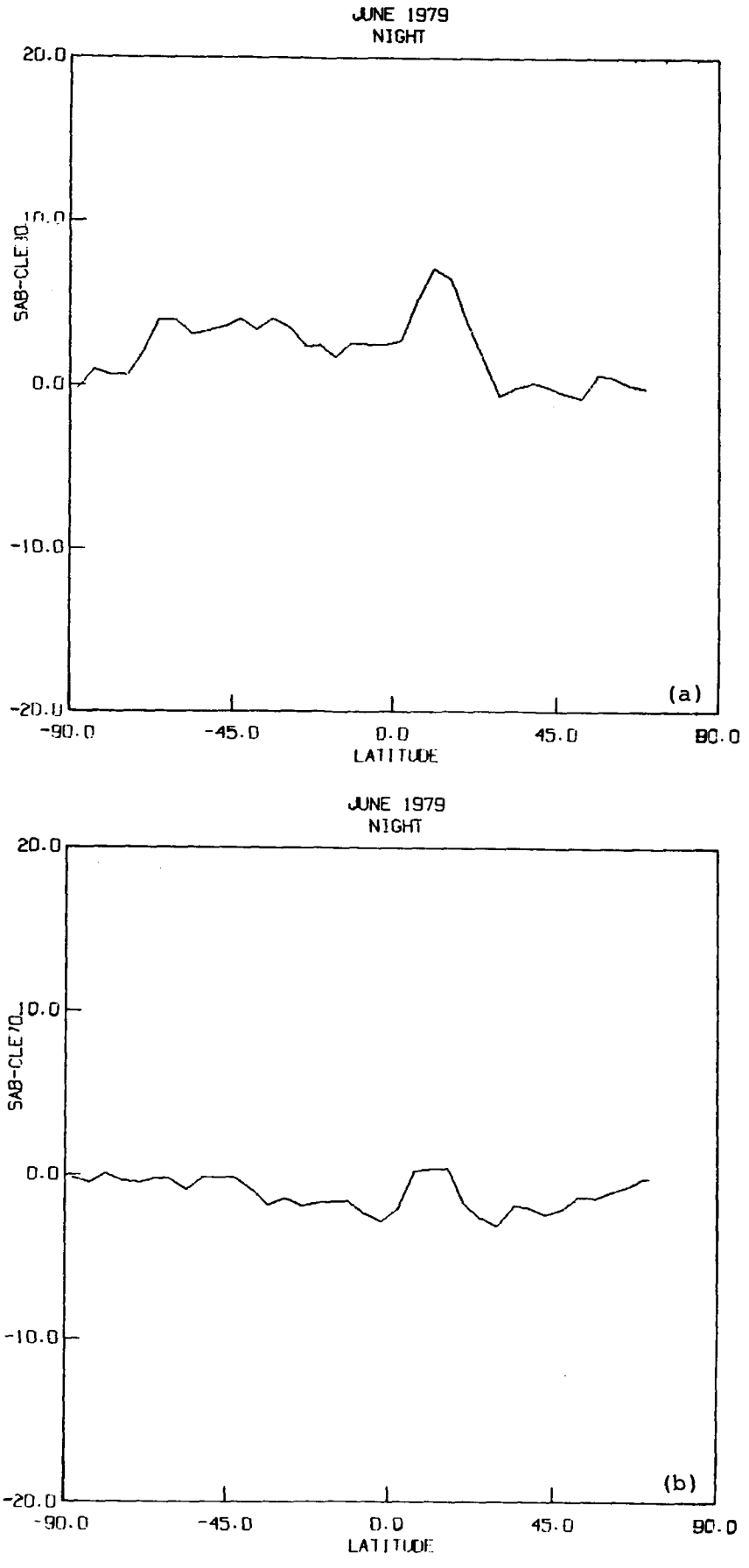

FIGURE 2.10 Zonally averaged monthly mean nighttime longwave flux differences (W/m^2) between SAB and CLE. CLE90 and CLE70 refer to cutoff at 90° and 70° cases with the MLE method. (a) CLE 90° case; (b) CLE 70° case.

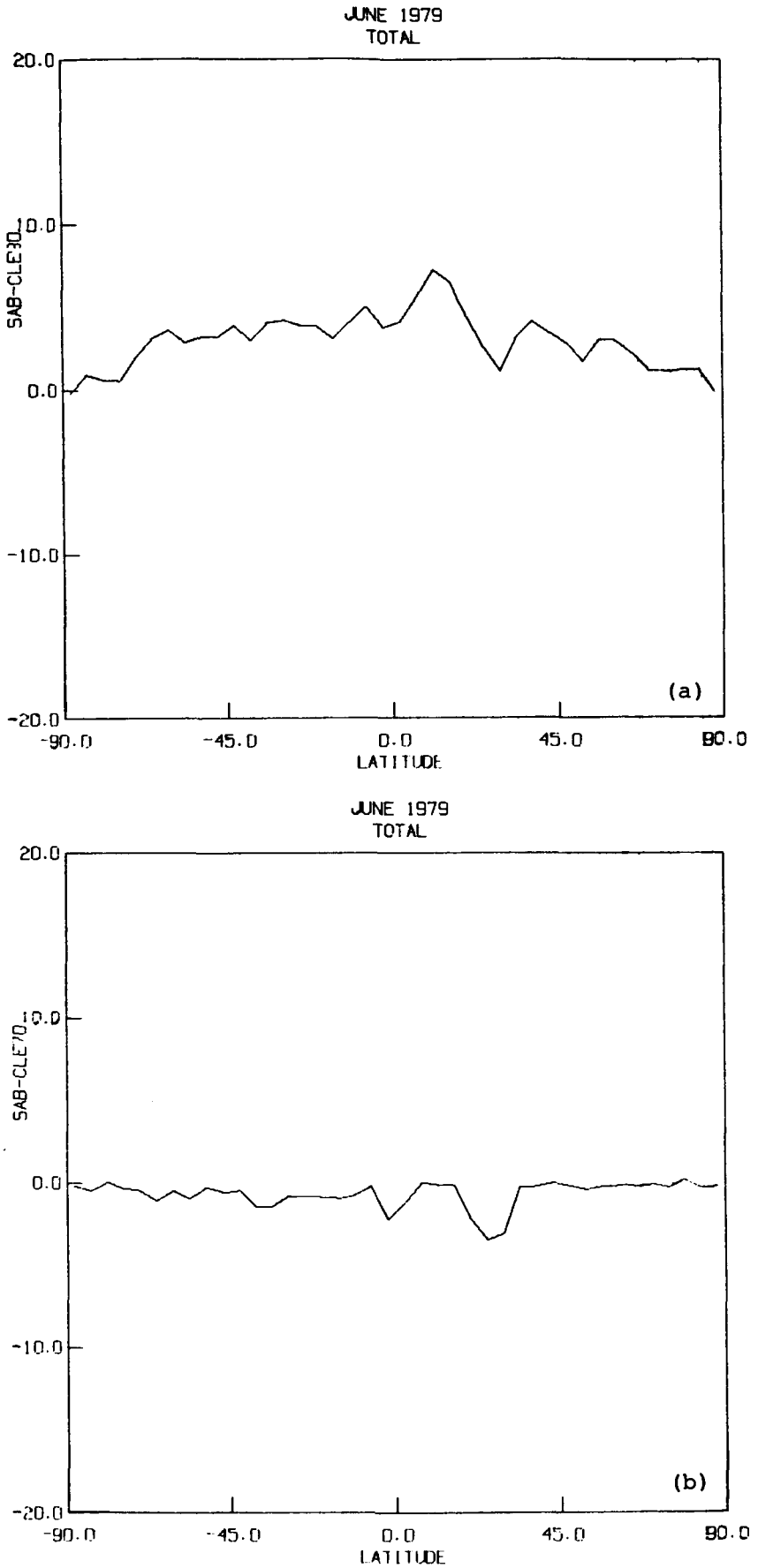

FIGURE 2.11 Zonally averaged monthly mean day, night averaged (total) longwave flux differences (W/m^2) between SAB and CLE. CLE90 and CLE 70 refer to cutoff at 90° and 70° cases with the MLE method. (a) CLE 90° case; (b) CLE 70° case.

TABLE 2.2 Global Averages Using SAB and MLE Methods.

Monthly Means for June 1979.

Radiation Budget Parameter	SAB Method	MLE Method			
		$\theta_s \leq 90°$		$\theta_s \leq 70°$	
		Mean	RMS Diff	Mean	RMS Diff
Instantaneous Albedo	0.2738±0.101	0.2820±0.103	0.019	0.2780±0.099	0.016
LW Flux (day)	244.3±23.4	239.4±22.4	6.36	244.4±23.4	3.79
LW Flux (night)	227.6±35.4	224.6±36.0	5.28	228.5±36.5	3.41
LW Flux (Total)	235.6±30.9	231.8±30.8	5.41	236.3±31.5	3.09

and 70^{o} cutoff cases are included in the table. Also included are the computed values with the SAB method, which provides the values for comparison. RMS differences of the MLE 90 and MLE 70 cases from the SAB case are also shown in the table. The instantaneous albedo values expressed as percentages are 28.1 and 27.8 for the MLE 90 and MLE 70 cases while the SAB gives a value of 27.4. The RMS difference is smaller in the MLE 70 case. Earlier results of comparisons with the zonal and TA means also support the conclusion that the 70^{o} cutoff case gives closer agreement with the SAB results. The longwave fluxes also lead to a similar conclusion. The MLE 70 method gives longwave flux values which differ from the SAB method by 0.5 to 0.9 W/m^2 while in the MLE 90 case the differences are of the order of 3 to 5 W/m^2. The RMS differences have also improved in the MLE 70 case.

2.1.4 Conclusions

Based upon the above comparisons, global, zonal and TA averages of the radiation budget parameters derived using the MLE method with CLE angular

models show a very good agreement with the parameters derived from the SAB method. The agreement is especially good at all the above spatial scales when observations above 70^{o} in satellite zenith angle are removed from the sample.

2.2 TARGET AREA STUDIES

To help further validate the MLE approach, 20 target areas have been chosen for detailed study. These target areas are shown on the ERB world grid (Fig. 2.12) and are denoted by symbols A through T. These are the same TAs used for detailed analysis by the ERBE team (VI-6-4 of ERBE release 3 specifications, ed. R. Green, April 1983; unpublished). In the Nimbus-7 global grid convention, the TAs are 25, 96, 330, 585, 662, 889, 1121, 1146, 1418, 1423, 1444, 1498, 1527, 1657, 1660, 1767, 1782, 1948, 1957, 2025.

2.2.1 Monthly Means

For these 20 TAs, monthly mean albedo and longwave fluxes are compared with the SAB values. When these TAs are classified purely on the basis of the underlying surface, they fall into these categories:

Land:	D,F,N,O,Q,R
Ocean:	C,E,G,H,K,M,P,S
Snow:	A,B,T
Desert:	I,J,L

Instantaneous albedo differences for the 20 TAs are shown in Figure 2.13a,b for the 90^{o} and 70^{o} cutoff cases. In both cases, ocean TAs seem to indicate small absolute differences with the SAB method compared to the TAs with land as underlying surface. Albedo values for the ocean TAs seem to differ from SAB values by 0.02 or less, with the only exception of H (TA 1146) which is in the equatorial Pacific and belongs to the ITCZ. There is also a general tendency for the albedo difference to decrease in the 70° case relative to

ORIGINAL PAGE IS
OF POOR QUALITY

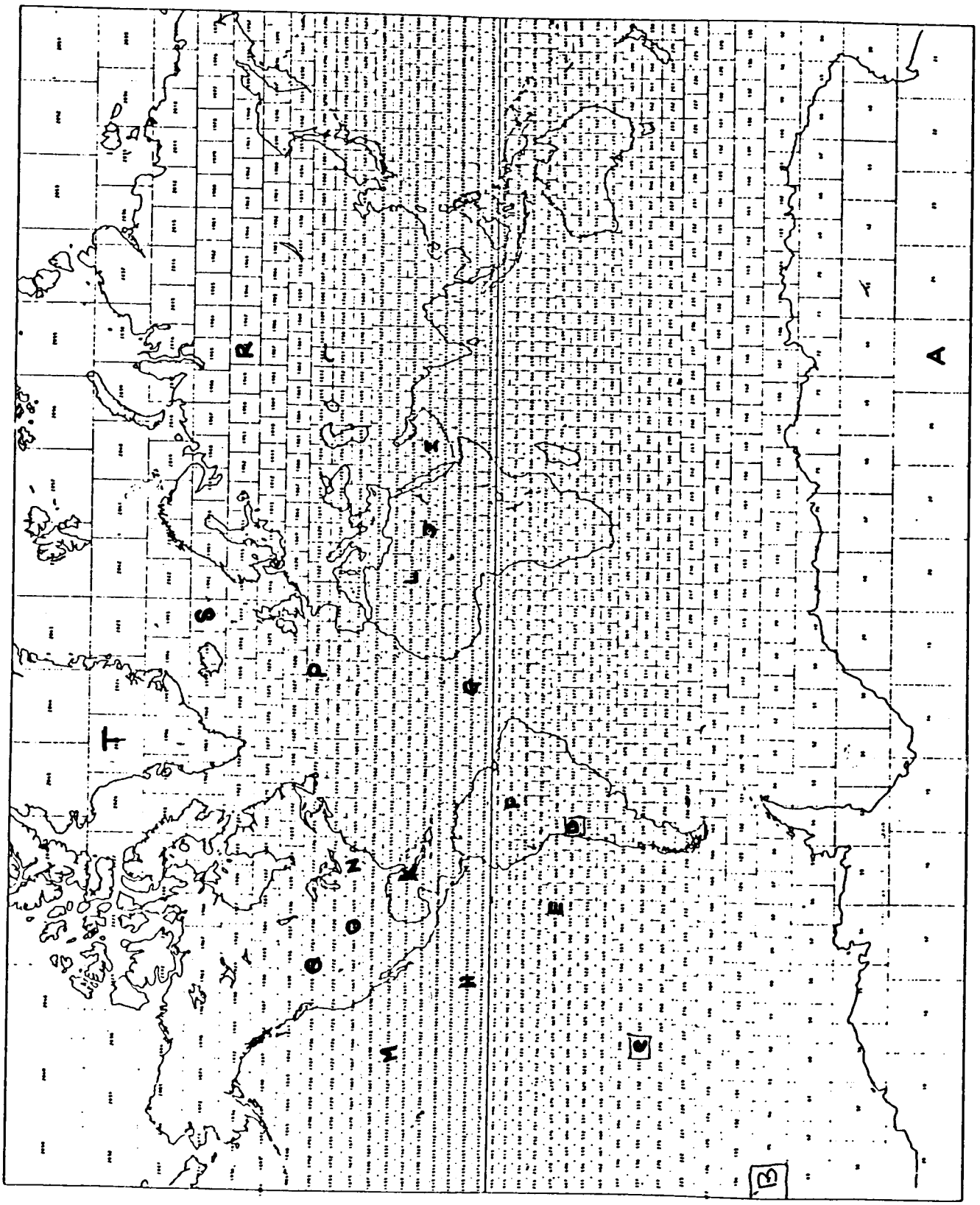

FIGURE 2.12 Nimbus-7 ERB equal area regions (Target Areas) displayed on a mercator projection.

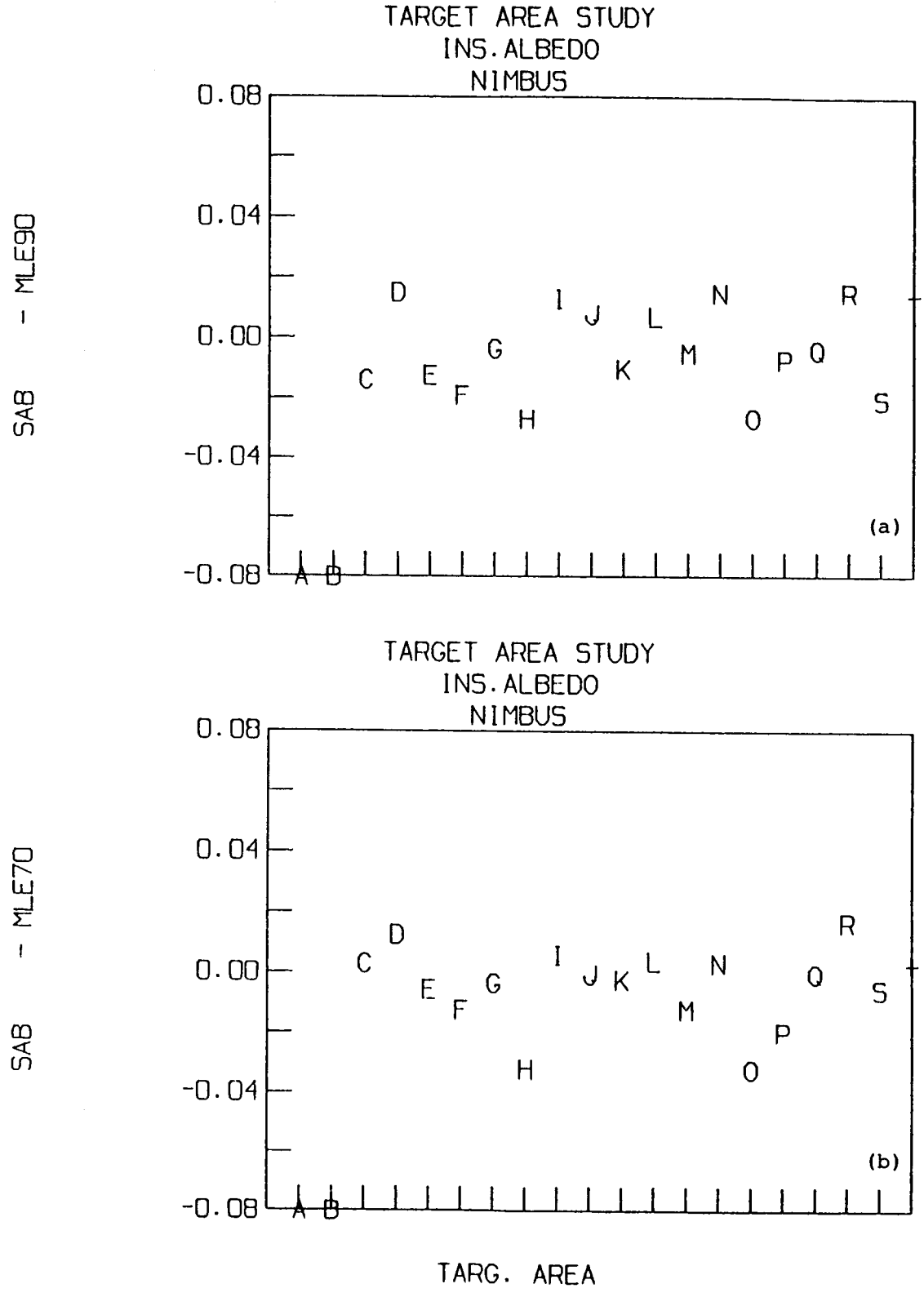

FIGURE 2.13 Monthly mean instantaneous albedo (as fractions) differences for 20 chosen target area regions, A through T. These areas are identified as A, B, etc. on Fig. 2.12. (a) CLE 90° case; (b) CLE 70° case.

the 90^{o} case. Here again, the primary exceptions are TAs H, M and P, all of which are ocean TAs.

Daytime longwave flux comparisons are shown in Figure 2.14a,b. For many TAs, the flux differences are in excess of 5 W/m^2 and for H (TA 1146) in excess of 10 W/m^2. In none of the cases is the MLE value larger than the SAB value. At 70^{o} cutoff, the flux differences are still positive, but dropped significantly. TA 1146 which belongs to the ITCZ is the only exception with a difference close to 9 W/m^2. Similar TA behavior is noticed in Figure 2.15a,b for the nighttime longwave fluxes. These values in general show better agreement with SAB. The improvement at 70^{o} cutoff is also apparent. The exception is G, the ocean TA 1121 in the equatorial east Atlantic. The total longwave flux shows a similar trend (Fig. 2.16a,b). It is noteworthy that TAs denoted by G and H stand out in their differences from the SAB by as much as 12 to 13 W/m^2 in total longwave flux for G and 0.03 in albedo for TA H.

2.2.2 Day to Day Dispersion

One of the primary advantages of the MLE method is that regional radiation budget parameters could be computed on a daily basis. For each day, therefore, a mean value and a standard deviation can be obtained for the albedo and longwave flux. This is not possible with the SAB method. The method provides a simple integrated value of the albedo or the longwave flux as a monthly mean. It is not possible to determine the variance in the flux in a day or the variation from day to day during the month. Use of the SAB method for intervals smaller than a month is investigated in section 5 and the degree of bias introduced due to use of smaller temporal interval and of different spatial scale averaging are discussed in that section.

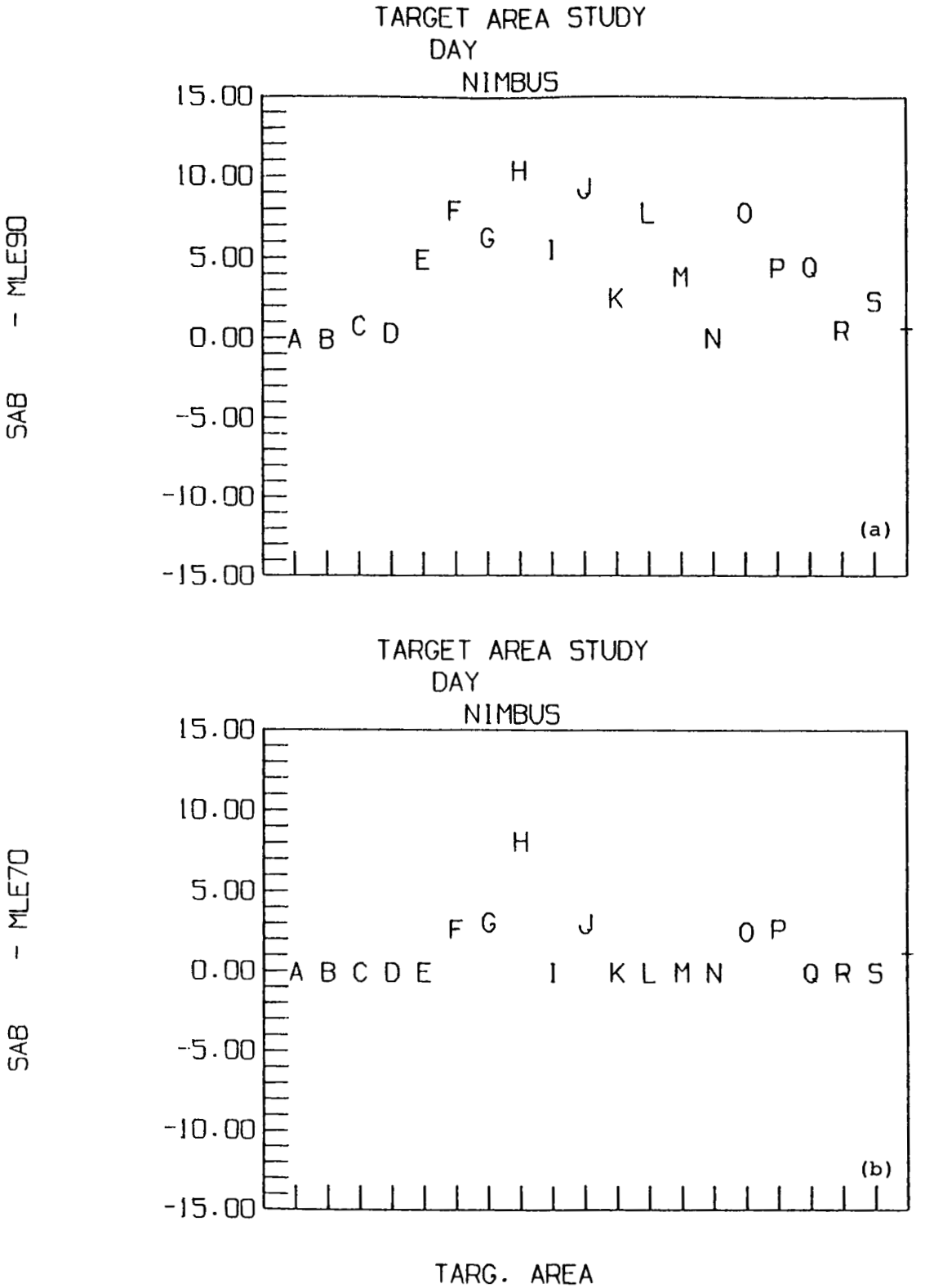

FIGURE 2.14 Monthly mean daytime longwave flux differences (W/m^2) for 20 chosen target area regions, A through T. These areas are identified as A, B, etc. on Fig. 2.12. (a) CLE 90° case; (b) CLE 70° case.

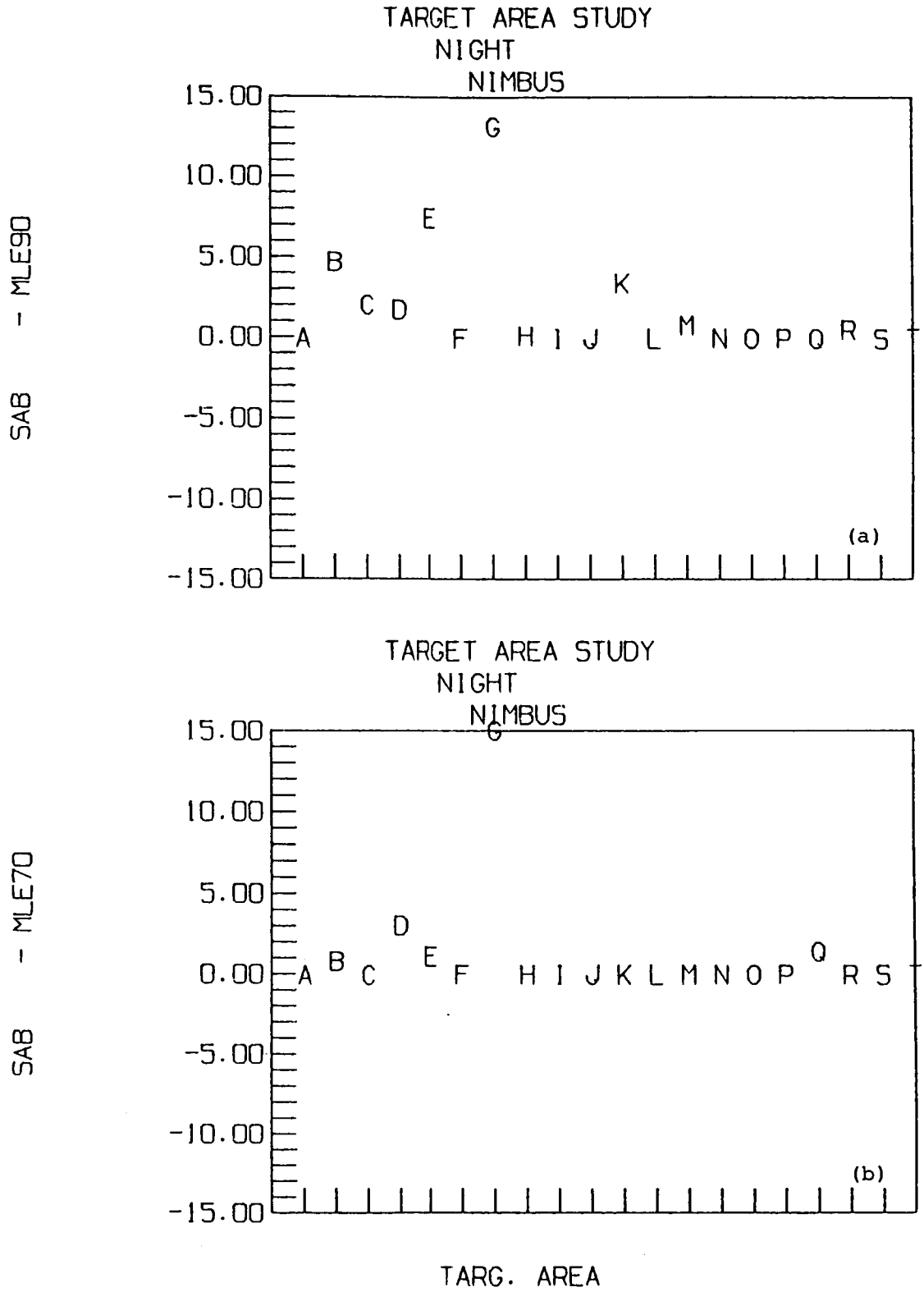

FIGURE 2.15 Monthly mean nighttime longwave flux differences (W/m^2) for 20 chosen target area regions, A through T. These areas are identified as A, B, etc. on Fig. 2.12. (a) CLE 90° case; (b) CLE 70° case.

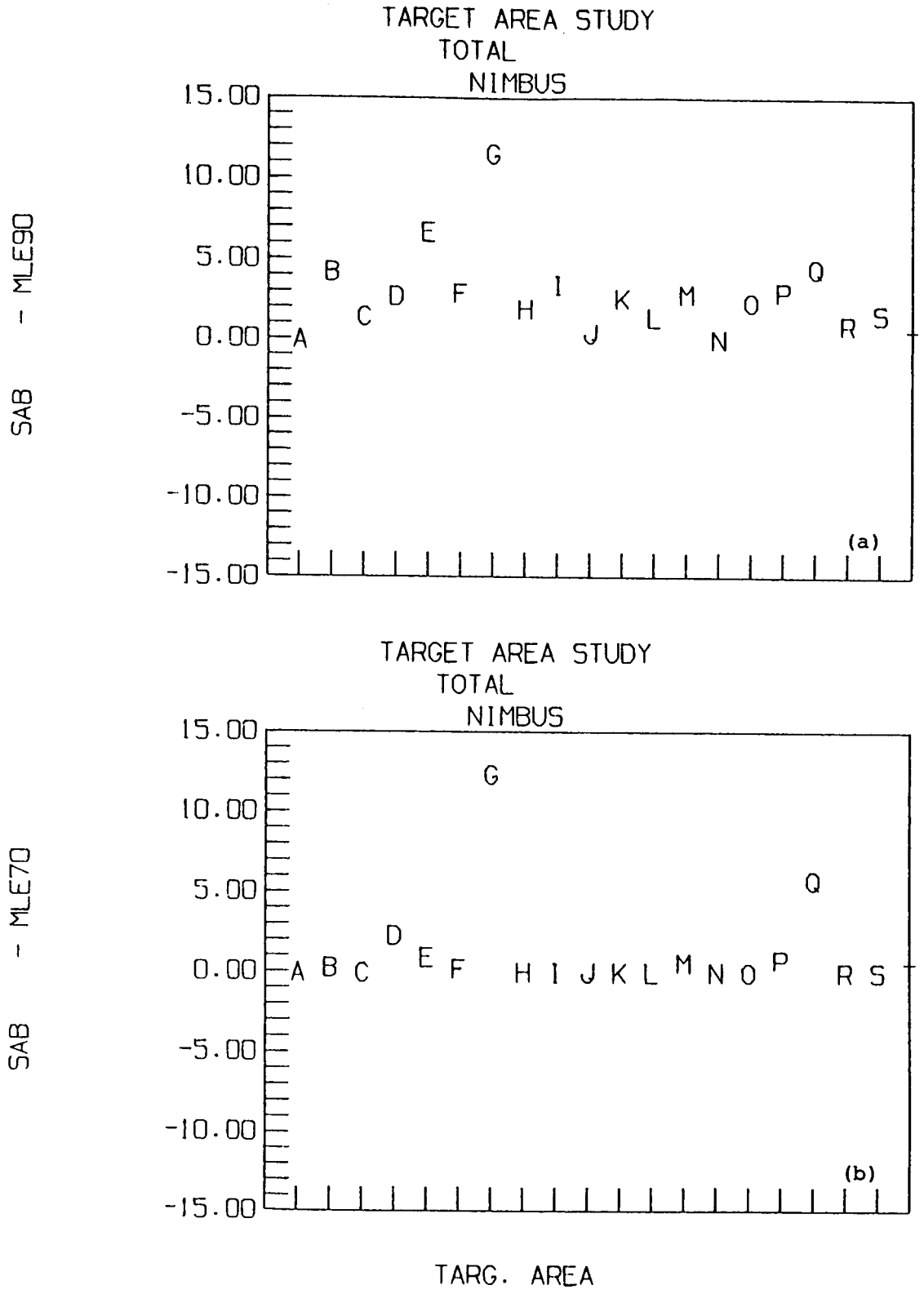

FIGURE 2.16 Monthly mean day, night average (total) longwave flux differences (W/m^2) for 20 chosen target area regions, A through T. These areas are identified as A, B, etc. on Fig. 2.12. (a) CLE 90° case; (b) CLE 70° case.

Daily mean values of the albedo with the associated standard deviation are shown in Figures 2.17, 2.18, 2.19 and 2.20. The surface characteristics for the TAs used in these figures are snow covered ocean (TA B), coastal land in South America (TA D), Desert (TA I), and land in continental U.S. (TA O), respectively. The values of monthly mean albedo are shown as lines across the figure for MLE 90 (9), for MLE 70 (7), and SAB (S). The day number is shown on the abscissa. Day 152 corresponds to June 1. TA 96, which is covered with snow over the ocean, did not have a value with the SAB method, due to inadequate sampling. Instantaneous albedo with the 90^{o} case is in excess of 0.70 while with 70^{o} cutoff it is closer to 0.60. The day-to-day variation in the albedo is appparent in the figure. The value of standard deviation on each day is also significant. Obviously, from a radiation standpoint, this is a very active TA. Figure 2.18 shows the instantaneous albedo for TA 585. The SAB value derived for this TA is slightly larger than the MLE value. The MLE 90 and MLE 70 (9, 7 cases) albedo values are almost identical. The effect of clouds is noticeable around day 157 and more prominently for day 167. The value of the standard deviation also increases on those days when clouds are present.

The case of the desert TA is shown in Figure 2.19. The albedo is close to 0.3 for all three cases (S, 9, 7, respectively). Meteorology and day number play no part in the albedo value. The standard deviation on any given day is very small and there is hardly any difference from day to day. Clouds do not appear in this region and no albedo changes take place. This TA, from a reflected flux point of view, is very inert. Figure 2.20 shows the daily variation of the albedo for a TA located in central U.S. The effect of clouds

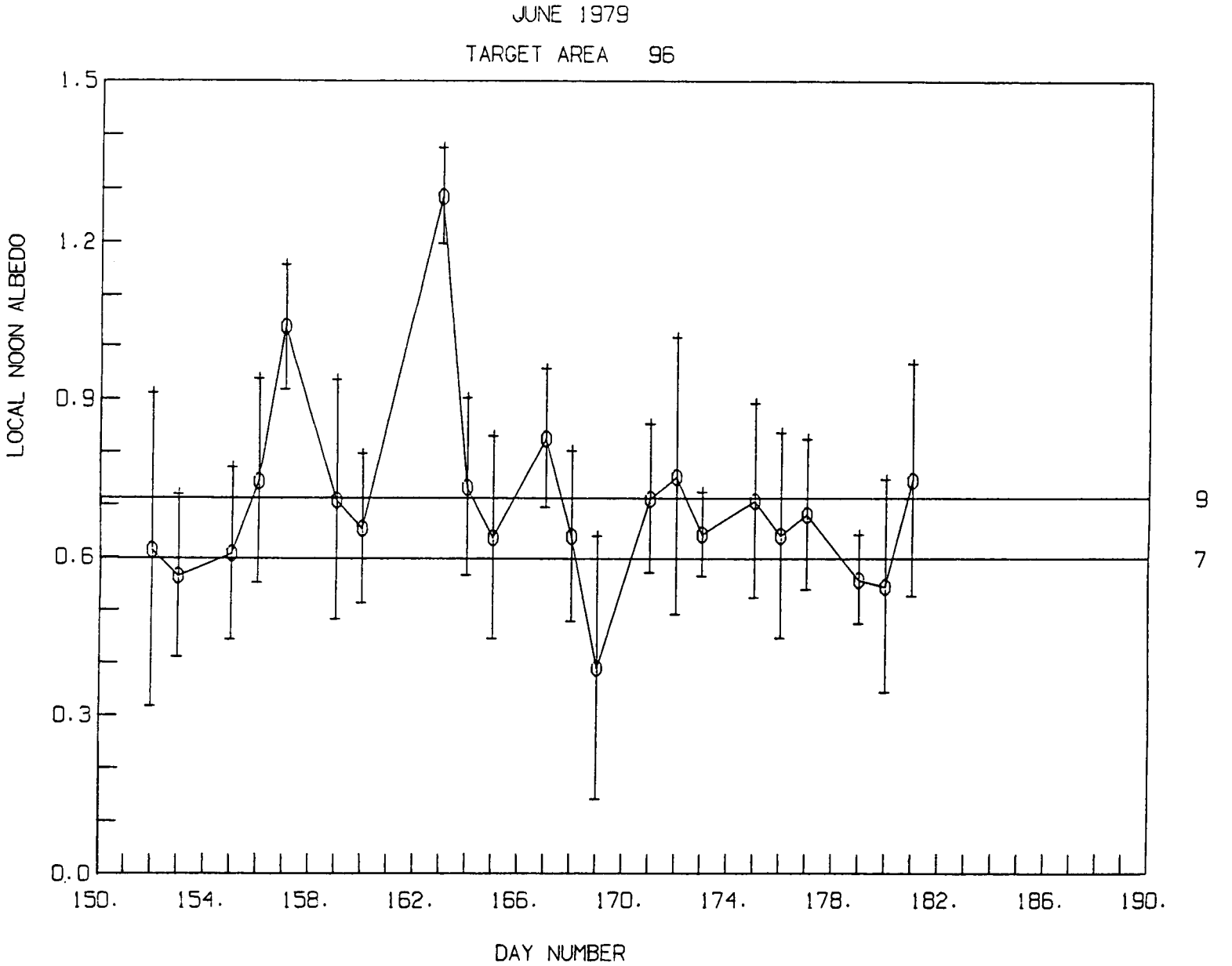

FIGURE 2.17 Instantaneous albedo statistics (daily mean and standard deviation) for TA 96 for each day of observation during June 1979. Monthly means are shown as horizontal lines denoted by 9 (for CLE 90° case) and by 7 (for CLE 70° case),

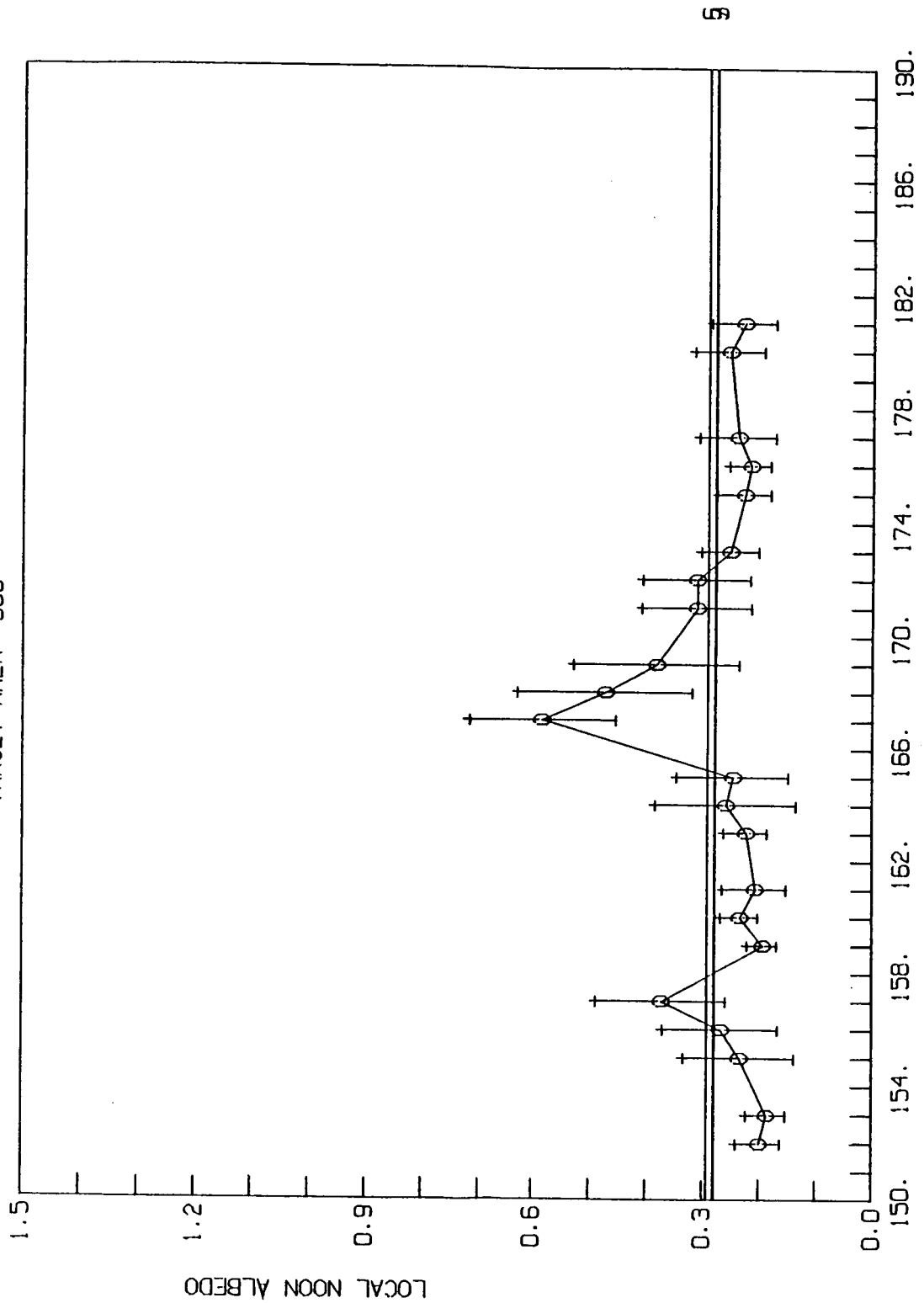

FIGURE 2.18 Instantaneous albedo statistics (daily mean and standard deviation) for TA 585 for each day of observation during June 1979. Monthly means are shown as horizontal lines denoted by 9 (for CLE 90° case), by 7 (for CLE 70° case), and by S (for SAB method).

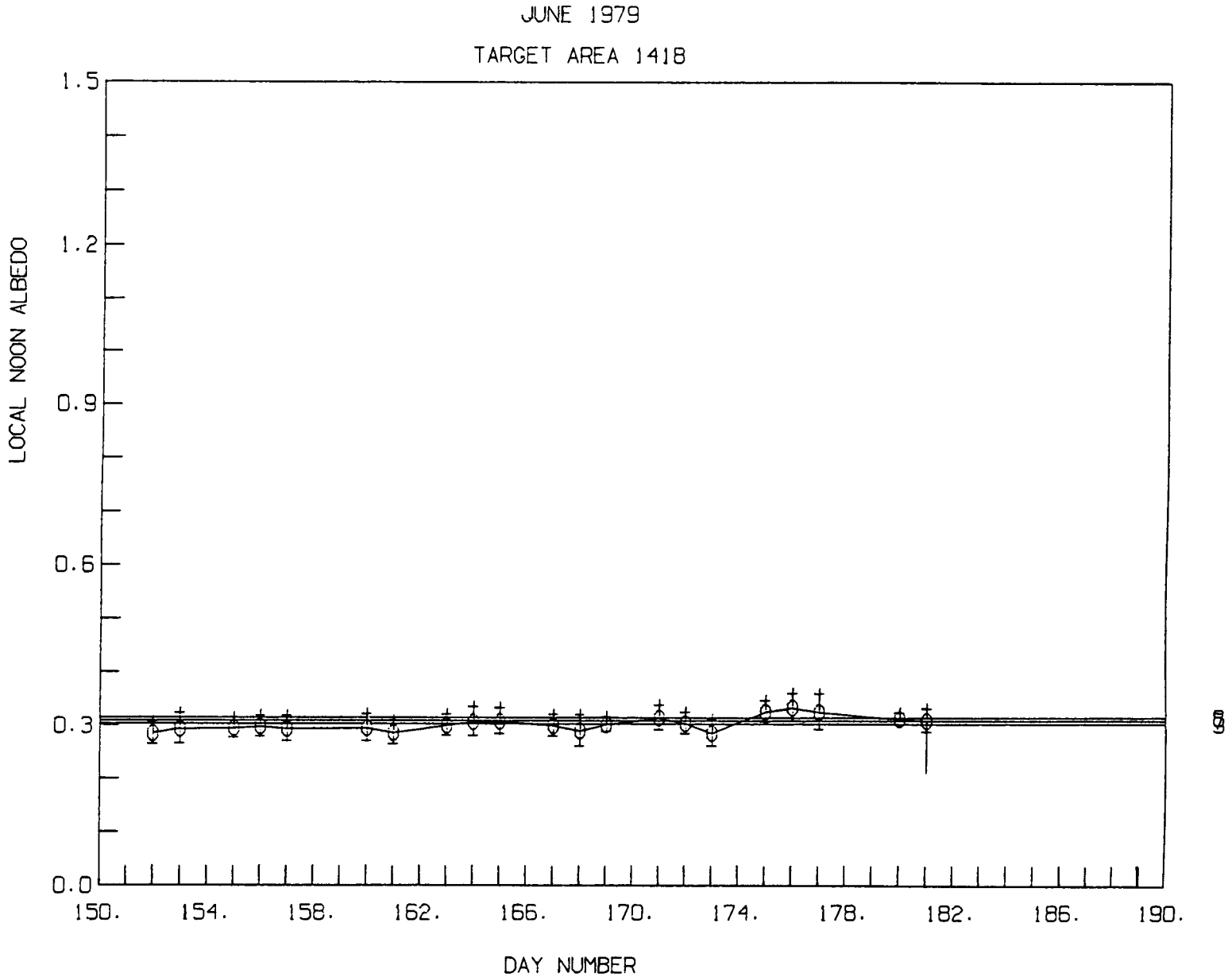

FIGURE 2.19 Instantaneous albedo statistics (daily mean and standard deviation) for TA 1418 for each day of observation during June 1979. Monthly means are shown as horizontal lines denoted by 9 (for CLE 90° case), by 7 (for CLE 70° case), and by S (for SAB method).

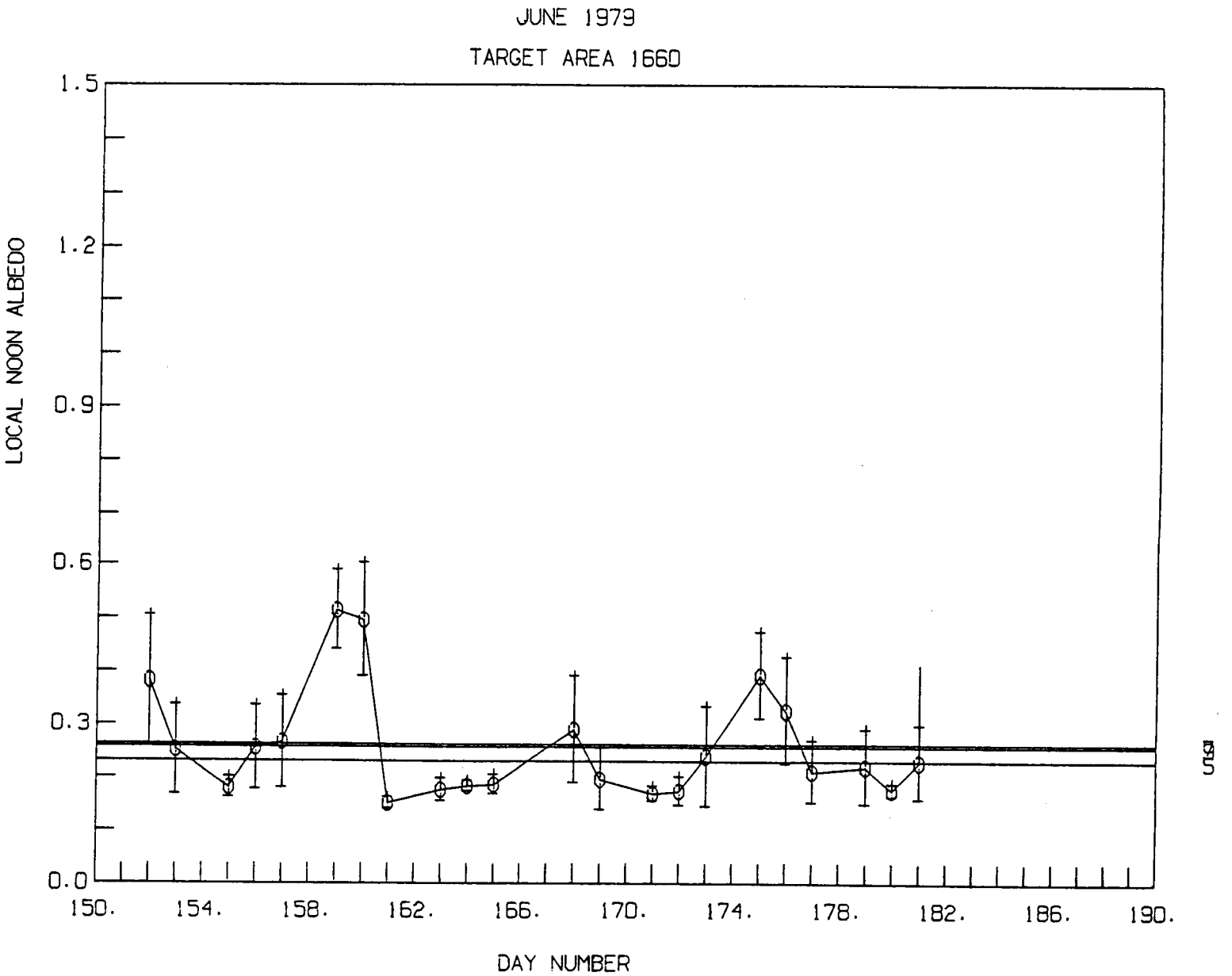

FIGURE 2.20 Instantaneous albedo statistics (daily mean and standard deviation) for TA 1660 for each day of observation during June 1979. Monthly means are shown as horizontal lines denoted by 9 (for CLE 90° case), by 7 (for CLE 70° case), and by S (for SAB method).

every few days is apparent from the albedo mean value. The SAB method gives an albedo value slightly smaller than the two MLE methods which are very nearly the same.

2.3 SCENE SELECTION ADEQUACY USING MLE

A clear validation of the scene selection accuracy using the MLE method is through comparison of the cloud identifications with other available cloud datasets. For this purpose, daily and monthly mean cloud amounts derived from the MLE method are compared with THIR cloud amounts in section 9. The total cloud amount is derived assuming that the mean cloud amounts in partly cloudy (5-50% cloud) and mostly cloudy (50-95% cloud) situations are 25% and 75% respectively, while the clear and cloudy cases are treated as 0% and 100% cloud. A different but an indirect way of the validation is possible by looking at the computed albedo values at different satellite zenith angle intervals. Earlier studies over the satellite zenith angle effect (Vemury et al., 1984) indicated an increase in albedo with satellite zenith angle, primarily due to increased cloud classification at those angles.

A scene identification reliability index is defined in Vemury (1985) to evaluate the degree to which the MLE method has been able to identify the scene correctly. The index provides the fraction of observations which are within one standard deviation (1 σ case) or two standard deviations (2 σ case) from the mean radiance values for the chosen scene. This index is thus a measure of how well the method performs under different conditions, for example, when longwave data only are used, or longwave and shortwave are used together, etc. This subsection will provide a brief analysis of these results.

2.3.1 Albedo Dependence on Satellite Zenith Angle

Biases in the computed reflected fluxes with satellite zenith angle using Nimbus-7 scanner data have been noted by Vemury et al. (1984) and Arking and Vemury (1984). Arking and Vemury divided the observatons into 4 groups depending upon the satellite zenith angle. These groups consist of $0\text{-}30^{\circ}$, $30^{\circ}\text{-}45^{\circ}$, $45^{\circ}\text{-}60^{\circ}$, and $60^{\circ}\text{-}90^{\circ}$. A similar breakdown of the instantaneous albedo into 4 groups is done in the present case for the values using the MLE method. The results for ocean TA 1121 are shown in Figure 2.21. The five different cases in the figure correspond to clear ocean, partly cloudy over ocean, mostly cloudy over ocean, overcast over ocean, and combined case. The four intervals in each of these cases correspond to angular intervals $0\text{-}30^{\circ}$, $30^{\circ}\text{-}45^{\circ}$, $45^{\circ}\text{-}60^{\circ}$, and $60^{\circ}\text{-}90^{\circ}$, denoted by 1, 2, 3,and 4. These results do not indicate albedo biases with satellite zenith angle interval. We interpret this to mean that the satellite zenith angle related biases do not appear with the MLE algorithm. One case of land and one case of desert are shown in Figures 2.22 and 2.23 respectively. These also support the above conclusion.

2.3.2 Scene Identification Reliability Index

The index is defined in Vemury (1985). The values of the index are computed for each of the 12 surfaces and are shown in four categories (also defined in Vemury, 1985) in Table 2.3. In the normal use of the longwave and shortwave together during daytime, 59.3% of the LW, SW observations on day

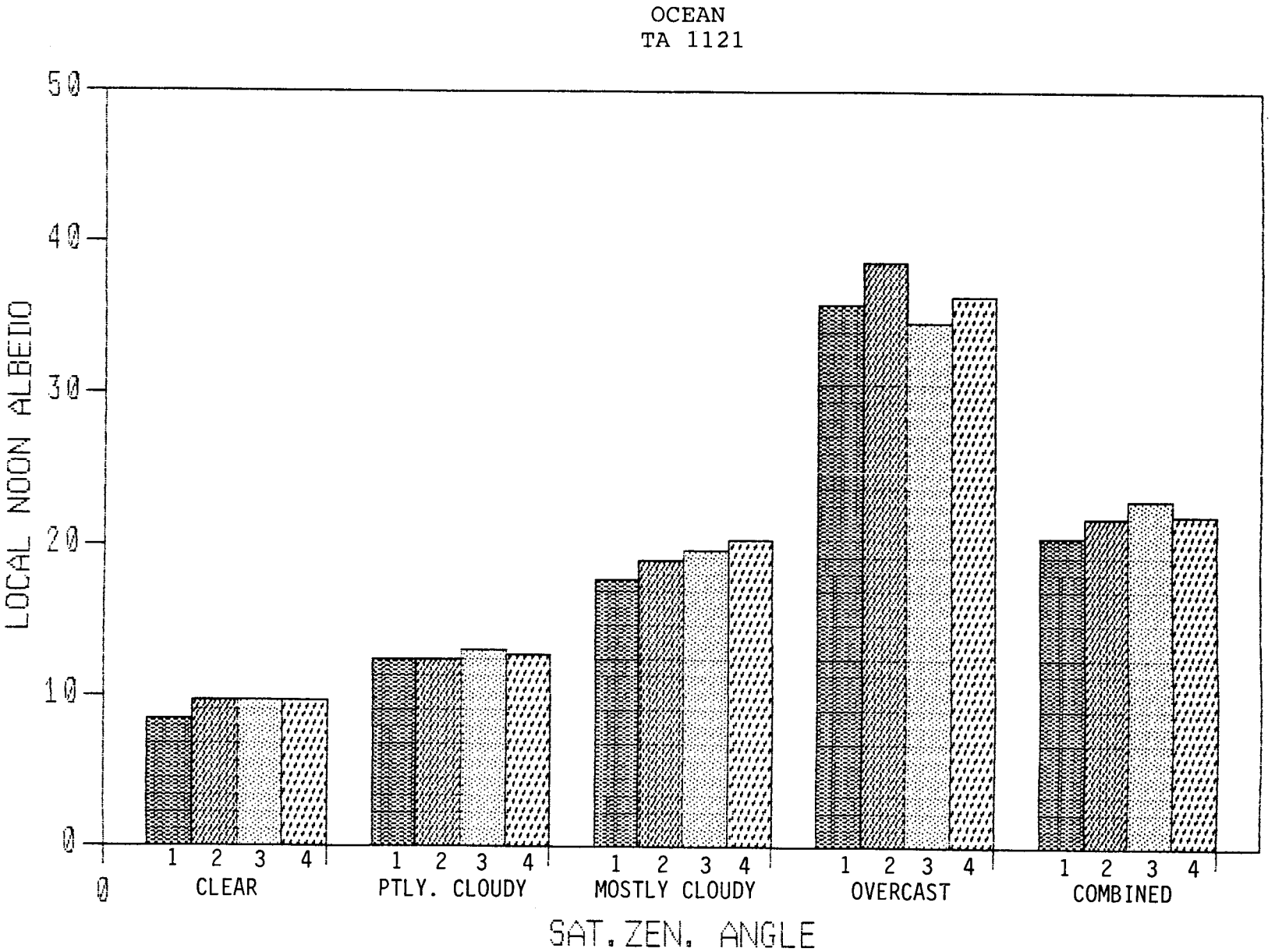

FIGURE 2.21 Dependence of instantaneous albedo for TA 1121 on the satellite zenith angle range (1: $0 < \theta \leq 30°$; 2: $30° < \theta \leq 45°$; 3: $45° < \theta \leq 60°$; 4: $60° < \theta \leq 90°$) for each of four cloud cover categories. The combined case is also shown.

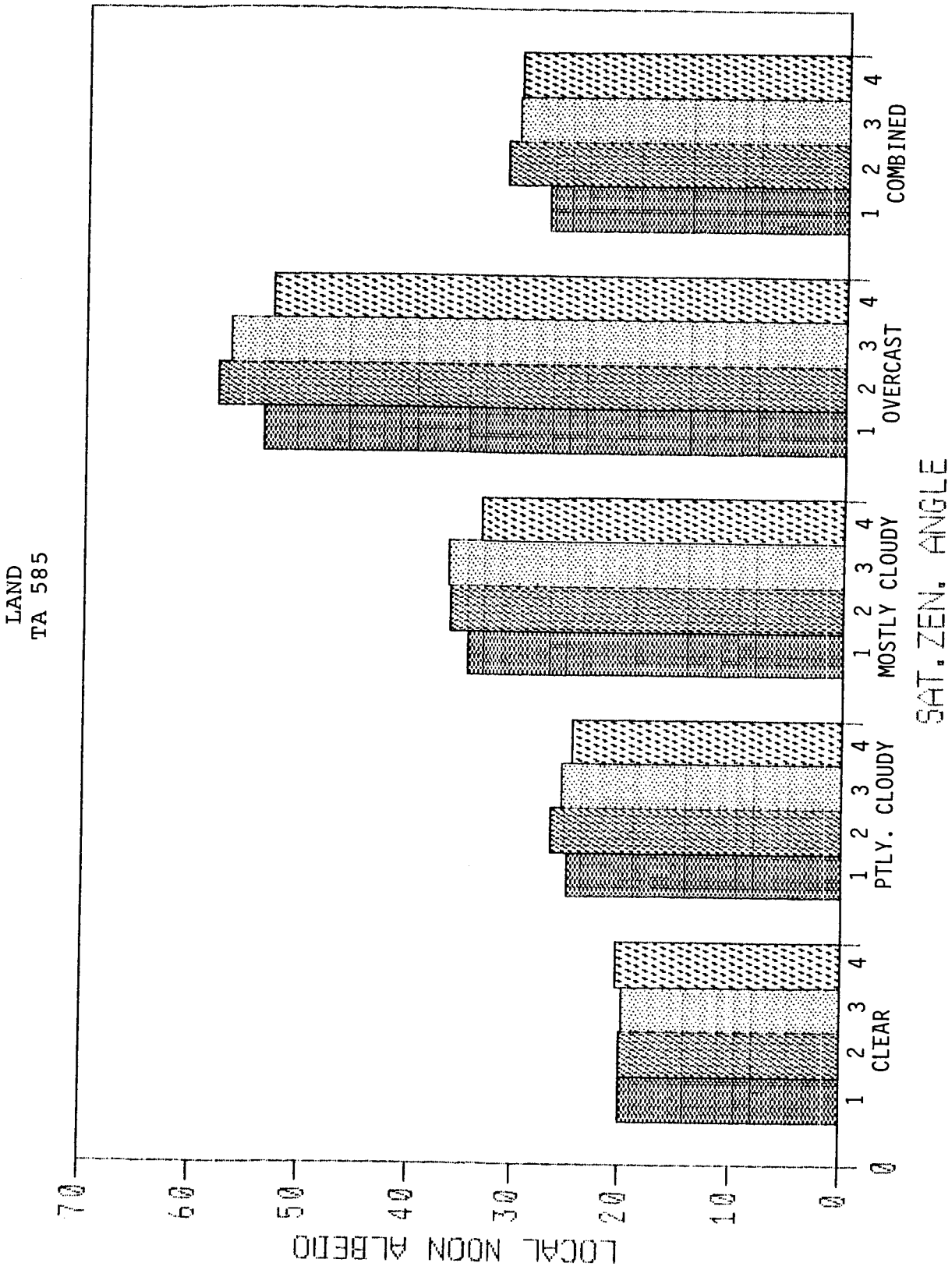

FIGURE 2.22 Dependence of instantaneous albedo for TA 585 on the satellite zenith angle range (1: $0 < \theta \leq 30°$; 2: $30° < \theta \leq 45°$; 3: $45° < \theta \leq 60°$; 4: $60° < \theta \leq 90°$) for each of four cloud cover categories. The combined case is also shown.

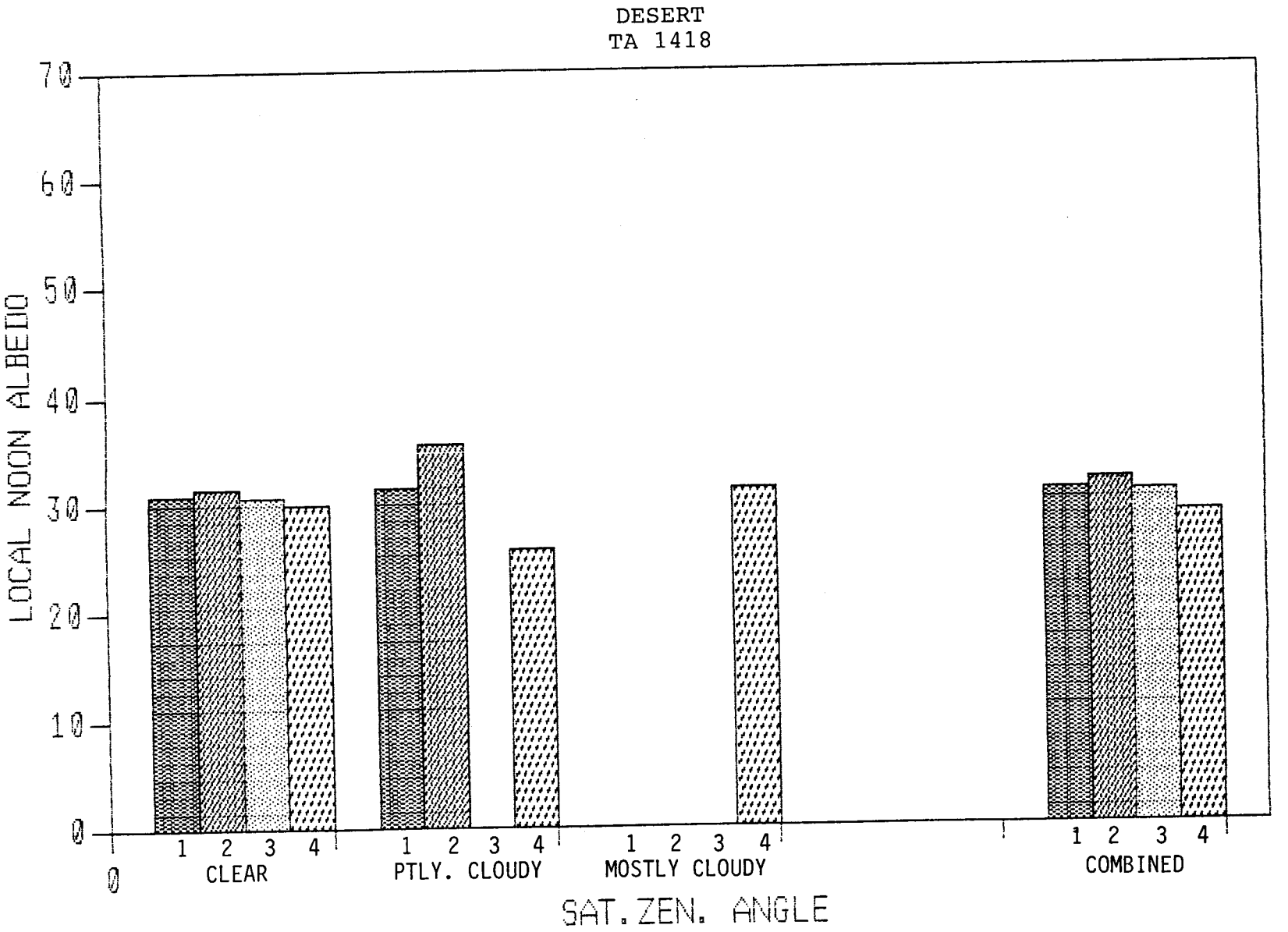

FIGURE 2.23 Dependence of instantaneous albedo for TA 1418 on the satellite zenith angle range (1: $0 < \theta \leq 30°$; 2: $30° < \theta \leq 45°$; 3: $45° < \theta \leq 60°$; 4: $60° < \theta \leq 90°$) for each of four cloud cover categories. The combined case is also shown.

TABLE 2.3 Scene identification reliability statistics using ERB-7 CLE models.

******** DAY 152 **********

	NCLA			NCLDAY			NCLNIT			NCSDAY		
	TOTAL	PRCNT .LT.1	PRCNT .LT.2	TOTAL	PRCNT .LT.1	PRCNT .LT.2	TOTAL	PRCNT .LT.1	PRCNT .LT.2	TOTAL	PRCNT .LT.1	PRCNT .LT.2
OCEAN	19298	0.6255	0.9578	25763	0.7397	0.9586	22970	0.8551	0.9744	19238	0.8955	0.9998
LAND	10907	0.6221	0.9697	13268	0.7343	0.9893	6120	0.9350	0.9954	10720	0.8857	0.9825
SNOW	7545	0.6467	0.9618	9104	0.8595	0.9986	29693	0.8921	0.9998	6436	0.7758	0.9699
DESERT	5035	0.4254	0.9676	6429	0.7121	0.9905	5062	0.6604	0.9176	5035	0.6107	0.9762
MIXED LAND/OCEAN	2162	0.6591	0.9695	2706	0.7480	0.9871	1451	0.9166	0.9883	2155	0.9086	0.9824
PARTLY CLOUDY/OCEAN	15914	0.6800	0.9929	22684	0.8316	0.9958	29260	0.9848	0.9999	15806	0.9015	0.9994
PARTLY CLOUDY/LAND	9303	0.7248	0.9920	13403	0.9287	1.0000	11222	0.9942	1.0000	9022	0.8202	0.9936
PARTLY CLOUDY/LAND,OCEAN MIX	1715	0.7417	0.9953	2512	0.8726	0.9976	2169	0.9991	1.0000	1694	0.9091	0.9988
MOSTLY CLOUDY/OCEAN	26044	0.5678	0.9756	32806	0.7717	0.9830	29877	0.8956	0.9995	25837	0.7716	0.9973
MOSTLY CLOUDY/LAND	11380	0.6435	0.9612	14484	0.8310	0.9783	6839	0.9649	0.9991	10899	0.8332	0.9908
MOSTLY CLOUDY/LAND,OCEAN MIX	2065	0.6145	0.9521	2767	0.7824	0.9675	1297	0.9414	1.0000	2000	0.8570	0.9980
COMPLETELY CLOUDY	68249	0.5429	0.9356	88386	0.7462	0.9562	83986	0.7174	0.9568	66755	0.7377	0.9801
	179617	0.5933	0.9586	234312	0.7776	0.9733	229946	0.8415	0.9795	175597	0.7968	0.9879

******** DAY 153 **********

	NCLA			NCLDAY			NCLNIT			NCSDAY		
	TOTAL	PRCNT .LT.1	PRCNT .LT.2	TOTAL	PRCNT .LT.1	PRCNT .LT.2	TOTAL	PRCNT .LT.1	PRCNT .LT.2	TOTAL	PRCNT .LT.1	PRCNT .LT.2
OCEAN	19683	0.6417	0.9580	25689	0.7515	0.9614	22474	0.8679	0.9802	19663	0.9015	0.9994
LAND	9795	0.6384	0.9776	12004	0.7412	0.9912	9142	0.9053	0.9937	9583	0.9056	0.9871
SNOW	7914	0.6639	0.9659	9197	0.8681	0.9986	27394	0.9291	0.9996	6756	0.7758	0.9741
DESERT	4695	0.4019	0.9627	6041	0.7297	0.9954	5161	0.6350	0.9337	4695	0.5789	0.9659
MIXED LAND/OCEAN	1933	0.6565	0.9824	2342	0.7494	0.9902	1721	0.9256	0.9954	1921	0.9099	0.9901
PARTLY CLOUDY/OCEAN	15119	0.6963	0.9933	21605	0.8354	0.9966	28458	0.9859	1.0000	15029	0.9180	0.9989
PARTLY CLOUDY/LAND	8540	0.7123	0.9930	12306	0.9312	0.9998	11904	0.9922	0.9999	8211	0.8088	0.9950
PARTLY CLOUDY/LAND,OCEAN MIX	1877	0.7342	0.9936	2603	0.8682	0.9977	2592	0.9981	1.0000	1850	0.8924	0.9978
MOSTLY CLOUDY/OCEAN	21918	0.5550	0.9786	28163	0.7761	0.9860	30113	0.8973	0.9999	21754	0.7520	0.9969
MOSTLY CLOUDY/LAND	10610	0.6559	0.9616	13461	0.8367	0.9762	6942	0.9569	0.9994	10213	0.8333	0.9951
MOSTLY CLOUDY/LAND,OCEAN MIX	2023	0.6683	0.9684	2567	0.8111	0.9805	1559	0.9416	1.0000	1950	0.8687	0.9974
COMPLETELY CLOUDY	62252	0.5351	0.9330	81083	0.7245	0.9519	82518	0.7290	0.9721	61083	0.7505	0.9790
	166359	0.5955	0.9591	217061	0.7743	0.9728	229978	0.8516	0.9862	162708	0.8027	0.9880

*NOTE: Percent in this table implies fraction of observations. This fraction represents the fractions of observations for which the measured radiance differs from the computed radiance for the scene type by $\pm 1\sigma$ in .LT.1 case and by $\pm 2\sigma$ for the .LT.2 case.

152 are within one standard deviation ($\pm 1\ \sigma$) of the means when the whole globe is considered. In the case of $\pm 2\ \sigma$, the number increases to 95.9%. If shortwave observations only are considered, percentage of observations within $\pm\ 1\ \sigma$ and $\pm\ 2\ \sigma$ are 79.7% and 98.8%, respectively. The PRCNT values noted in the table are really fractions and not percentages. The values for day 153 are also shown in the table and the general pattern of scene categorization is the same from day to day. For the individual scene types for a given day, the values are shown in each category in the table and are also shown in the histograms in Figures 2.24 and 2.25 for the $1\ \sigma$ and $2\ \sigma$ cases respectively. At the $1\ \sigma$ level, most surfaces indicate values at the 60% level except for the desert case. At the $2\ \sigma$ level (Fig. 2.25), the fractions are close to 1.0 in all cases, indicating that more than 95% of the observations in each category are within $2\ \sigma$ of the respective means.

2.4 CONCLUSIONS

Several improvements in the datasets and algorithms are made in the present study. Most of the analyses on the radiation budget parameters (section 2.1), target area related studies (section 2.2), and scene selection statistics (2.3) are repeated with the "improved baseline" results. The new results improve and confirm the conclusions of the earlier study. The results in this study are based upon the "CLE" angular models.

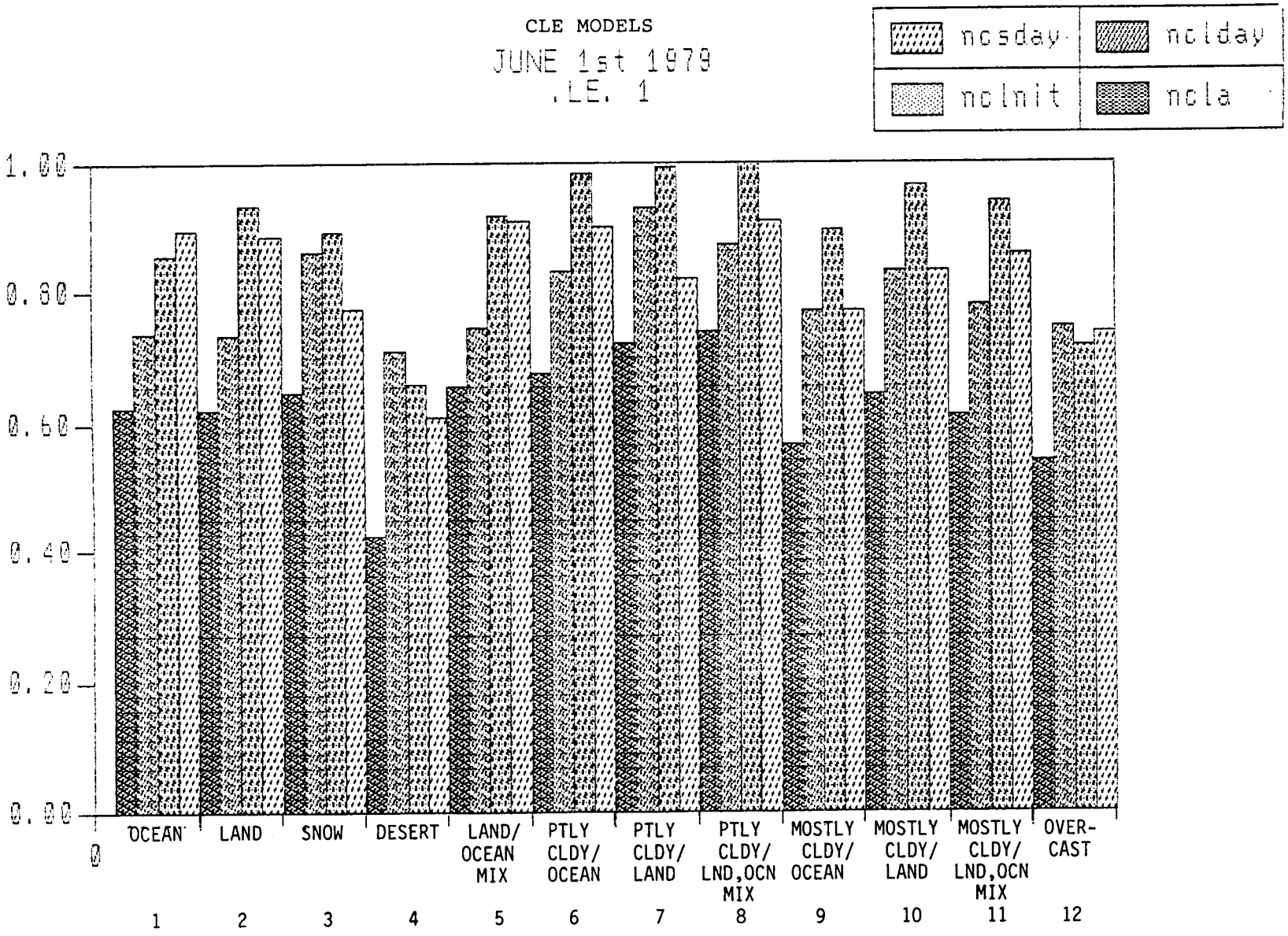

FIGURE 2.24 Scene identification reliability statistics for June 1, 1979. The fractions represent the fractions of observations for the scene type which differ from the bin means by less than or equal to 1 σ (.LE.1 in the title). Fractions under NCLA are computed using both shortwave and longwave radiances. NCLDAY and NCSDAY represent fractions of LW and SW observations during daytime, which differ from bin means by less than or equal to 1 σ. NCLNIT represents the fraction of LW observations at night.

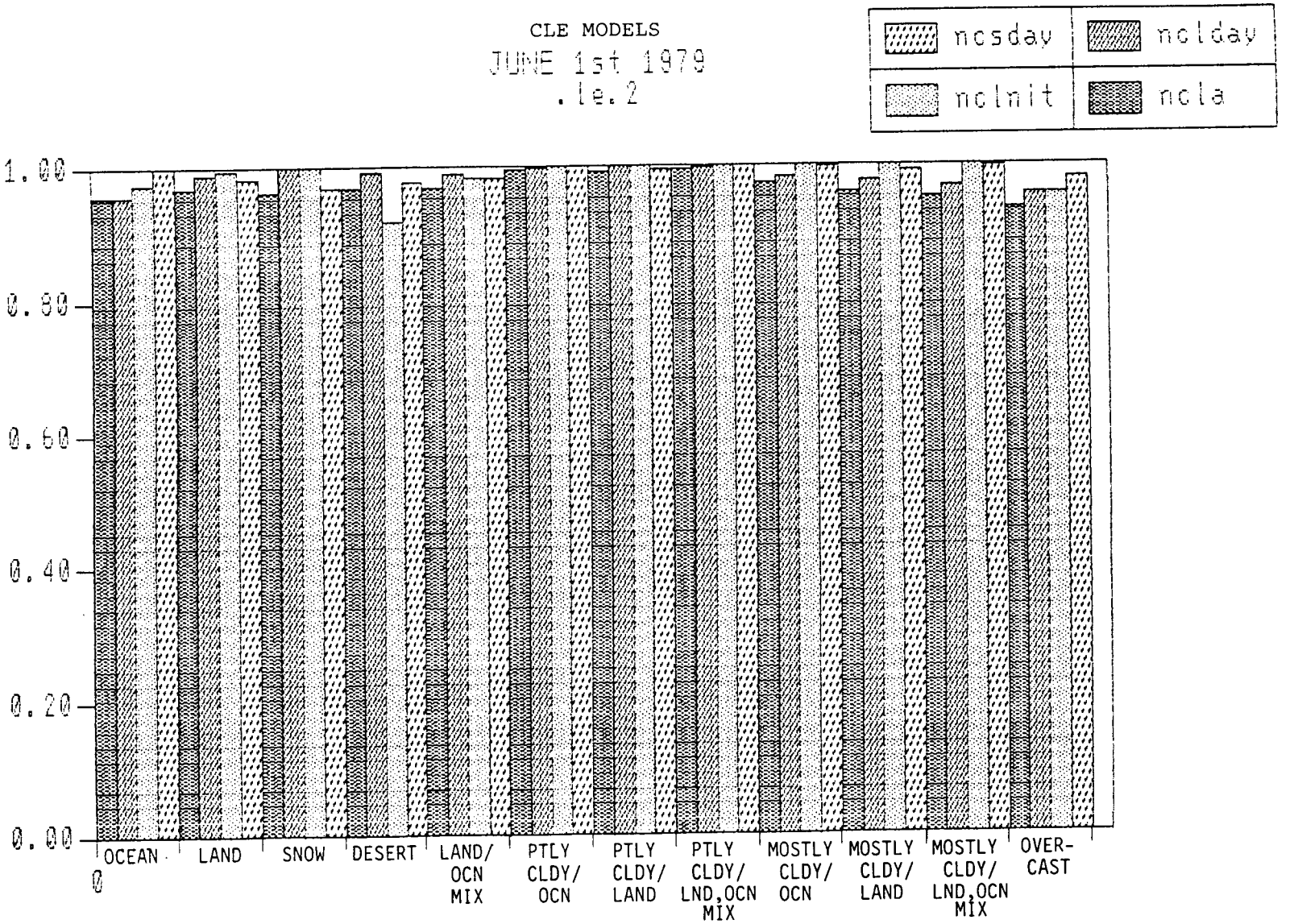

FIGURE 2.25 Scene identification reliability statistics for June 1, 1979. The fractions represent the fractions of observations for the scene type which differ from the bin means by less than or equal to 2 σ (.LE.2 in the title). Fractions under NCLA are computed using both shortwave and longwave radiances. NCLDAY and NCSDAY represent fractions of LW and SW observations during daytime, which differ from bin means by less than or equal to 2 σ NCLNIT represents the fraction of LW observations at night.

SECTION 3

EFFECT OF GOES MODELS

Angular distribution models play a very important role in the estimation of the radiation budget quantities. They are necessary in the scene selection process using the MLE method and they are also used to convert the measured radiances to instantaneous reflected fluxes. The models derived from Nimbus-7 ERB referred to as ERB-7 models are primarily for noontime conditions. Since two of the three ERBE instruments will be orbiting at times different from noon, it is important to know the effect on the computed reflected flux using bidirectional models derived from the geostationary GOES satellite. The results in this section will deal with the use of bidirectional models derived from GOES.

3.1 EFFECT ON BUDGET PARAMETERS

Of primary interest in this study is the effect of GOES models on the instantaneous albedo and day and night longwave flux values. To evaluate the effect of truncation on these parameters, the radiance values obtained at satellite zenith angle greater than a specified zenith angle θ_c are not considered in the computation. A value of $\theta_c = 90^o$ would correspond to the use of the entire sample. Values of θ_c up to 40^o are used in steps of 10^o each time. At these cutoff angles, global mean values of the instantaneous albedo, daytime and nighttime longwave fluxes are obtained and are presented in Table 3.1. These results are for June 1, 1979 or day 152 of 1979.

TABLE 3.1 Use of GOES Models (Day 152, Sat. Zen. Cutoff Study)

	90°	80°	70°	60°	50°	40°
Inst. Albedo	.2865	.2844	.2798	.2723	.2677	.2577
Day (LW)	237.7	239.9	242.0	242.6	243.3	243.7
Night (LW)	227.5	230.4	232.3	232.5	232.5	231.8

TABLE 3.2a. Effect of Satellite Zenith Angle Cutoff
Using Nimbus-7 Bidirectional Models (Vemury, 1985)

MLE

Daily Global Averages
June 1, 1979

Description	NIMBUS 90°	NIMBUS 80°	NIMBUS 70°	NIMBUS 60°	NIMBUS 50°	NIMBUS 40°
Inst. Albedo	0.2812	0.2802	0.2787	0.2727	0.2693	0.266
LW Flux (day)	236.7007	239.5793	241.5121	242.1980	242.7481	243.595
LW Flux (night)	228.1264	231.0569	232.5696	232.6121	232.6225	231.838
Total	230.5099	233.3534	235.3143	235.7682	236.3256	236.467

TABLE 3.2b. Number of TAs Sampled at Each Cutoff Angle.
The maximum number over the globe is 2070 TAs.
(Nimbus-7 Models)

SAMPLE SIZES

Number of TAs Used — Max. Number = 2070 TAs

Description	NIMBUS 90°	NIMBUS 70°	NIMBUS 60°	NIMBUS 50°	NIMBUS 40°
Inst. Albedo	1849	1828	1717	1507	1204
LW Flux (day)	1849	1828	1717	1507	1201
LW Flux (night)	1781	1741	1583	1345	1088
LW Flux (Total)	2070	2070	2040	1919	1672

TABLE 3.3 Use of GOES Models

SAMPLE SIZES

	90°	80°	70°	60°	50°	40°
Ins Albedo	1854	1850	1828	1717	1507	1201
Day LW Flux	1864	1854	1836	1767	1552	1230
Night LW Flux	1913	1884	1846	1709	1488	1194

Results of a similar study using ERB-7 models are discussed in Vemury (1985) and shown in Table 3.2a. There are some differences between the inputs for the two studies, but the overall results indicate a similar trend. The amount of decrease in the instantaneous albedo (28.65 at 90^{o} to 25.77 at 40^{o}) using GOES models is almost double the corresponding decrease (28.1 to 26.7) using ERB-7 models. This could imply that the ERB-7 models are better (more appropriate) in reducing the effect of scene identification deficiencies at large zenith angles. The daytime longwave fluxes show an increase of 4.6 W/m^2 between 90^{o} and 40^{o} cases using GOES models. With the ERB-7 models, this increase for the day-time is 6.8 W/m^2. The corresponding night time values are 4.3 W/m^2 with GOES models and 3.7 m^2 with ERB-7 models.

The numbers of TAs that contributed to the global mean in each of the above cases are shown in Table 3.3. Similar to the ERB-7 case (Table 3.2b), the drop in the number of TAs contributing to the global mean is significant at lower zenith angle thresholds. In the case of instantaneous albedo, the number of TAs providing the global mean is 1201 out of a possible 2070 for the entire globe. Similar decrease in sampling occurs with day and night longwave fluxes also.

3.2 EFFECT ON CLOUD AMOUNT

Effect of the models on the choice of scene from observed radiances at different cutoff angles is presented in Tables 3.4a, 3.4b, and 3.4c. Hemispherical and global cloud amounts, as chosen by the scene identification process, are shown for the daytime and nighttime observations in Tables 3.4a and 3.4b respectively, and in Table 3.4c for the day-night average cloud

TABLE 3.4a. Cloud Hemispherical Averages Using GOES Models.

Daytime June 1, 1979

	Cutoff Angle					
Description	90°	80°	70°	60°	50°	40°
Northern	58.19	56.64	55.59	55.18	54.06	54.17
Southern	52.35	49.57	46.44	45.01	44.99	44.39
Global	55.39	53.26	51.21	50.33	49.78	49.64

TABLE 3.4b. Cloud Hemispherical Averages Using GOES Models.

Nighttime June 1, 1979

	Cutoff Angle					
Description	90°	80°	70°	60°	50°	40°
Northern	65.63	63.40	62.81	64.74	65.81	67.35
Southern	52.09	49.09	47.89	49.34	48.85	49.64
Global	58.67	56.02	55.13	56.83	57.04	58.03

TABLE 3.4c. Cloud Hemispherical Averages Using GOES Models.

Day, Night Average June 1, 1979

	Cutoff Angle					
Description	90°	80°	70°	60°	50°	40°
Northern	60.93	59.37	58.44	58.22	58.20	58.59
Southern	51.81	49.47	47.29	47.00	46.68	47.16
Global	56.37	54.22	52.87	52.91	52.45	52.87

amount. For the daytime for example, the decrease in cloud classification for the northern hemisphere is about 4% while the drop in the southern hemisphere is almost 8% at 40^{o} cutoff angle. Nighttime results show a different trend; in both hemispheres the cloud amount values drop to a minimum around 70^{o} cutoff angle and increase again at smaller zenith angles. Any conclusions on the basis of the nighttime results are not appropriate. The primary reason is that no separate nighttime longwave models exist in the algorithms and the scene selection at night depends only on the longwave radiances. Table 3.4c presents the cloud amount values for the day-night average at the same cutoff angles. The results indicate that there is a slight overall increase in the cloud classification at larger satellite zenith angles.

3.3 CONCLUSION

The instantaneous albedo computed with GOES models shows greater sensitivity to cutoff angle compared with ERB-7 models. Longwave fluxes (day/night) are sensitive nearly to the same degree.

SECTION 4

EFFECT OF CORRELATION COEFFICIENTS

The scene selection using the MLE method is dependent upon the sample means and standard deviations of both the reflected and emitted radiance as well as on the correlation coefficient between the shortwave and longwave radiances in the sample. Both the shortwave and longwave radiance samples are assumed to follow normal distributions. The correlation coefficient varies from scene to scene and from angle to angle. The objective of the present analysis is to evaluate the sensitivity of scene selection algorithm and the derived radiation budget parameters to the use of a correlation coefficient of zero.

4.1 GLOBAL AVERAGES WITH COR = 0

In the portion of the algorithm dealing with scene identification, the value of the correlation coefficient (COR) is set equal to zero and the values of the radiation budget quantities are computed. The values derived thus are shown in Table 4.1, along with the corresponding values for the nominal case referred to here as MLE. The computations were performed for three different days in June, viz., June 1, June 10, and June 20, 1979. In all cases, the difference in the instantaneous global albedo is of the order of 0.01. The longwave fluxes also show extremely close agreement.

Results of the comparison for the three days for observations with satellite zenith angle less than or equal to 70° are shown in Table 4.2. At the global level, the means tend to show extremely good agreement.

TABLE 4.1 Effect of Using Zero Correlation Coefficient in the MLE Method on the Global Mean Values

	Satellite Zenith Angle ≤ 90°					
	June 1, 1979		June 10, 1979		June 20, 1979	
	MLE	COR = 0	MLE	COR = 0	MLE	COR = 0
Inst. Albedo	0.2818	0.2819	0.2802	0.2801	0.2860	0.2860
Daytime LW Flux	238.0838	238.0747	240.7887	240.7839	239.9365	239.9353
Nighttime LW Flux	222.9440	222.9448	224.9933	224.9934	222.4142	224.4150
Total LW Flux	230.3005	230.2961	233.0801	233.0786	232.9910	232.9911

TABLE 4.2 Effect of Using Zero Correlation Coefficient in the MLE Method on the Global Mean Values

	Satellite Zenith Angle ≤ 70°					
	June 1, 1979		June 10, 1979		June 20, 1979	
	MLE	COR = 0	MLE	COR = 0	MLE	COR = 0
Ins. Albedo	0.2787	0.2786	0.2768	0.2766	0.2827	0.2826
Daytime LW Flux	243.1234	243.1288	245.8293	245.8348	245.1041	245.1044
Nighttime LW Flux	227.7964	227.7965	228.9910	228.9908	228.4153	228.4149
Total LW Flux	235.3695	235.3691	237.6886	237.6912	237.5795	237.5800

4.2 TARGET AREA AND ZONAL MEAN VALUES

The radiation budget parameters for all the target areas (TAs) for the case of COR = 0 are compared with the nominal case and the resulting linear regression relationships are computed. Table 4.3 presents parameters of the regression derived from the results for the satellite zenith angle cutoff case of 90^{o} and Table 4.4 shows the same for the cutoff case of 70^{o}. A and B in the table are the intercept and the gradient and R is the correlation coefficient. In all cases, the value of R is 1.0, indicating perfect correlation between the results obtained with COR = 0.0 in the algorithm and the nominal results. The intercepts in the case of longwave flux comparison are non-zero but are extremely small. For the nighttime, for which the correlation coefficient plays no part at all, the difference is due to the way the scene selection and flux computations are performed. The scene selection algorithm provided by NASA/LaRC treats all observations with solar zenith angle greater than 90^{o} as nighttime observations. The flux computation procedure which is part of the Nimbus-7 ERB algorithm uses a value of 88^{o} for the day-night distinction. Thus the nighttime differences in the intercept are generic to the code differences and are not therefore real.

Also shown in the tables 4.3 and 4.4 are the global mean RMS differences between the two cases computed using all target area means. At 90^{o} satellite zenith angle cutoff, the RMS deviation of the instantaneous global mean albedo is 0.16 on June 1, 1979. This difference drops to 0.14 when the zenith angle cutoff is set at 70^{o}. The RMS differences at nighttime are different from zero due to the algorithms discussed in the previous paragraph.

TABLE 4.3 Coefficients of Linear Regressionand Correlation Coefficient (R) Between TA Means Using Zero Correlation Case and Normal MLE Method. A is Intercept; B is Gradient. All observations are used.

Description	June 1, 1979 Sat. Zen. Angle ⩽ 90°				June 10, 1979 Sat. Zen. Angle ⩽ 90°				June 20, 1979 Sat. Zen. Angle ⩽ 90°			
	A	B	R	RMS Diff	A	B	R	RMS Diff	A	B	R	RMS Diff
Ins. Albedo	0.0	1.000	1.000	0.0016	0.0	0.999	1.0	0.0018	0.000	0.999	1.000	0.0018
LW Flux (Day)	-0.037	1.000	1.000	0.0941	-0.031	1.000	1.000	0.112	-0.009	1.000	1.000	0.1081
LW Flux (Night)	-0.002	1.000	1.000	0.0291	-0.005	1.000	1.000	0.0389	-0.001	1.000	1.000	0.0360
LW Flux (Total)	-0.018	1.000	1.000	0.0543	-0.020	1.000	1.000	0.0583	-0.018	1.000	1.000	0.0574

TABLE 4.4 Coefficients of Linear Regression (A,B) and Correlation Coefficient (R) Between TA Means Using Zero Correlation Case and Normal MLE Method. A is intercept; B is gradient. Observations with Satellite Zenith Angle ⩽ 70° only are kept.

Desc.	June 1, 1979 Sat. Zen. Angle ⩽ 70°				June 10, 1979 Sat. Zen. Angle ⩽ 70°				June 20, 1979 Sat. Zen. Angle ⩽ 70°			
	A	B	R	RMS Diff	A	B	R	RMS Diff	A	B	R	RMS Diff
Ins. Albedo	0.000	1.000	1.000	0.0014	0.000	0.999	1.000	0.0016	0.000	0.999	1.000	0.0018
LW Flux (Day)	0.004	1.000	1.000	0.0660	-0.015	1.000	1.000	0.0901	-0.014	1.000	1.000	0.0777
LW Flux (Night)	0.000	1.000	1.000	0.0121	0.002	1.000	1.000	0.0202	-0.004	1.000	1.000	0.0209
LW Flux (Total)	-0.002	1.000	1.000	0.0391	-0.0018	1.000	1.000	0.0508	-0.007	1.000	1.000	0.0391

The zonal means are compared for the 90^{o} and 70^{o} cutoff cases separately. Differences in the zonally averaged instantaneous albedoes are shown in Figure 4.1a,b for the 90^{o} and 70^{o} case respectively. The daytime, nighttime, and total (day, night mean) longwave flux differences are shown in Figures 4.2, 4.3 and 4.4. At both the 90^{o} and 70^{o} cutoff angles, the effect of COR = 0 is quite insignificant. The results are similar for the June 10 and June 20 cases.

4.3 CONCLUSIONS

Analysis of the results of this study indicate that accurate knowledge of the correlation coefficients between the shortwave and longwave radiances is not an important factor in the final radiation budget parameter estimation at any of the spatial scales of interest.

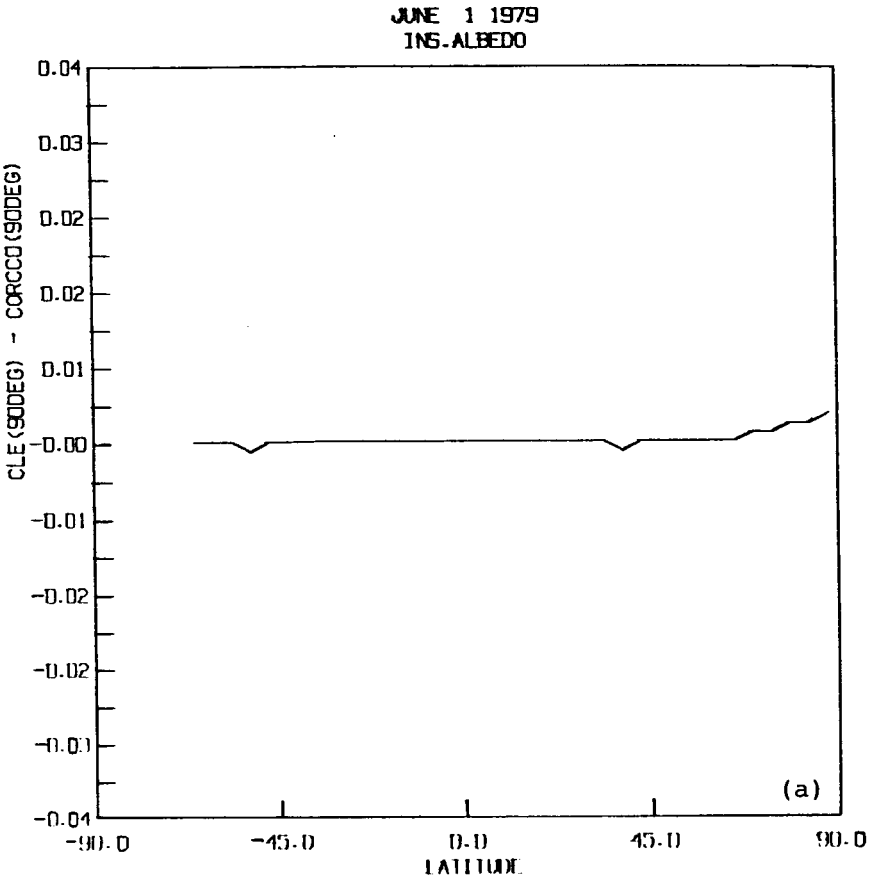

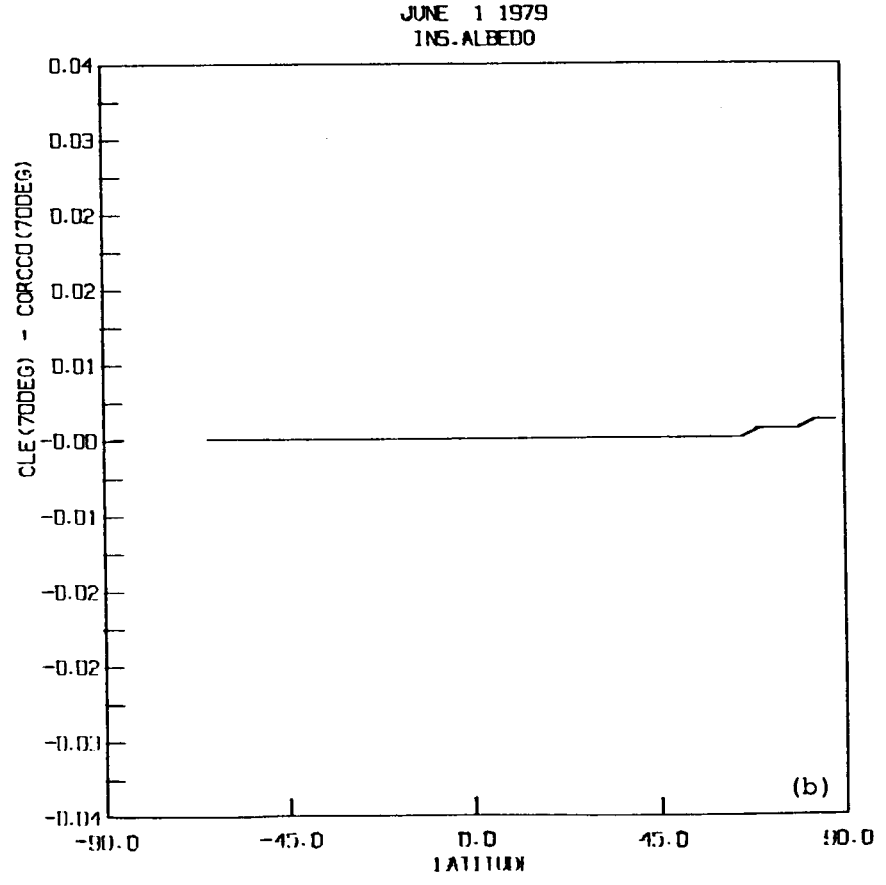

FIGURE 4.1 Instantaneous albedo differences between the normal MLE and COR = 0 cases. (a) Observations up to 90° are kept; (b) observations up to 70° only are kept.

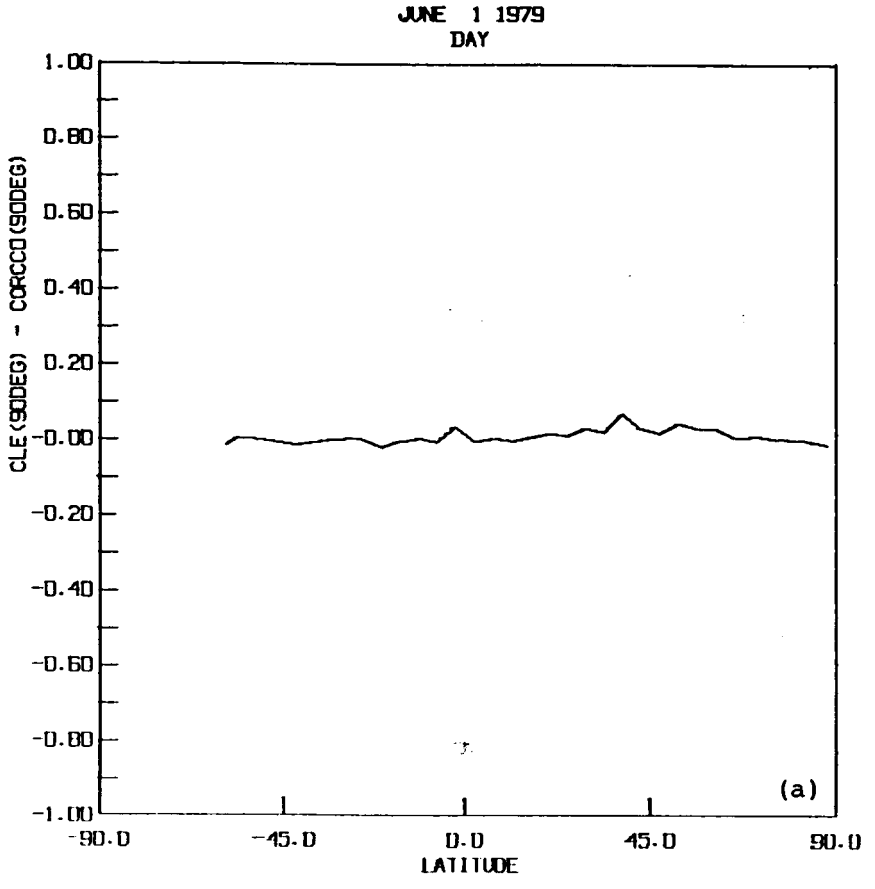

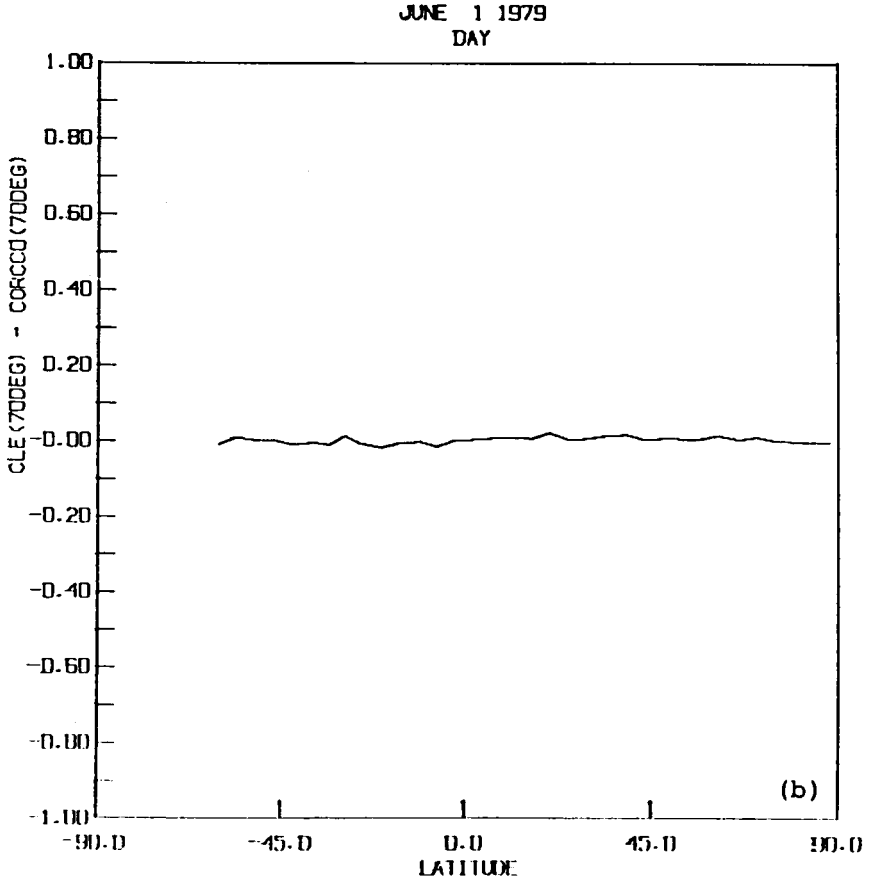

FIGURE 4.2 Daytime longwave flux differences between the normal MLE and COR = 0 cases (units: W/m^2). (a) Observations up to 90°; (b) observations up to 70°.

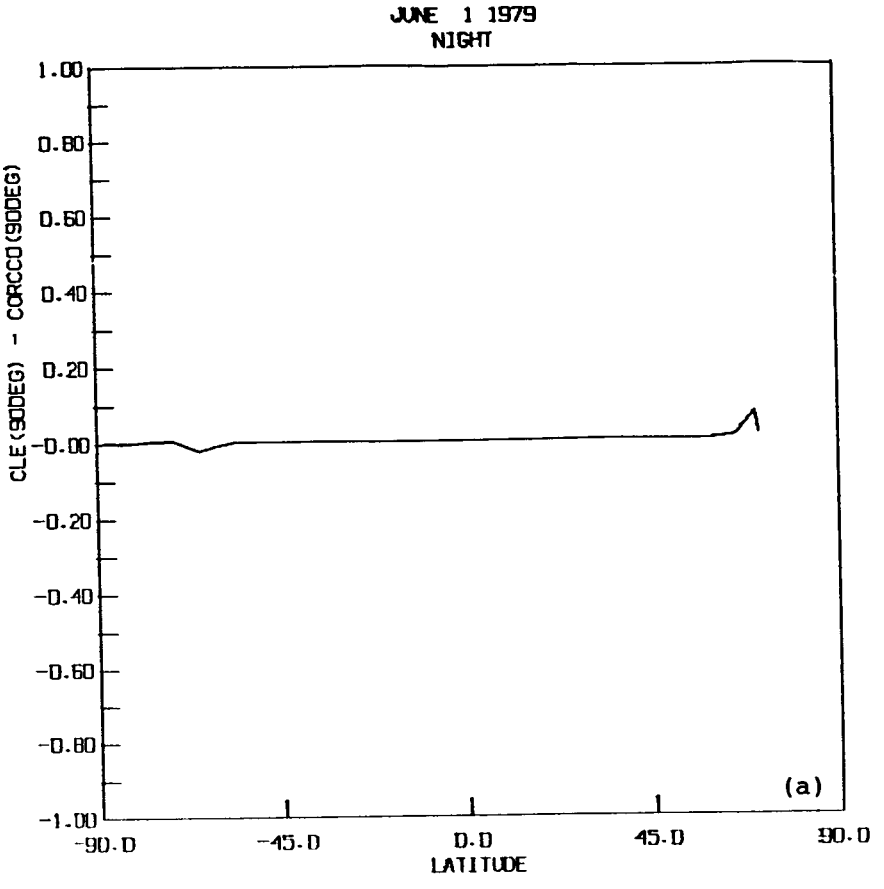

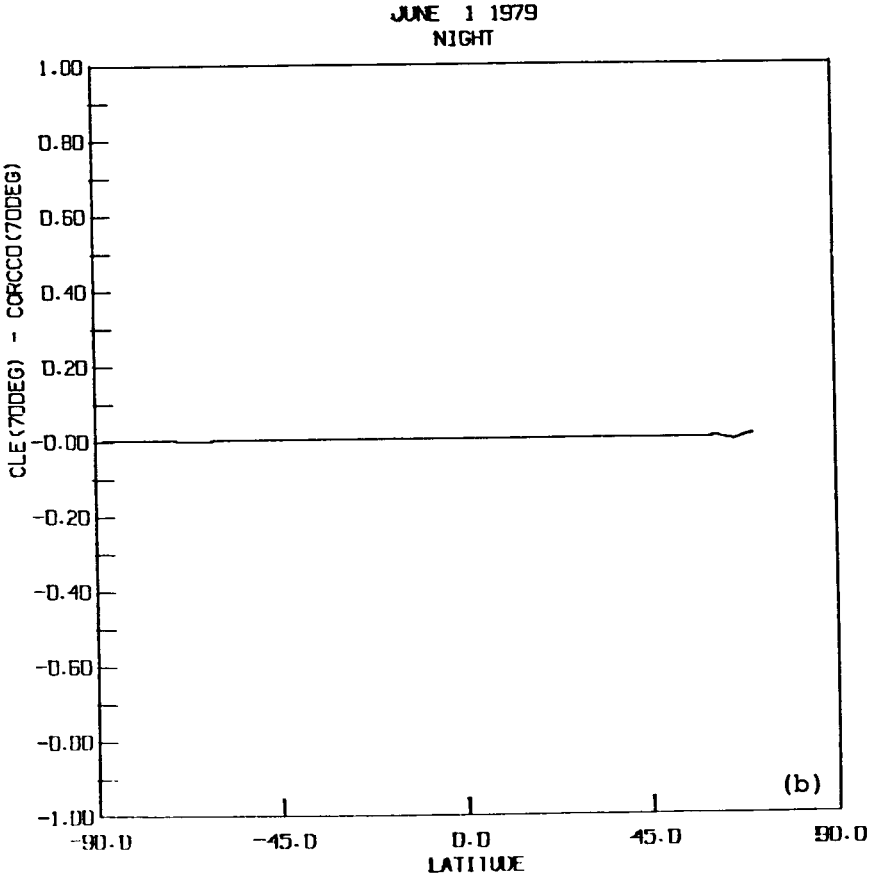

FIGURE 4.3 Nighttime longwave flux differences between the normal MLE and COR = 0 cases (units: W/m^2). (a) Observations up to 90°; (b) observations up to 70°.

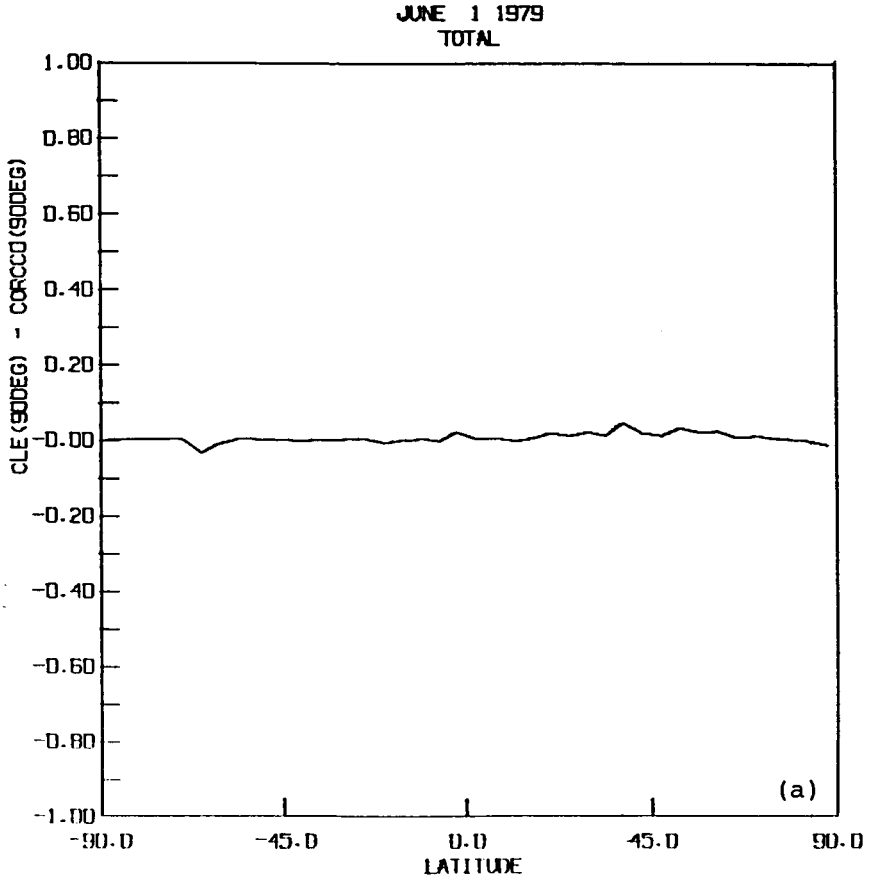

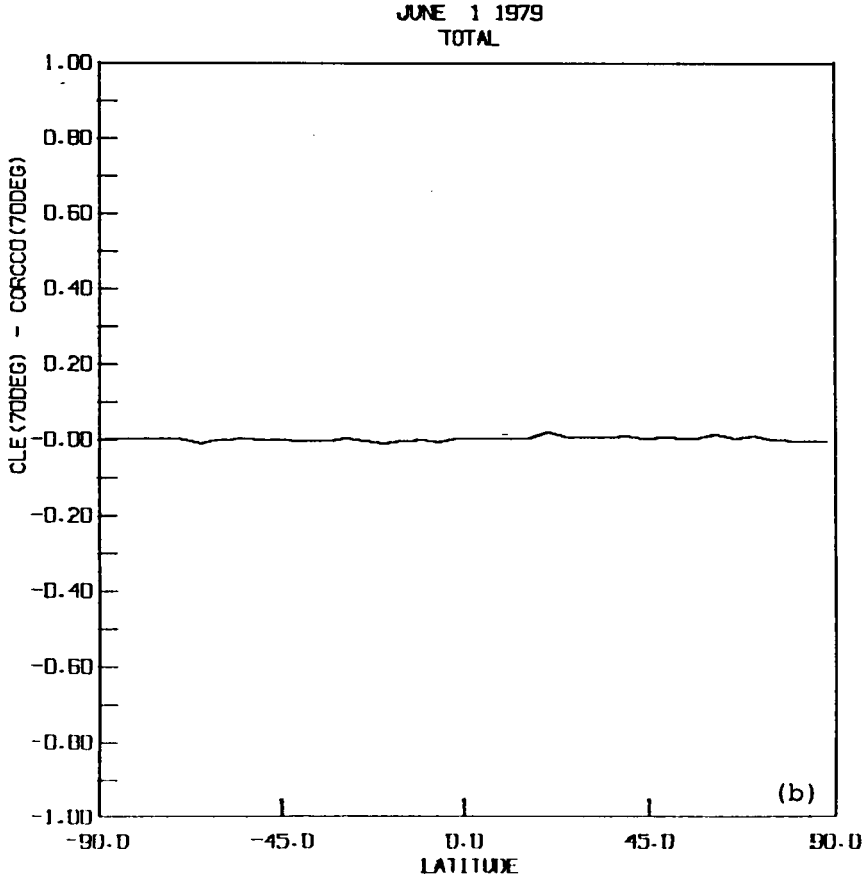

FIGURE 4.4 Day-night mean (total) longwave flux differences (W/m^2) between the normal MLE and COR = 0 cases. (a) Observations up to 90°; (b) observations up to 70°.

SECTION 5

SAMPLING STUDIES FOR SAB METHOD

Sorting into Angular Bins (SAB) method provides the validation dataset for comparison of the results with the MLE methods and different variations of it discussed in this report. SAB method involves computing angular bin averages for each target area and integrating with proper solid angle weights to obtain a flux. Any sampling biases due to differences in angular views or due to the temporal sampling interval could lead to corresponding biases in the flux estimates. This section addresses the questions relating to sampling sizes and their distribution with the number of days used in averaging and sampling differences at different viewing angles and their impact on individual TA fluxes.

The results of this study are presented in a separate report (Sorting into Angular Bins (SAB) Sampling Study, STC Technical Report 2087, January 1986). Details on the study conducted and results of the anlysis are presented in that report. For purposes of completeness only, the conclusions derived from that study are given below:

- Global mean radiation budget parameters do not show great sensitivity to the temporal interval with the SAB method.

- Zonal mean and rms differences relative to the 23 days improve significantly from the 5-day interval to the 11- or 12-day interval.

- No sampling biases or differences in radiation budget parameters are noted between the first half and second half of the month.

- Total number of TAs contributing to the global mean drops substantially in the 5-day case, e.g., for the albedo, only 25% of the globe is sampled. The rest of the TAs are rejected due to poor angular coverage.

- Certain TAs indicate excessive sampling in some azimuth ranges. The undersampled bin means also contribute to the flux estimation and, through large uncertainties in those bins, introduce errors into the computed fluxes.

- At the TA level, among the azimuth intervals, no systematic sampling biases associated with temporal interval are noticed.

- The flux integral receives biggest weight from the means of the bins in the interval 30^{o}–60^{o} in zenith. Poor sampling in this region could lead to errors in the computed flux. The 6-day case shows generally poor sampling in most bins, with bin numbers less than 58. This bin number corresponds to zenith angle of 63^{o}.

SECTION 6

USE OF NCLE MODELS

The CLE models used in section 2.0 are the reflectance and emission models which have been developed using cloud selection from THIR. Subsequently, it was found that the inclusion of ultraviolet reflectances from TOMS instrument on Nimbus-7 improved the cloud selection, particularly in the case of low-lying cloud. The new cloud input is used to develop new sets of bidirectional models for reflected radiation and of emission models for longwave radiation. These models are referred to as NCLE models. This section deals with an investigation of the effect of NCLE models on the scene selection and on the derived radiation budget parameters. The results with NCLE models are then compared with the results of the SAB method in a manner similar to the discussion in section 2. It soon became apparent that the NCLE models produced results which are essentially similar to those with the CLE models. A few aspects of the comparison only are discussed to avoid repetition.

6.1 RADIATION BUDGET PARAMETERS

6.1.1 Global Mean Parameters

Table 6.1 presents the results of the MLE method using NCLE models. The new algorithm included minor changes in the software provided by NASA/LaRC. The results in Table 6.1 should be compared with those in Table 2.1. Values resulting from the SAB method are shown since that constitutes the final

TABLE 6.1 Use of NCLE Models.
June 1979

ERB PARAMETER	SAB	MLE/NCLE Sat.Zen.Angle ≤ 90°		MLE/NCLE Sat.Zen.Angle ≤ 70°	
		Mean	RMS Diff.	Mean	RMS Diff.
Ins. Albedo	0.2738±0.101	0.2839±0.102	0.021	0.2779±0.099	0.016
LW Flux (Day)	244.3±23.3	239.1±22.2	6.66	244.4±23.3	3.75
LW Flux (Night)	227.6±35.4	224.5±35.5	5.09	228.6±36.4	3.34
LW Flux (Total)	235.6±30.9	231.6±30.5	5.30	236.4±31.5	2.81

TABLE 6.2 SAB, MLE Parameter Regression Relationships
Using NCLE Models.

Param	Intercept	Gradient	Corr. Coeff.	RMS Diff.
90° Case				
Inst. Albedo	0.012	1.001	0.992	0.021
LW flux (day)	3.48	0.996	0.990	6.66
LW flux (night)	-1.88	0.995	0.993	5.09
LW flux (Total)	0.30	0.982	0.995	5.30
70° Case				
Inst. Albedo	0.016	0.954	0.993	0.016
LW flux (day)	1.42	0.996	0.993	3.75
LW flux (night)	-0.88	1.008	0.996	3.34
LW flux (Total)	-0.67	1.006	0.997	2.81

baseline for all comparisons. It is immediately obvious from the table that the NCLE models and CLE models produce very similar results for the global values of the parameters. At the 90^{o} cutoff, the instantaneous albedo is higher by 0.20 (28.4 with NCLE versus 28.2 with CLE; refer to Table 2.2). The longwave flux values differ by only 0.1 to 0.3 W/m^2. At the 70^{o} cutoff the differences are even less significant. Thus the NCLE models tend to keep up the agreement between the SAB and MLE methods, particularly at 70^{o} cutoff in satellite zenith angle.

For the purpose of completeness, the parameters of the linear regression between the MLE and SAB results are presented in Table 6.2. Both the 90^{o} and 70^{o} cases are shown. The RMS differences improve at the 70^{o} cutoff, particularly for the longwave fluxes.

6.1.2 Zonal Averages

Differences in the zonal averages between SAB and MLE using NCLE models are shown in Figures 6.1 through 6.4 for instantaneous albedo, longwave flux for day, night, and total, respectively. The general behavior of these differences is extremely similar to the CLE and SAB differences discussed in section 2.1.2.

6.1.3 Target Area Comparisons

Target area parameters derived with NCLE models are compared in a regression procedure with SAB method values as in section 2.1.1. The results are extremely similar and are not shown to avoid repetition. The parameters of the linear regression, however, are listed in Table 6.2.

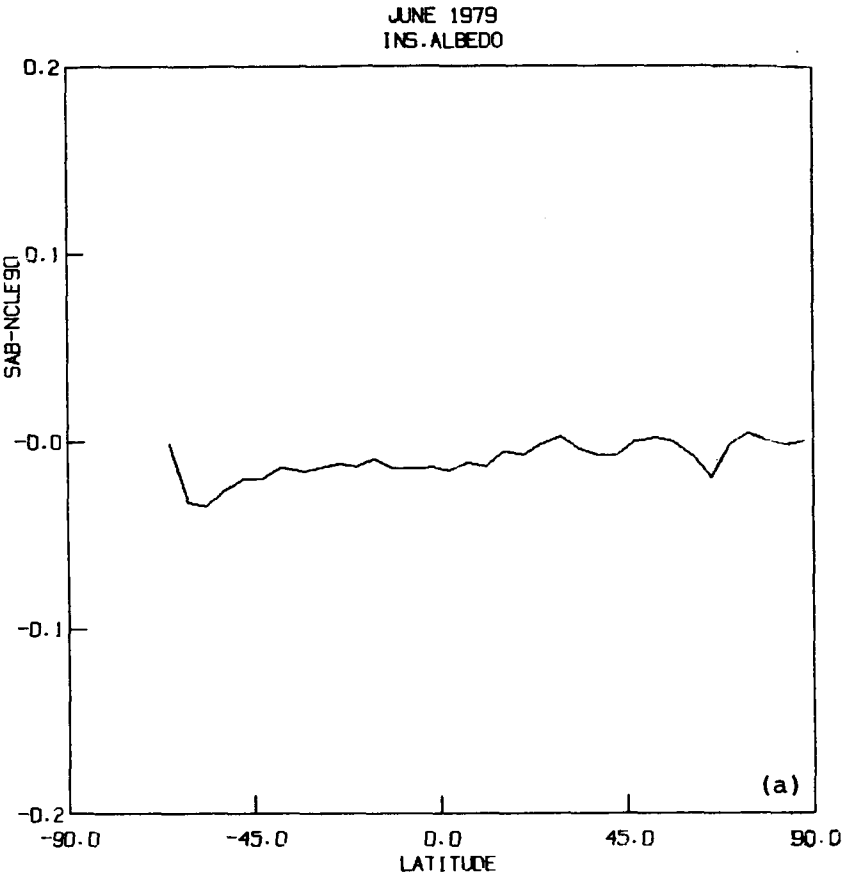

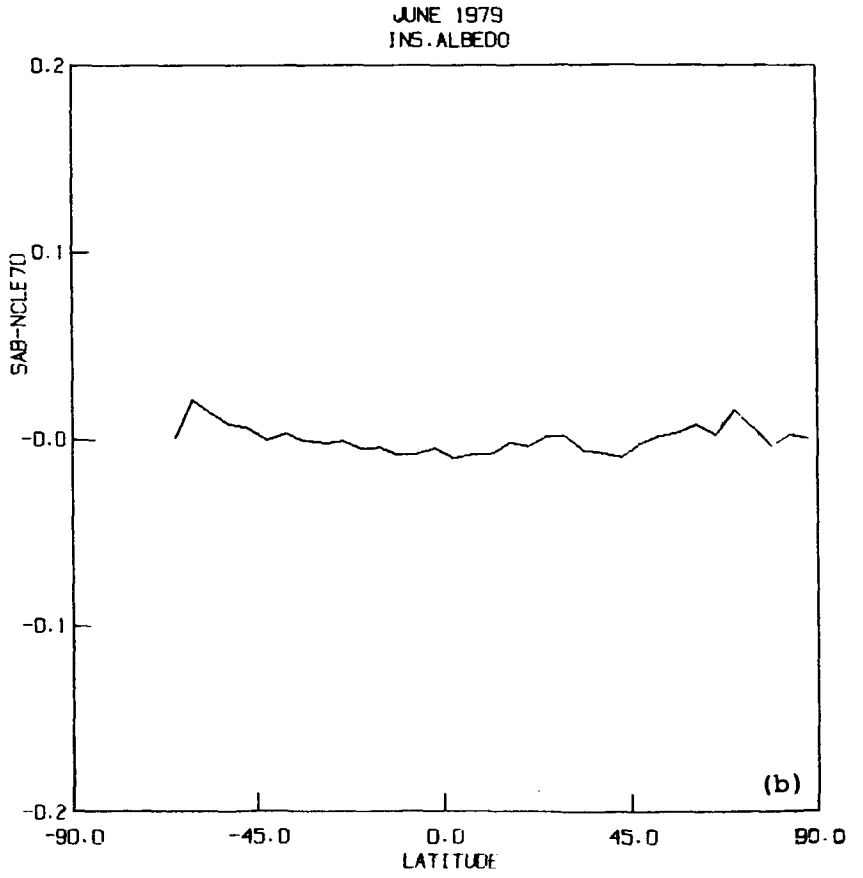

FIGURE 6.1 Zonally averaged monthly mean instantaneous albedo differences between SAB and MLE-NCLE methods. Results for June 1979. (a) All observations up to 90 are retained; (b) only observations up to 70° are retained.

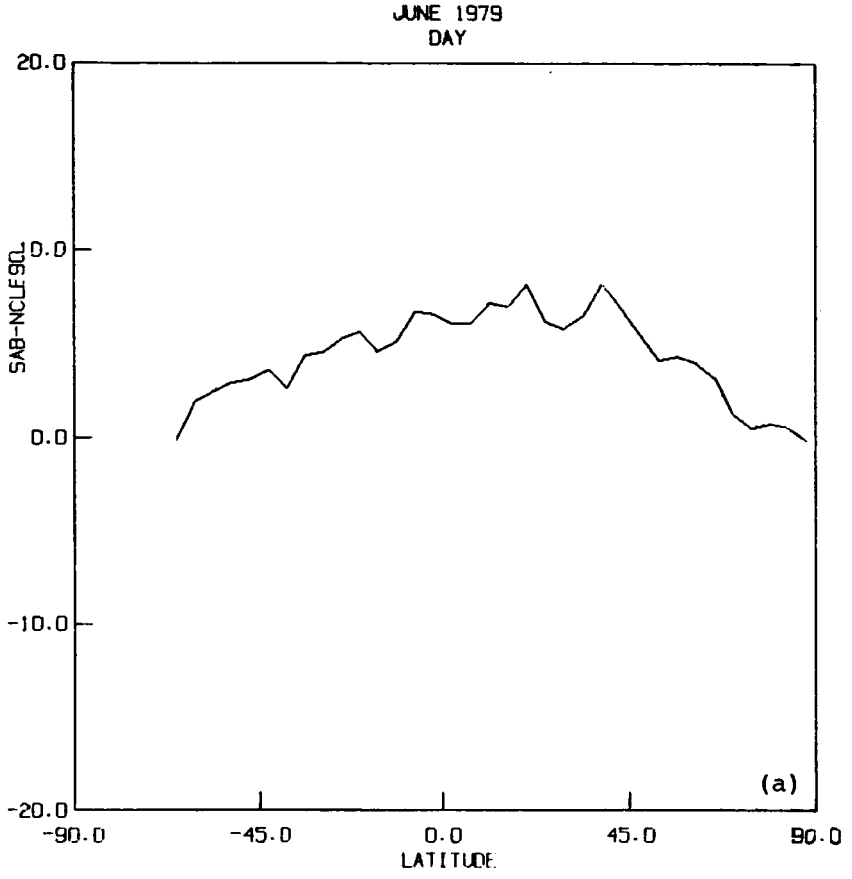

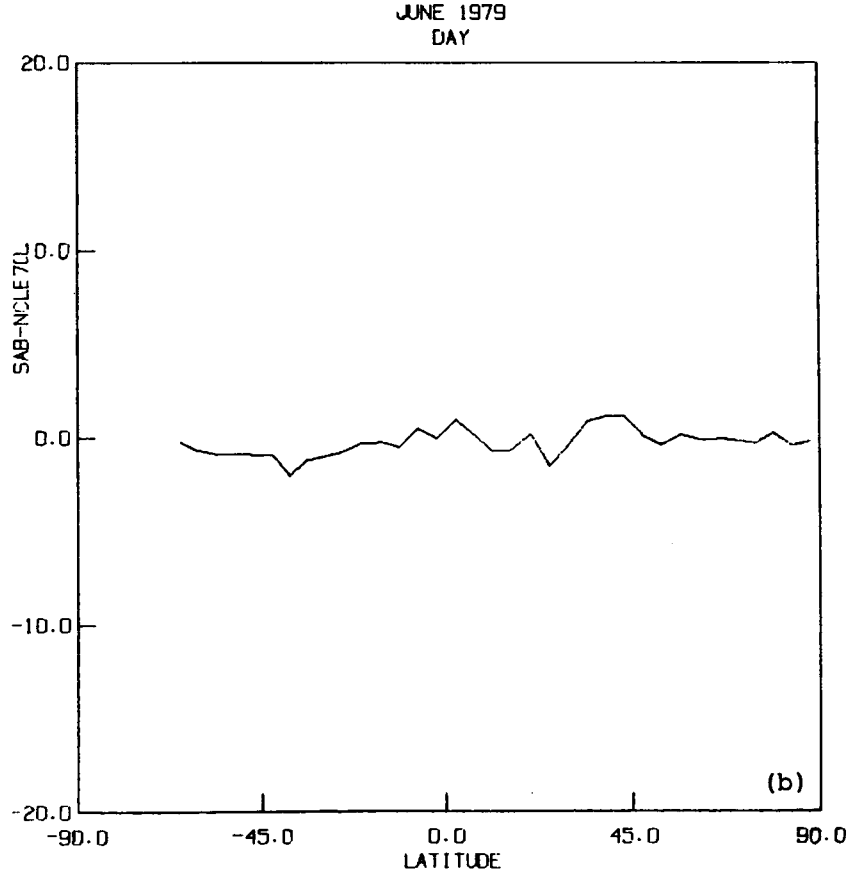

FIGURE 6.2 Zonally averaged monthly mean daytime longwave flux differences between SAB and MLE-NCLE methods. Results for June 1979. (a) All observations up to 90° are retained; (b) only observations up to 70° are retained.

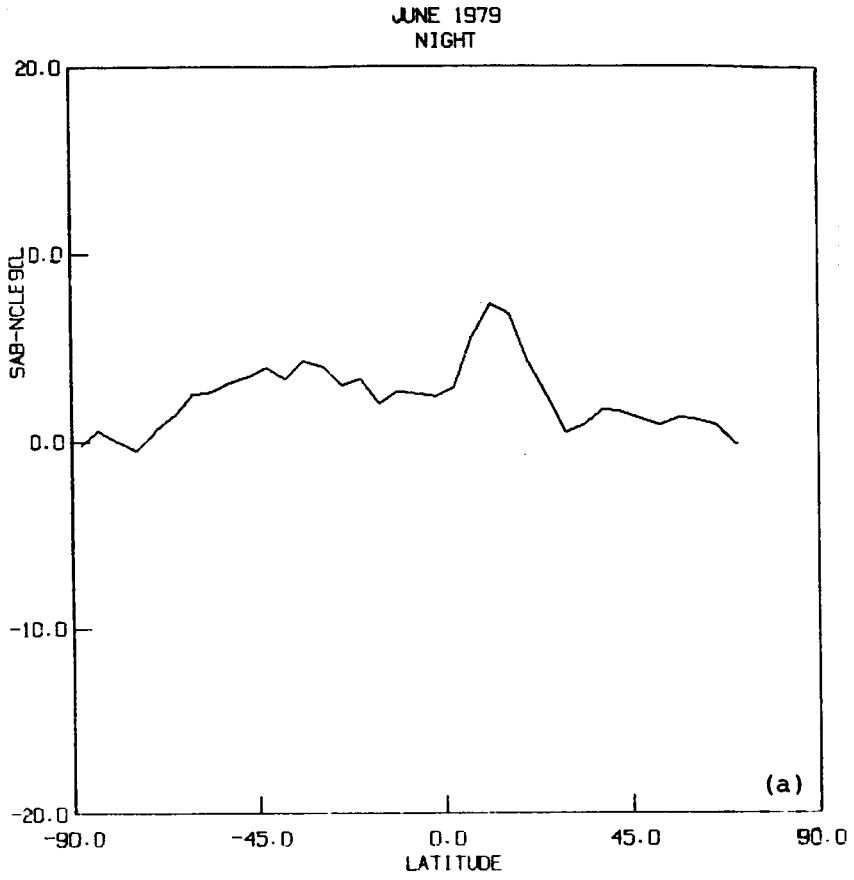

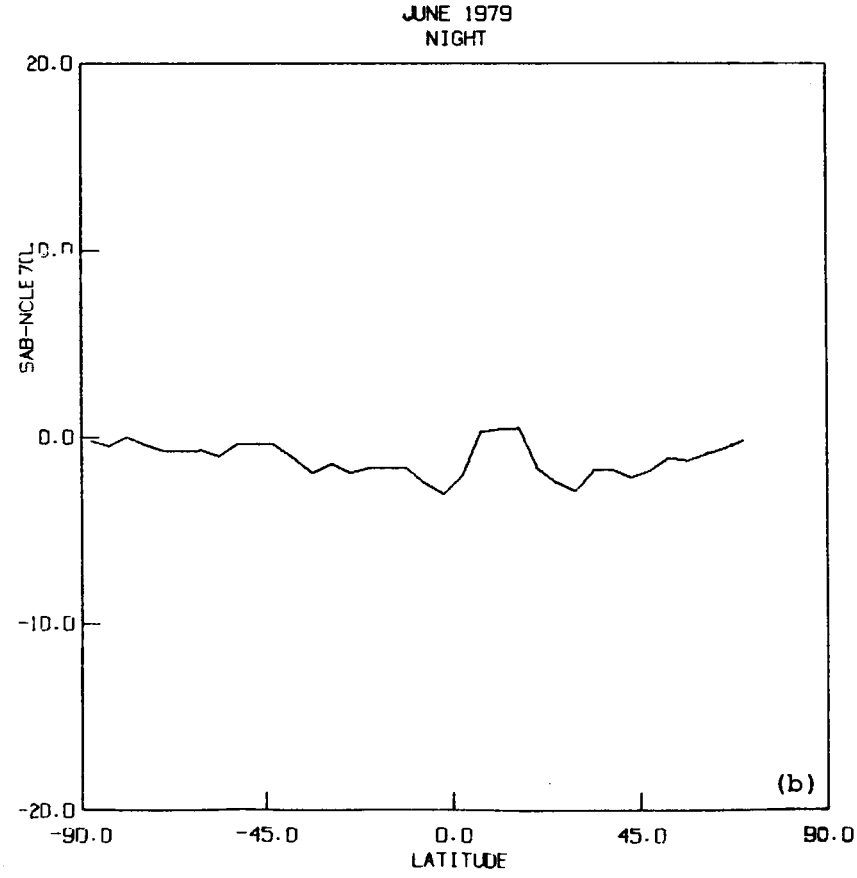

FIGURE 6.3 Zonally averaged monthly mean nighttime longwave flux differences between SAB and MLE-NCLE methods. Results for June 1979. (a) All observations up to 90° are retained; (b) only observations up to 70° are retained.

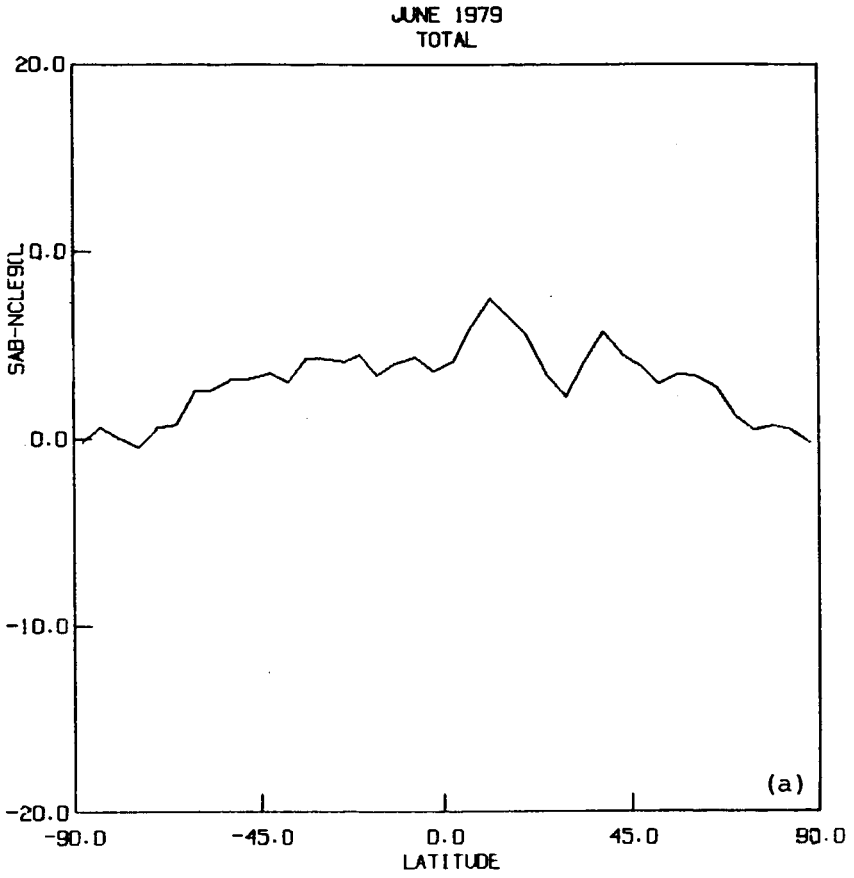

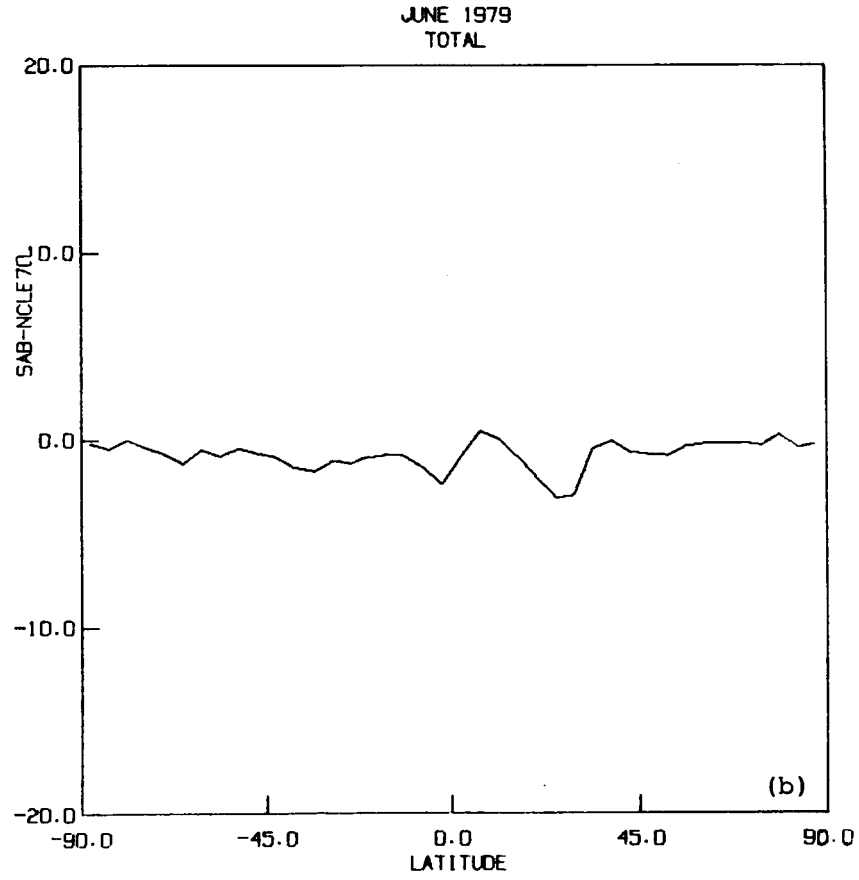

FIGURE 6.4 Zonally averaged monthly mean day, night average (total) longwave flux differences between SAB and MLE-NCLE methods. Results for June 1979. (a) All observations up to 90° are retained; (b) only observations up to 70° are retained.

Mercator maps of the parameter differences for the 70^{o} case are shown in Figures 6.5 to 6.8. Once again, the differences in the contours are nominal.

6.2 TARGET AREA STUDIES

Daily variations of the albedo using the MLE-NCLE method are shown for four target areas in Figures 6.9 to 6.12. These are the same TAs that are used in the discussion in section 2.2.2. Many of the results are repetitive. On closer scrutiny, small differences appear. For example, in Figure 6.9 for TA 96, the value of the 90^{o} cutoff case is slightly smaller than the one in Figure 2.17. Similarly, the 70^{o} cutoff case value is slightly higher. The values of the standard deviation in the local noon albedo on days 152, 153 and 167 smaller using NCLE models, but is larger on day 157. Minor differences of a similar nature are noticeable for the other TAs also. But overall, the effect on the computed albedo values due to the use of NCLE models is very small.

6.3 SCENE SELECTION ADEQUACY

6.3.1 Cloud Identification Using NCLE Models

The results in section 6.1 and 6.2 indicate that the radiation budget parameters are not affected when the NCLE models replace the CLE models. There is, however, an effect on the cloud identification when the NCLE models are used. Daytime, nighttime, and day-night average cloud amounts using the CLE and NCLE models are shown in Table 6.3 for June 10, 1979. The cloud amount computation procedure from the clear, partly cloudy, mostly cloudy, and overcast statistics is discussed in a later section dealing with validation of cloud identification.

TABLE 6.3 Computed Cloud Amounts
June 10, 1979

	Day		Night		Average	
Description	CLE	NCLE	CLE	NCLE	CLE	NCLE
Northern	54.84	55.38	57.22	56.64	55.50	55.62
Southern	45.46	49.62	47.52	49.33	46.96	49.33
Global	50.34	52.62	52.20	52.86	51.23	52.47

The results in Table 6.3 indicate that the average cloud amount in the northern hemisphere has remained the same with the NCLE models, but the southern hemisphere cloud amount has increased from 46.9 to 49.3. The global cloud amount has increased slightly to 52.5 from 51.2. Cloud amount in the southern hemisphere increased both during daytime (4.2) and nighttime (1.8). Northern hemisphere cloud amount increased during daytime, but decreased during the nighttime. NCLE models decrease the north, south differences in cloud amount. During both day and night, these differences using CLE models are near 10%, but they drop to about 5 or 6% with NCLE models. The daytime global mean cloud amount increased by 2.3% above the CLE value, while there is a minor change in the nighttime value. The additonal cloud identification using NCLE models can be attributed to the use of the TOMS ultraviolet reflectivities. The effect of this addition is to identify the low level cloudiness which is missed by the IR. The increase in the derived global cloud amount during the day is thus consistent with the above. The nighttime result should not be affected since the TOMS has no observations at night.

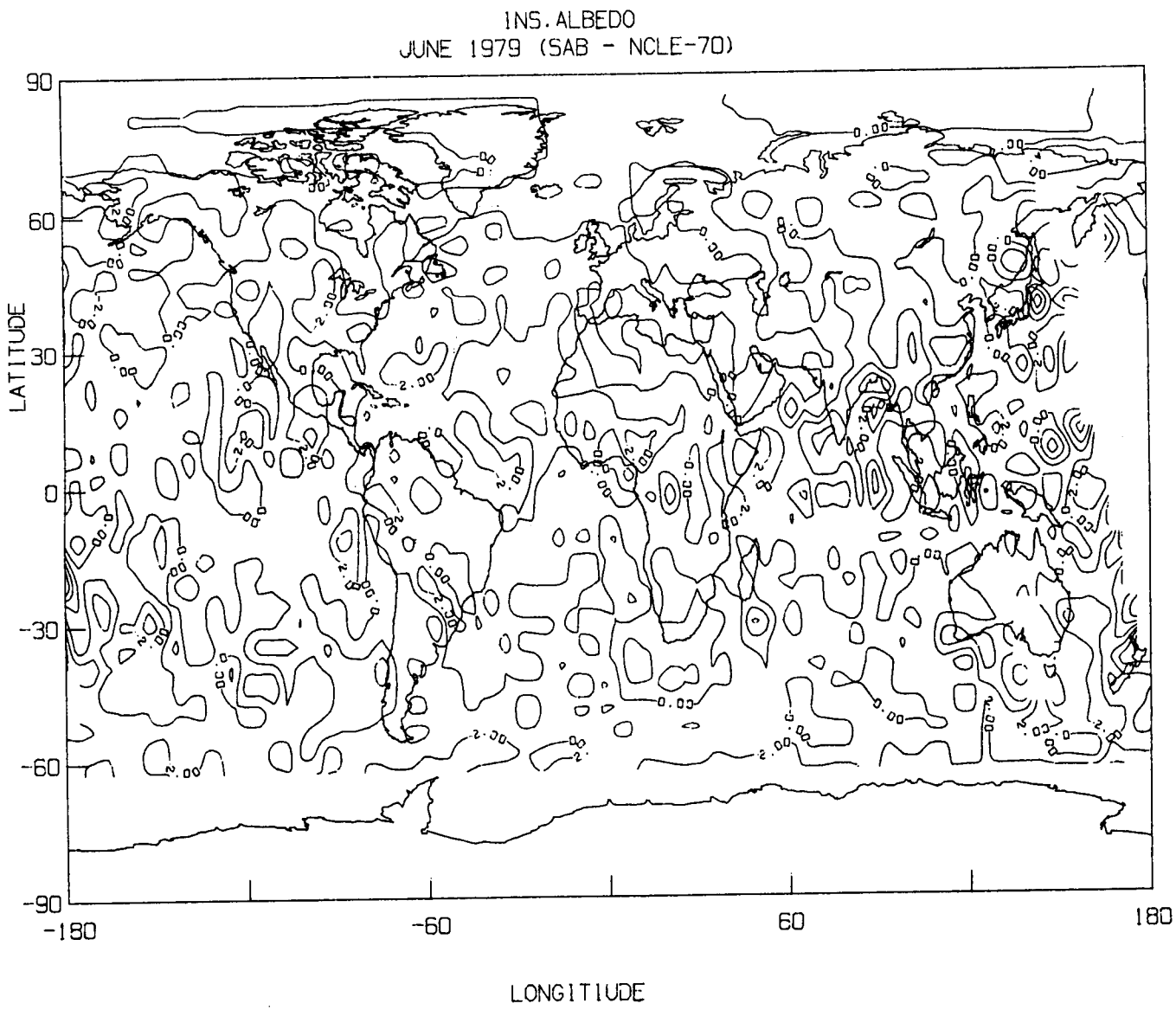

FIGURE 6.5 Mercator map of monthly mean instantaneous albedo (as percentages) differences between SAB and MLE-NCLE methods. Cutoff angle with MLE-NCLE method is 70° in satellite zenith angle.

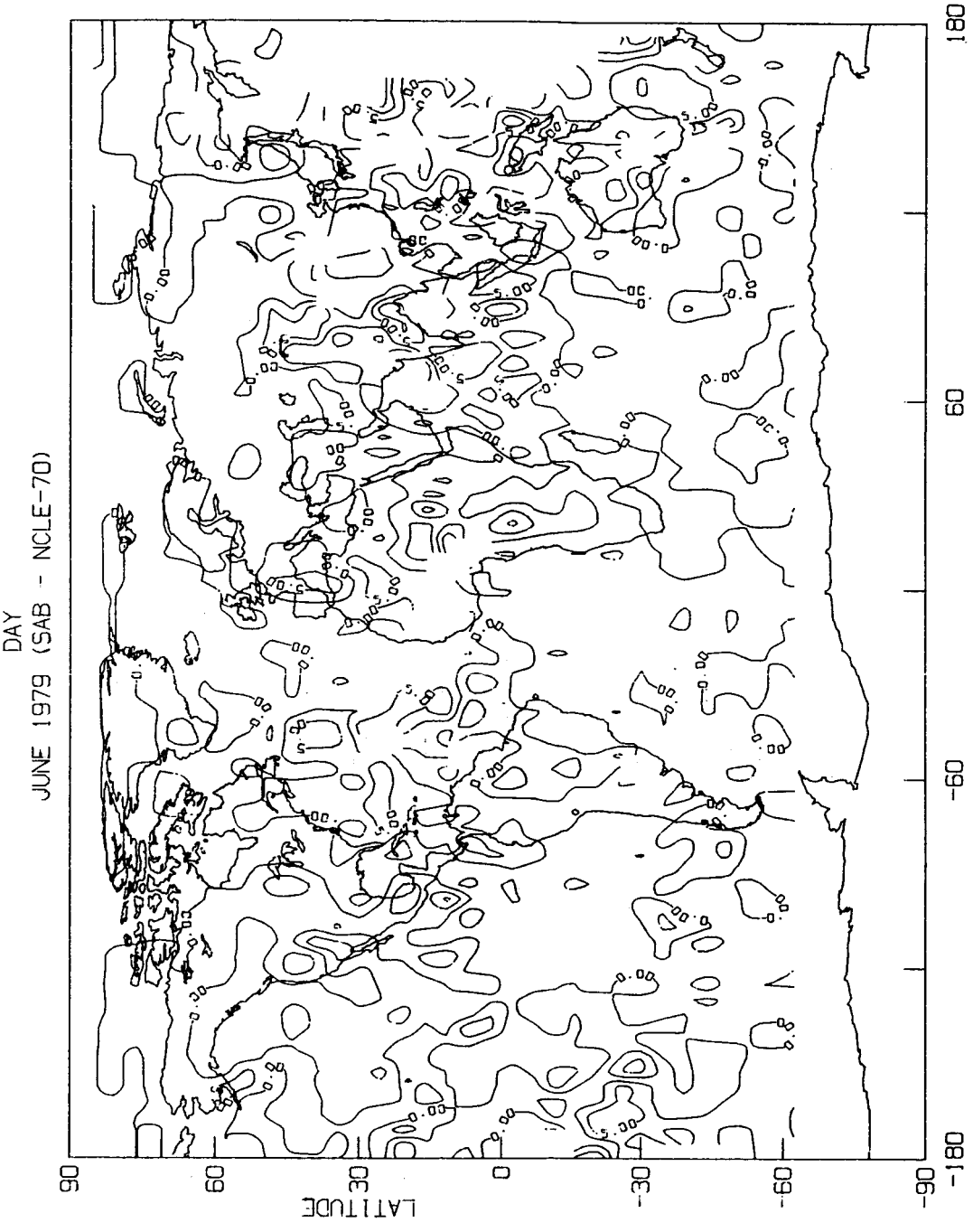

FIGURE 6.6 Mercator map of monthly mean daytime longwave flux differences between SAB and MLE-NCLE methods. Cutoff angle with MLE-NCLE method is 70° in satellite zenith angle.

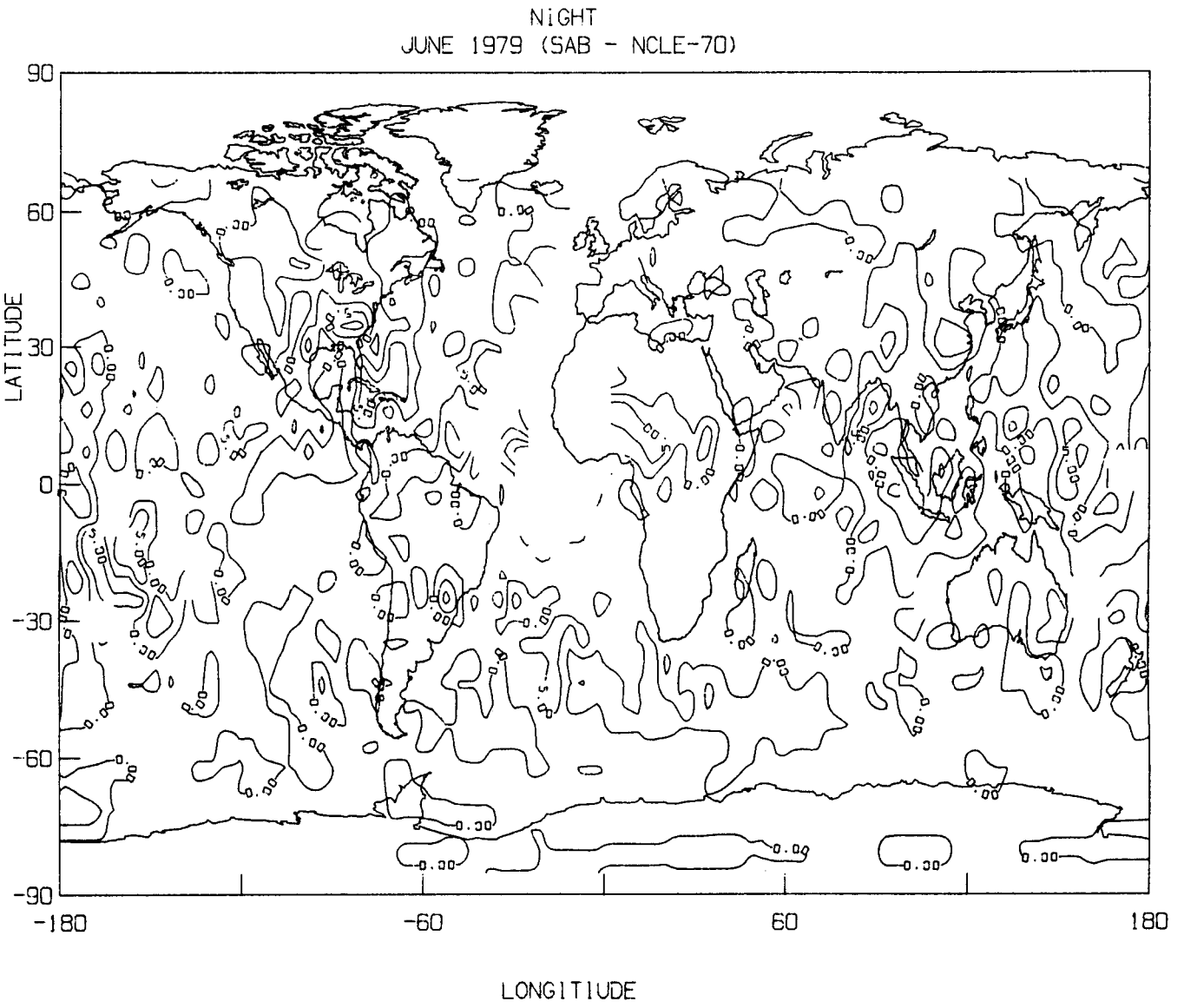

FIGURE 6.7 Mercator map of monthly mean nighttime longwave flux differences between SAB and MLE-NCLE methods. Cutoff angle with MLE-NCLE method is 70° in satellite zenith angle.

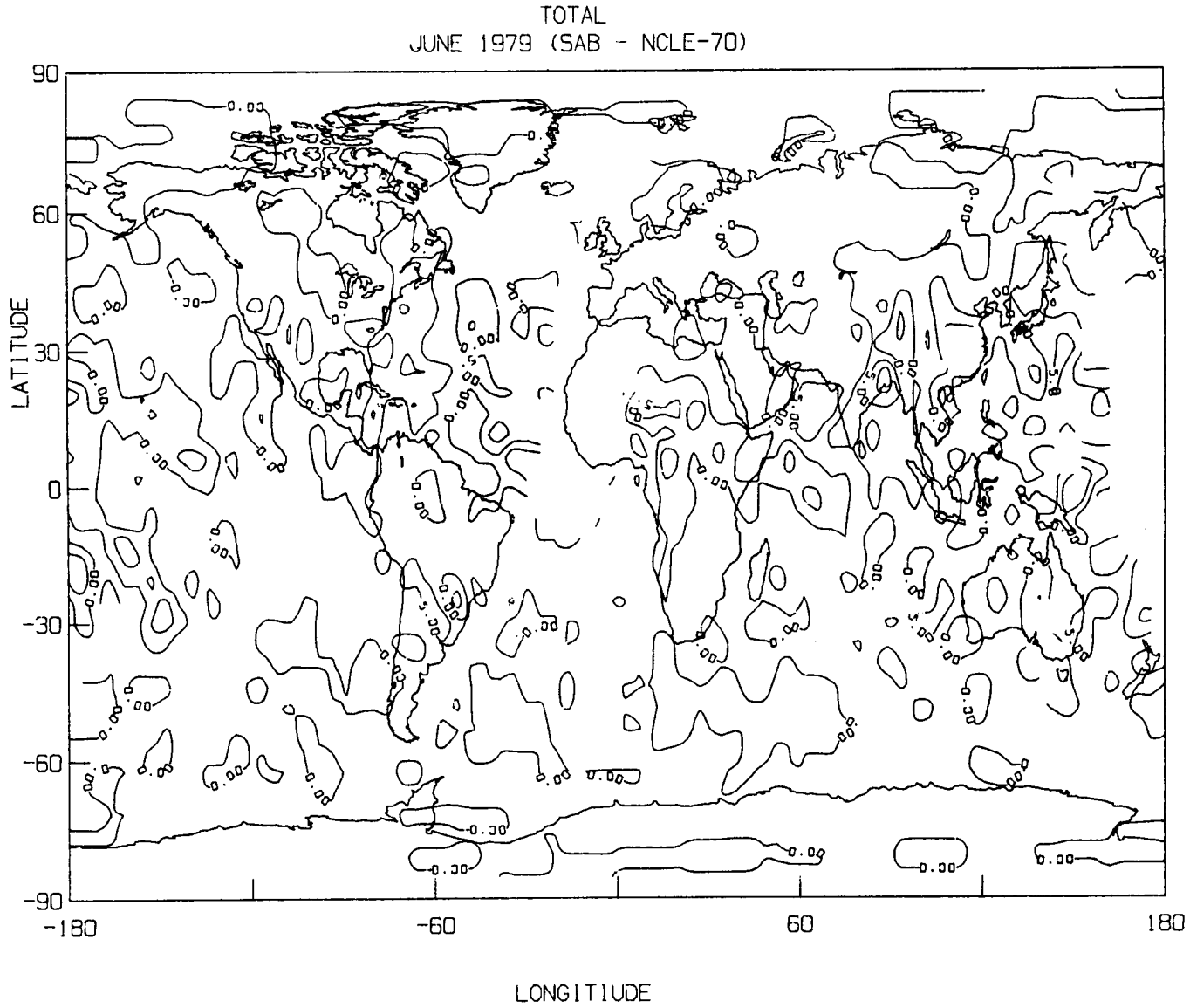

FIGURE 6.8 Mercator map of monthly mean day, night average (total) longwave flux differences between SAB and MLE-NCLE methods. Cutoff angle with MLE-NCLE method is 70° in satellite zenith angle.

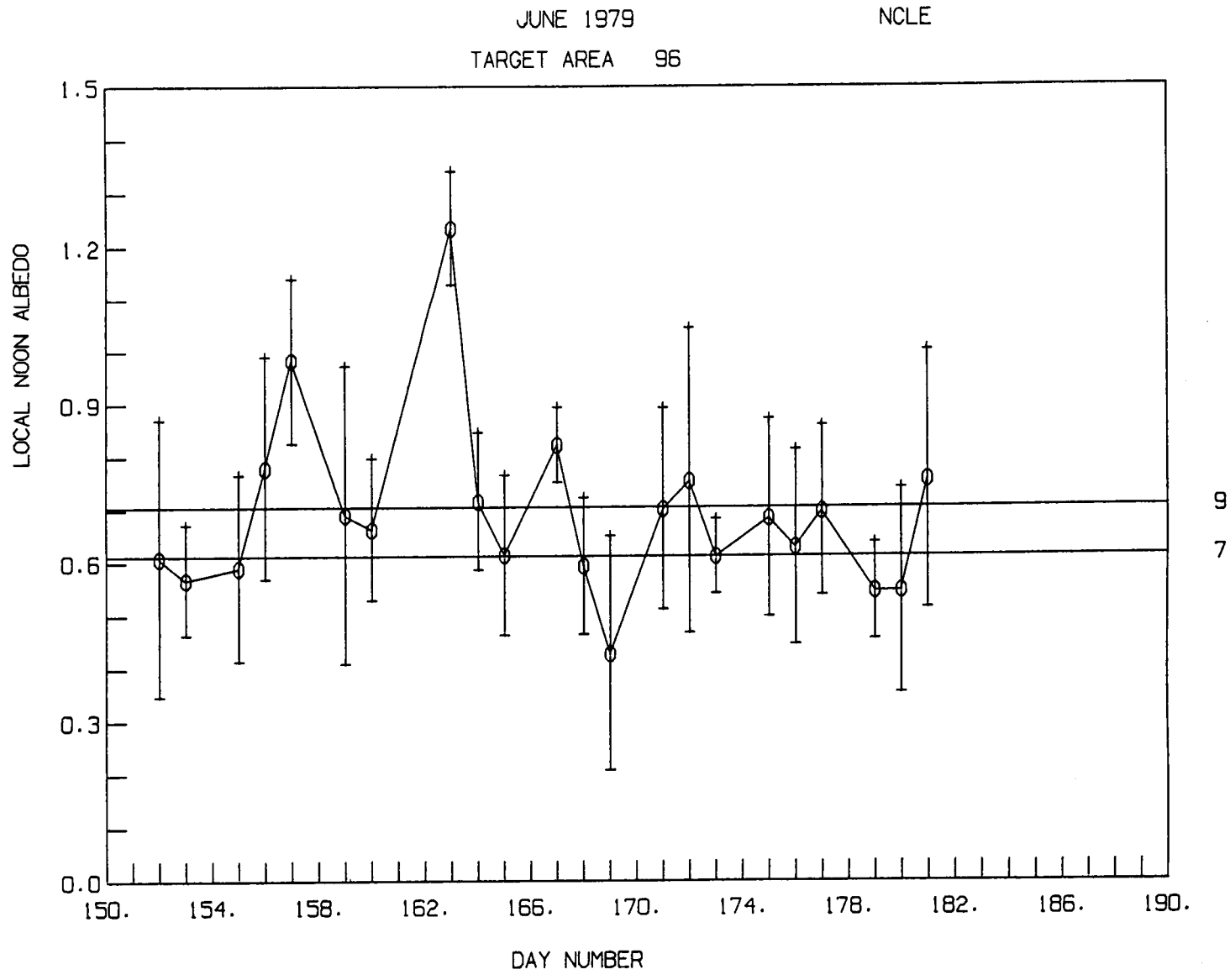

FIGURE 6.9 Mean and standard deviation of instantaneous albedo for TA 96 for each day of observation during June 1979, using MLE-NCLE method.

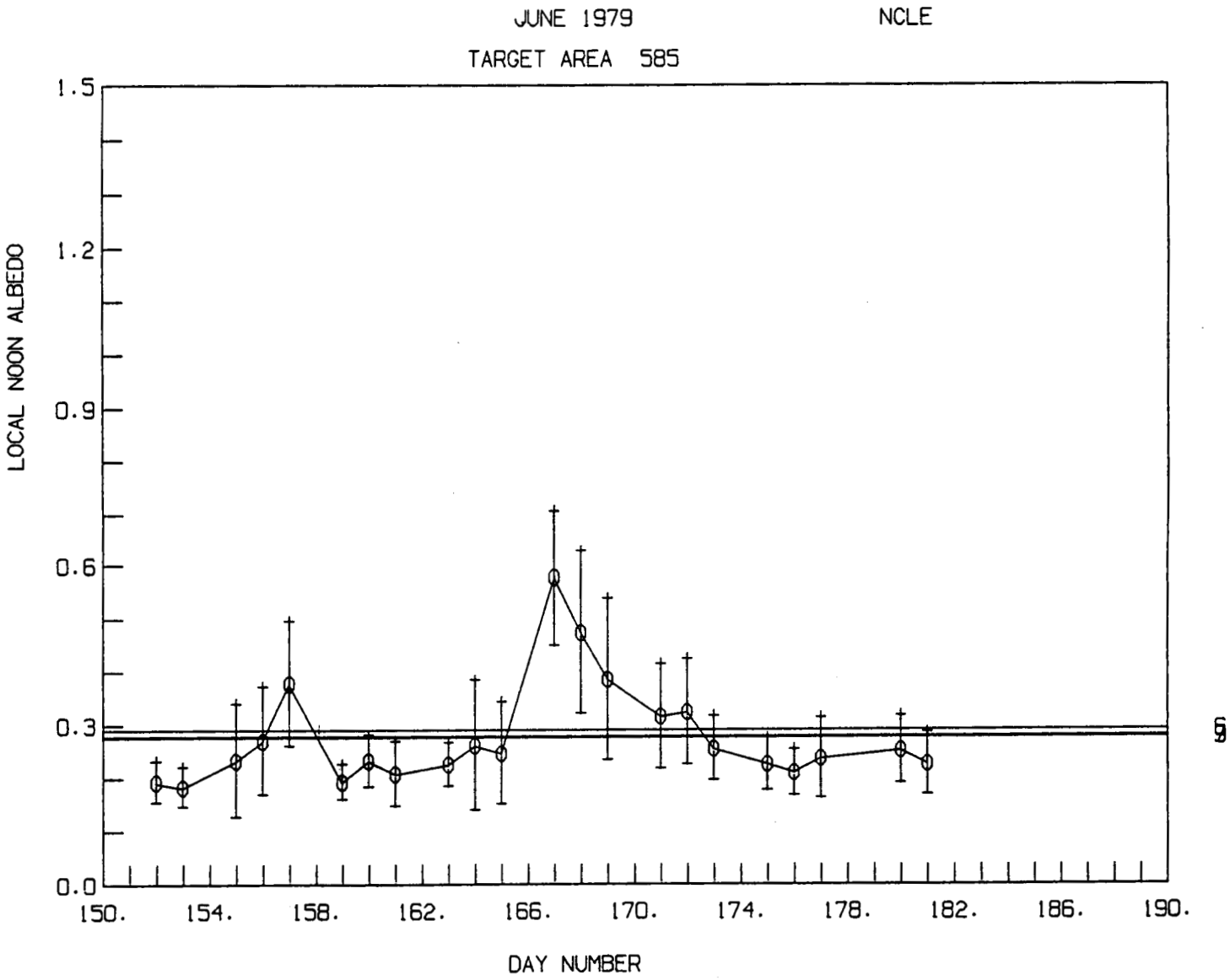

FIGURE 6.10 **Mean and standard deviation of instantaneous albedo for TA 585 for each day of observation during June 1979, using MLE-NCLE method.**

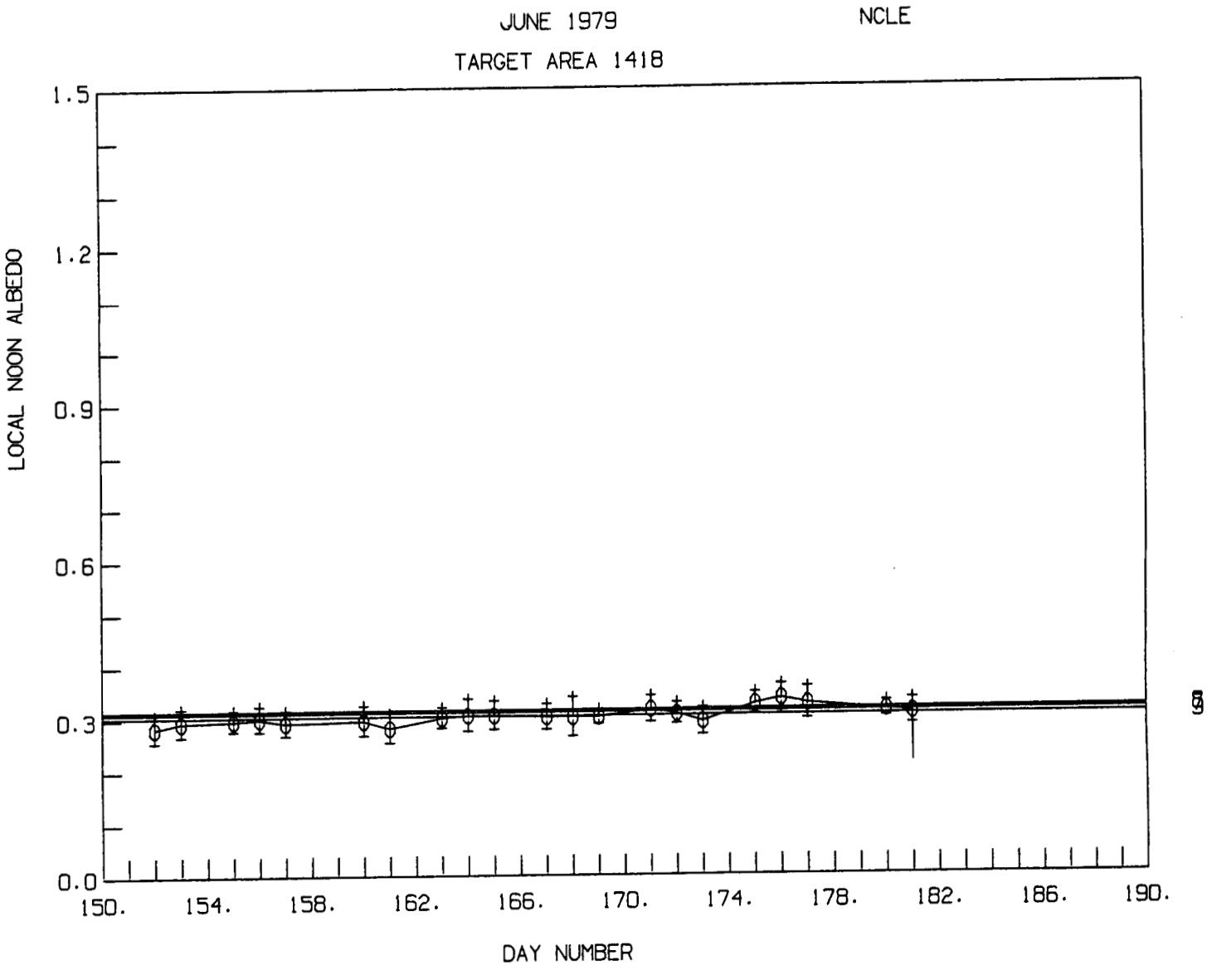

FIGURE 6.11 Mean and standard deviation of instantaneous albedo for TA 1418 for each day of observation during June 1979, using MLE-NCLE method.

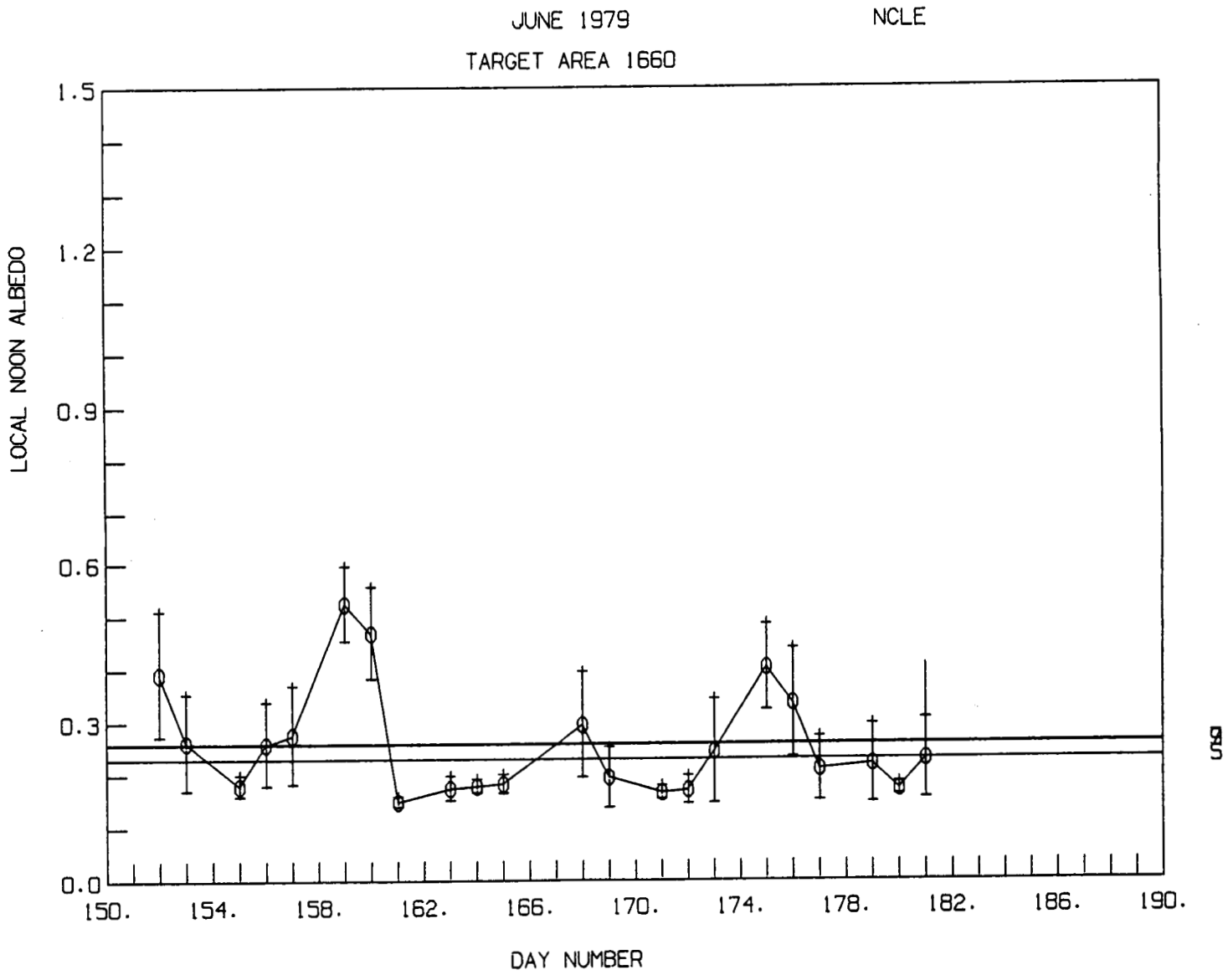

FIGURE 6.12 Mean and standard deviation of instantaneous albedo for TA 1660 for each day of observation during June 1979, using MLE-NCLE method.

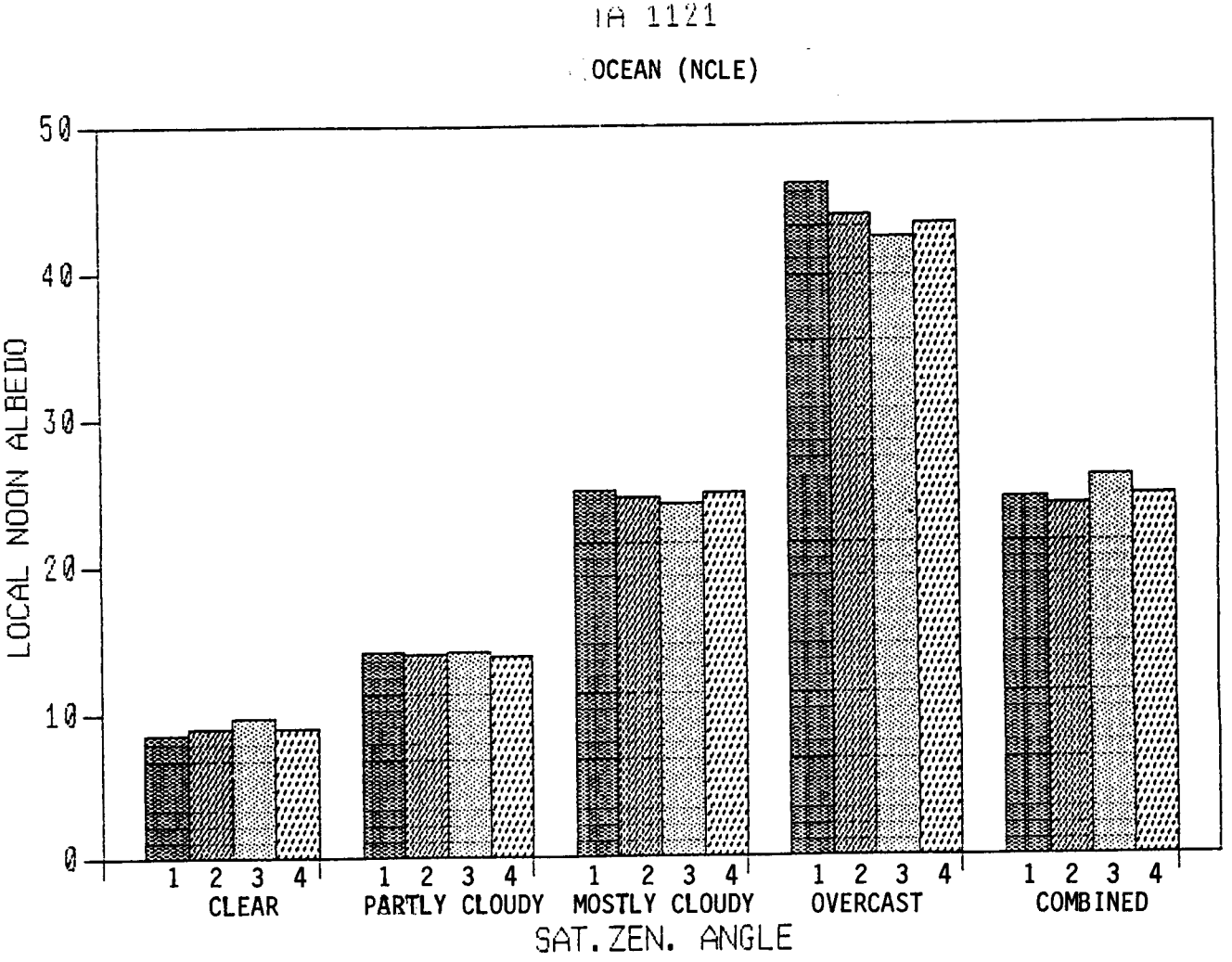

FIGURE 6.13 Dependence of instantaneous albedo for TA 1121 on the satellite zenith angle range (1: $0 < \theta \leq 30°$; 2: $30° < \theta \leq 45°$; 3: $45° < \theta \leq 60°$; 4: $60° < \theta \leq 90°$) for each of four cloud cover categories. The combined case is also shown.

6.3.2 Albedo Dependence on Satellite Zenith Angle

The effect of satellite zenith angle averaging for instantaneous albedo is shown in Figure 6.13 for an ocean TA 1121. The corresponding figure using CLE models is Figure 2.21. The five categories in the figure are, as before, clear case (0-5% cloud), partly cloudy (5-50% cloud), mostly cloudy (50-90% cloud), and overcast (95% and above cloud). Under each category, the four satellite zenith angle intervals are shown. There are slight differences in the individual values between Figures 2.21 and 6.14. The overall result is that there are no specific satellite zenith angle related biases in the computed albedo. Similar conclusions can be drawn from the results in Figure 6.14 for land TA 585 and Figure 6.15 for the desert TA 1418. The blank regions, particularly in Figure 6.15 are due to the absence of observations in that satellite zenith angle range for the scene type.

6.3.3 Scene Identification Reliability Index

Results regarding the scene reliability are shown in Table 6.4 for day 152 (June 1) and day 153. At the global level, nearly 95% to 98% of the observations are within 2 σ of the radiance means in all cases. At the $\pm 1\ \sigma$ level, the fractions have generally dropped. This is an indication that for the new models, the standard deviation for a given angular bin is generally smaller so that a smaller fraction of the observations is within 1 σ. The exception, however, is the nighttime, where the global values at both the 1 σ and 2 levels remain the same as with the CLE models.

For the case of individual scenes, we note that the clear scene fractions are smaller with NCLE models in the case of NCLA (daytime shortwave

and longwave together), NCSDAY (daytime shortwave cases only) than with the CLE models. Fractions corresponding to mostly cloudy and overcast scenes are considerably larger for the daytime longwave at both 1 σ and 2 σ levels. At the 2 σ level, all scene types show fractions between 0.95 and 1.00. We thus draw the conclusion that more than 95% of the observations in all categories are within 2 σ of the respective radiance mean values.

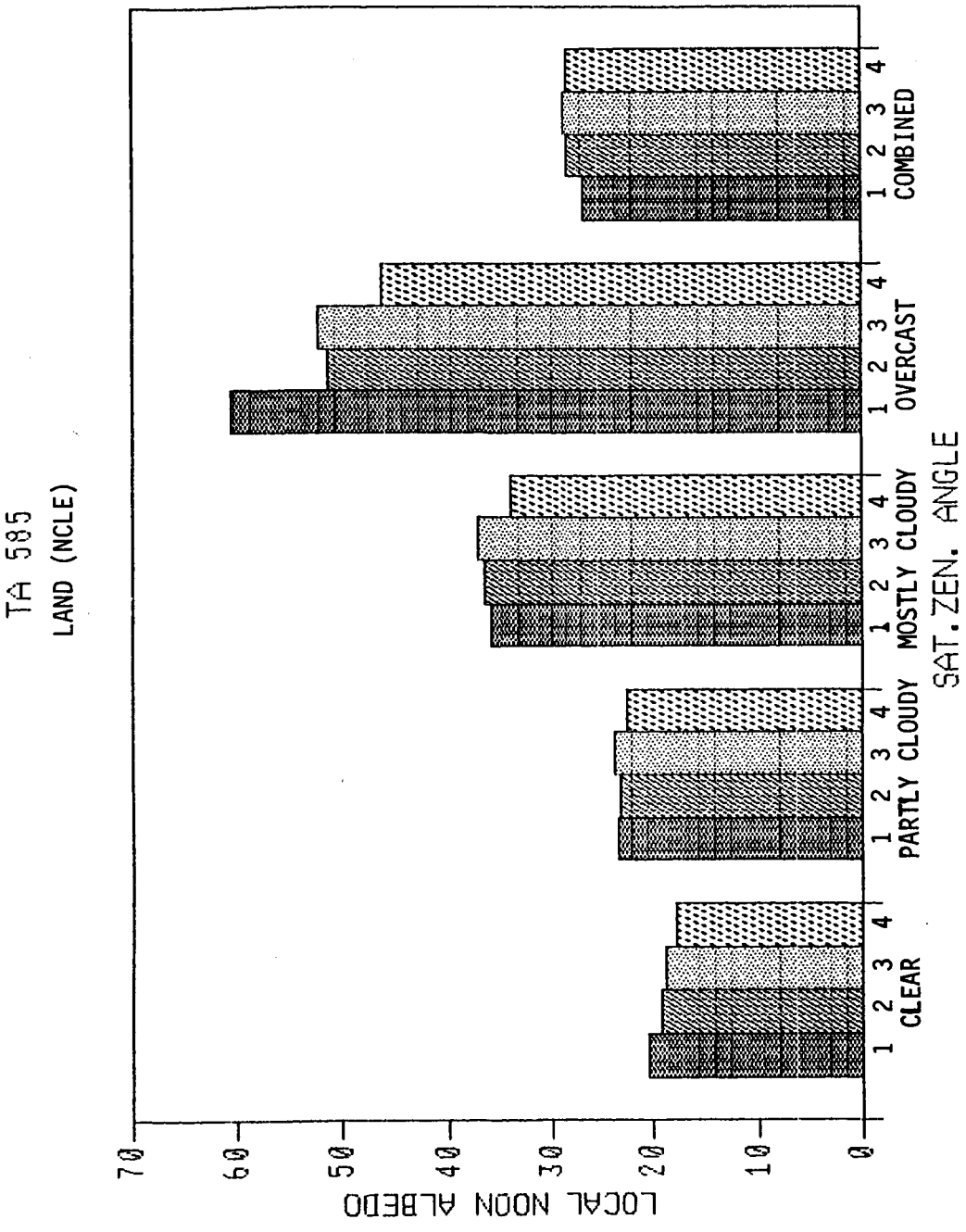

FIGURE 6.14 Dependence of instantaneous albedo for TA 585 on the satellite zenith angle range (1: $0 < \theta \leq 30°$; 2: $30° < \theta \leq 45°$; 3: $45° < \theta \leq 60°$; 4: $60° < \theta \leq 90°$) for each of four cloud cover categories. The combined case is also shown.

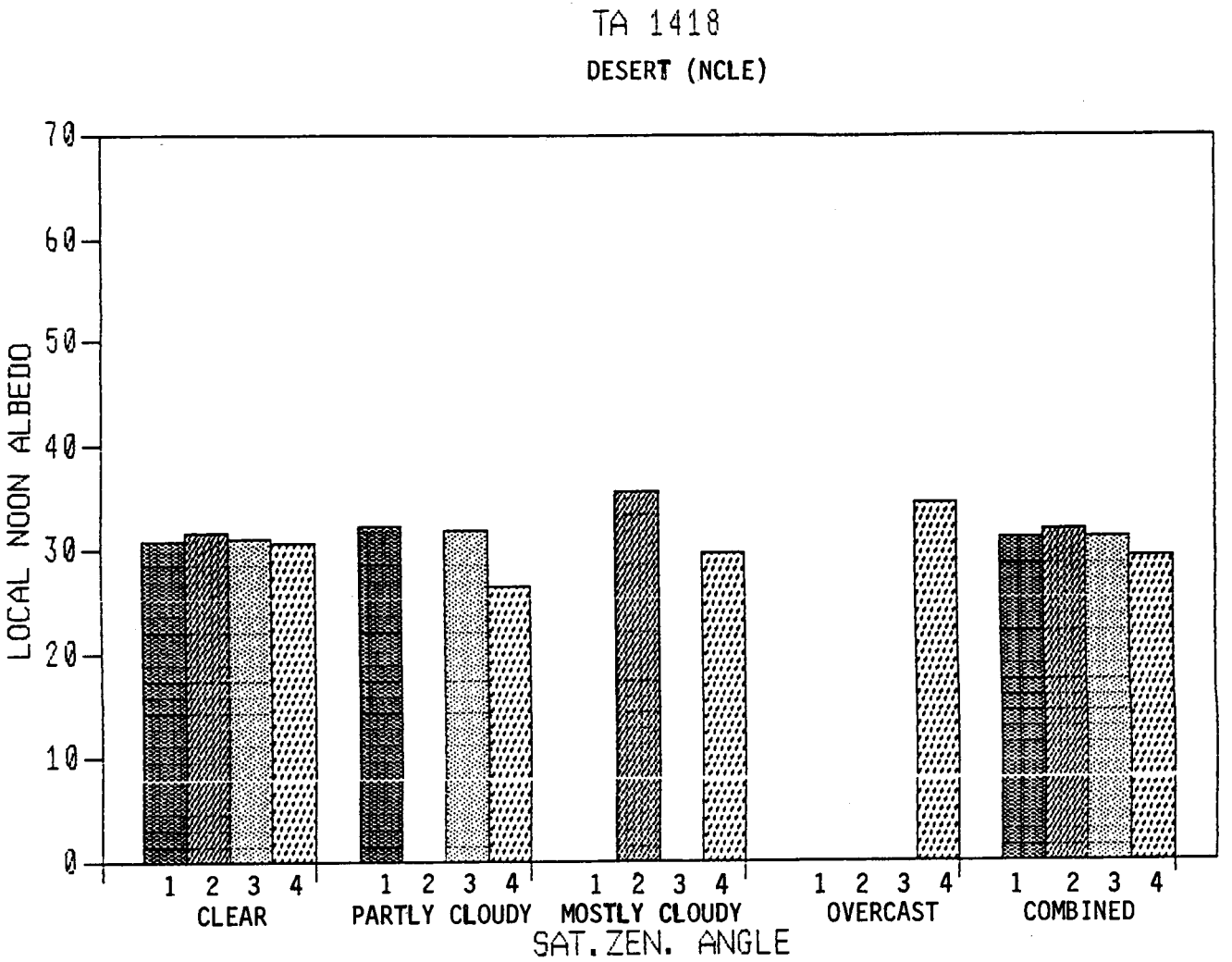

FIGURE 6.15 Dependence of instantaneous albedo for TA 1418 on the satellite zenith angle range (1: $0 < \theta \leq 30°$; 2: $30° < \theta \leq 45°$; 3: $45° < \theta \leq 60°$; 4: $60° < \theta \leq 90°$) for each of four cloud cover categories. The combined case is also shown.

TABLE 6.4. Scene Identification Reliability Statistics with NCLE Models.

****
* NIMBUS-7 *
****

******** DAY 152 **********

	NCLA			NCLDAY			NCLNIT			NCSDAY		
	TOTAL	PRCNT .LT.1	PRCNT .LT.2	TOTAL	PRCNT .LT.1	PRCNT .LT.2	TOTAL	PRCNT .LT.1	PRCNT .LT.2	TOTAL	PRCNT .LT.1	PRCNT .LT.2
OCEAN	12813	0.4481	0.9287	18880	0.7213	0.9444	21665	0.9097	0.9854	12800	0.6949	0.9977
LAND	7140	0.5882	0.9744	8957	0.7304	0.9849	4627	0.9447	0.9987	7110	0.8609	0.9920
SNOW	2032	0.3110	0.8445	2795	0.4608	0.9377	14917	0.6754	0.9787	1857	0.7044	0.8869
DESERT	3725	0.4483	0.9595	4787	0.6917	0.9914	4219	0.7440	0.9412	3725	0.6722	0.9646
MIXED LAND/OCEAN	1748	0.6133	0.9765	2268	0.7474	0.9819	1362	0.9317	0.9868	1747	0.8632	0.9920
PARTLY CLOUDY/OCEAN	24862	0.6043	0.9794	32474	0.7766	0.9904	38347	0.9414	0.9988	24499	0.8479	0.9963
PARTLY CLOUDY/LAND	11137	0.5990	0.9831	14831	0.8022	0.9946	8529	0.9968	0.9999	11014	0.8050	0.9921
PARTLY CLOUDY/LAND,OCEAN MIX	1977	0.6029	0.9681	2627	0.7606	0.9825	1816	0.9939	0.9994	1971	0.8549	0.9883
MOSTLY CLOUDY/OCEAN	32290	0.5835	0.9727	41005	0.8385	0.9898	45068	0.9760	0.9999	31523	0.7517	0.9883
MOSTLY CLOUDY/LAND	12717	0.6768	0.9760	17033	0.9126	0.9996	11092	0.9890	0.9990	12190	0.7782	0.9829
MOSTLY CLOUDY/LAND,OCEAN MIX	2564	0.5846	0.9434	3537	0.8931	0.9983	2556	0.9437	0.9969	2406	0.7111	0.9667
COMPLETELY CLOUDY	66611	0.4862	0.9340	85118	0.8045	0.9763	75748	0.6815	0.9279	64754	0.6085	0.9575
	179616	0.5430	0.9549	234312	0.7987	0.9816	229946	0.8435	0.9720	175596	0.7173	0.9769

******** DAY 153 **********

	NCLA			NCLDAY			NCLNIT			NCSDAY		
	TOTAL	PRCNT .LT.1	PRCNT .LT.2	TOTAL	PRCNT .LT.1	PRCNT .LT.2	TOTAL	PRCNT .LT.1	PRCNT .LT.2	TOTAL	PRCNT .LT.1	PRCNT .LT.2
OCEAN	12859	0.4706	0.9393	18599	0.7448	0.9562	20754	0.9072	0.9895	12844	0.6953	0.9942
LAND	6847	0.6115	0.9845	8649	0.7366	0.9883	7445	0.9631	0.9997	6813	0.8751	0.9952
SNOW	2014	0.2929	0.8466	2684	0.3882	0.9136	13815	0.6588	0.9746	1852	0.7511	0.9028
DESERT	3510	0.3741	0.9593	4414	0.6928	0.9957	4330	0.7353	0.9637	3510	0.5986	0.9635
MIXED LAND/OCEAN	1569	0.6284	0.9834	1962	0.7630	0.9837	1778	0.9758	1.0000	1560	0.8712	0.9974
PARTLY CLOUDY/OCEAN	24460	0.6268	0.9806	31627	0.7834	0.9915	37593	0.9359	0.9984	24109	0.8647	0.9965
PARTLY CLOUDY/LAND	9557	0.6215	0.9861	13250	0.8223	0.9960	9673	0.9984	1.0000	9450	0.8302	0.9934
PARTLY CLOUDY/LAND,OCEAN MIX	2051	0.6465	0.9756	2664	0.7988	0.9921	2048	0.9858	0.9976	2033	0.8667	0.9872
MOSTLY CLOUDY/OCEAN	27406	0.5733	0.9699	35071	0.8521	0.9908	44284	0.9788	1.0000	26619	0.7280	0.9849
MOSTLY CLOUDY/LAND	12305	0.6833	0.9777	16087	0.9166	0.9993	11051	0.9886	0.9987	11751	0.7838	0.9857
MOSTLY CLOUDY/LAND,OCEAN MIX	2406	0.6259	0.9613	3149	0.8892	0.9978	2643	0.9599	0.9974	2277	0.7536	0.9776
COMPLETELY CLOUDY	61367	0.4870	0.9400	78905	0.7903	0.9812	74564	0.7002	0.9405	59882	0.6240	0.9581
	166351	0.5484	0.9585	217061	0.7989	0.9845	229978	0.8518	0.9772	162700	0.7245	0.9771

Note: PRCNT should read fraction. The values of the fractions for less than 1 and 2 cases are shown for surface category and for each classification criterion. Results are shown for day 152 (June 1) and day 153 (June 2) only.

6.4 CONCLUSIONS

The analysis of results with the NCLE models indicates generally that the radiation budget parameters are not affected because of the new models. Scene identification categories have changed as indicated by the cloud amount values computed (section 6.3.1) and the scene reliability fractions (section 6.3.3). But these changes are apparently not enough to change the ERB parameters.

SECTION 7

ANALYSIS FOR AN ADDITIONAL MONTH

Most of the analyses so far have been for the month of June 1979. Extensive studies using several methods are also conducted on certain specific days in the month. This section presents the results for the month of December 1979. Results for SAB are taken from an unpublished report (The Angular Binning Alternatives for Narrow Field-of-View Data Processing, P. Davis and C. Herman, Presented at Nimbus-7 Experiment Team Meeting, May 1984) on the use of SAB for December. Using NCLE models and revised software, the radiation budget parameters are computed.

The target area averaged parameters using SAB are not available to make a consistent comparison at the TA level. So zonal means are used for those parameters that are available from an application of the SAB method.

A comparison of the zonal means of instantaneous albedo using SAB and MLE (NCLE) methods is shown in Figure 7.1. The MLE (NCLE) method is the MLE method which uses improved (NCLE) angular models and modified scene selection algorithm. Also shown, beside the figure, are the zonal mean instantaneous albedo values with the NCLE and SAB methods for each of the 40 latitude bands. NCLE in the figure refers to the MLE (NCLE) method as described above.

Shown in Figure 7.2 are the total emitted flux comparisons between the two cases. The zonal mean total longwave fluxes from the two methods are

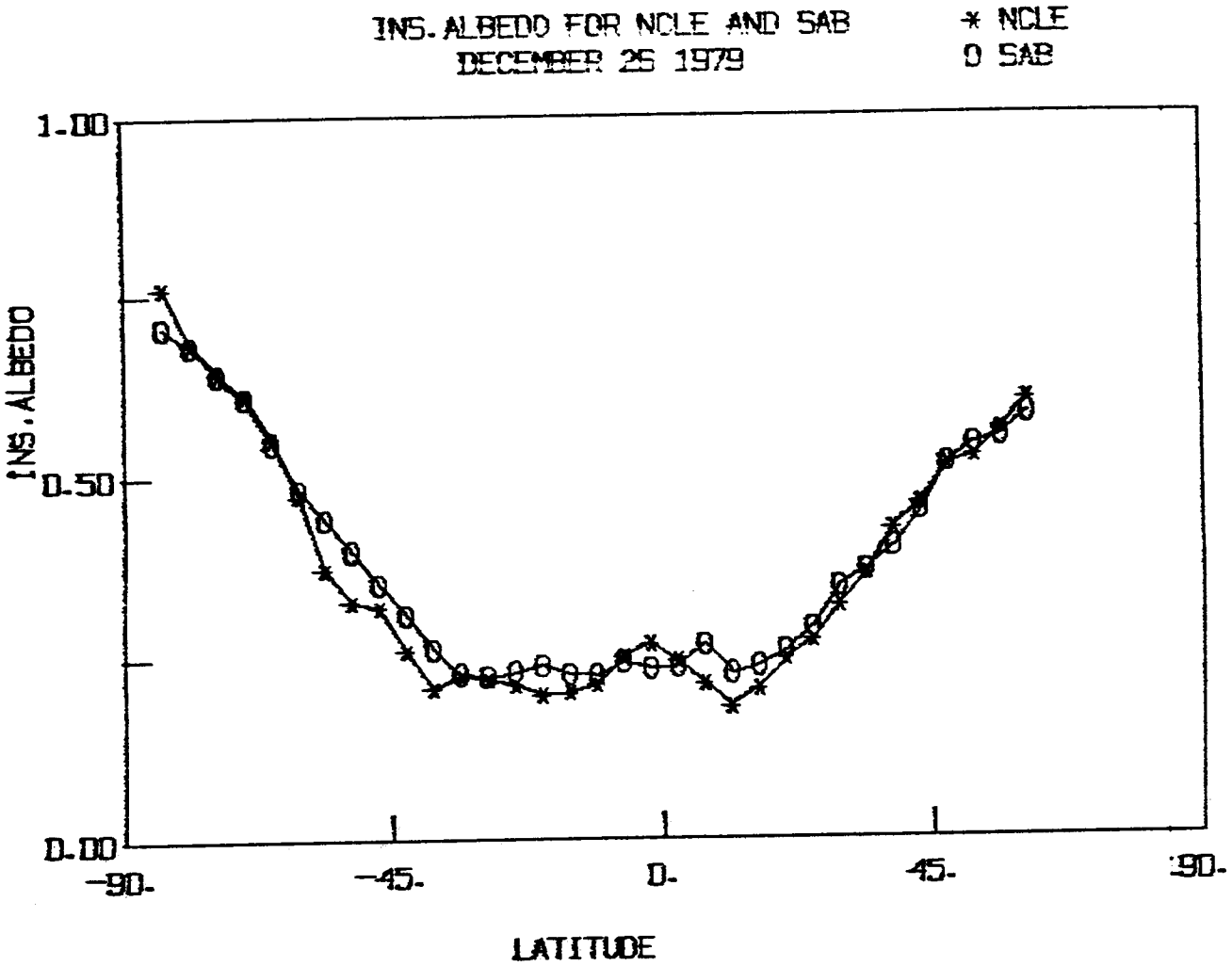

LATITUDE	NCLE	SAB
-87.75	0.0000	0.7130
-83.25	0.7626	0.7080
-78.75	0.6853	0.6820
-74.25	0.6457	0.6420
-69.75	0.6148	0.6100
-65.25	0.5551	0.5490
-60.75	0.4764	0.4830
-56.25	0.3744	0.4420
-51.75	0.3293	0.3990
-47.25	0.3216	0.3530
-42.75	0.2620	0.3110
-38.25	0.2095	0.2630
-33.75	0.2264	0.2290
-29.25	0.2217	0.2250
-24.75	0.2141	0.2320
-20.25	0.2008	0.2400
-15.75	0.2034	0.2280
-11.25	0.2146	0.2270
-6.75	0.2538	0.2450
-2.25	0.2702	0.2360
2.25	0.2473	0.2380
6.75	0.2156	0.2680
11.25	0.1829	0.2290
15.75	0.2081	0.2390
20.25	0.2494	0.2600
24.75	0.2742	0.2910
29.25	0.3230	0.3480
33.75	0.3660	0.3710
38.25	0.4277	0.4020
42.75	0.4623	0.4520
47.25	0.5153	0.5170
51.75	0.5269	0.5430
56.25	0.5643	0.5540
60.75	0.6064	0.5840
65.25	0.0000	0.0000
69.75	0.0000	0.0000
74.25	0.0000	0.0000
78.75	0.0000	0.0000
83.25	0.0000	0.0000
87.75	0.0000	0.0000

FIGURE 7.1 Zonally averaged instantaneous albedo comparison using SAB and MLE-NCLE methods. Data during December 1979 are used. Zonal averages are shown in the table at right.

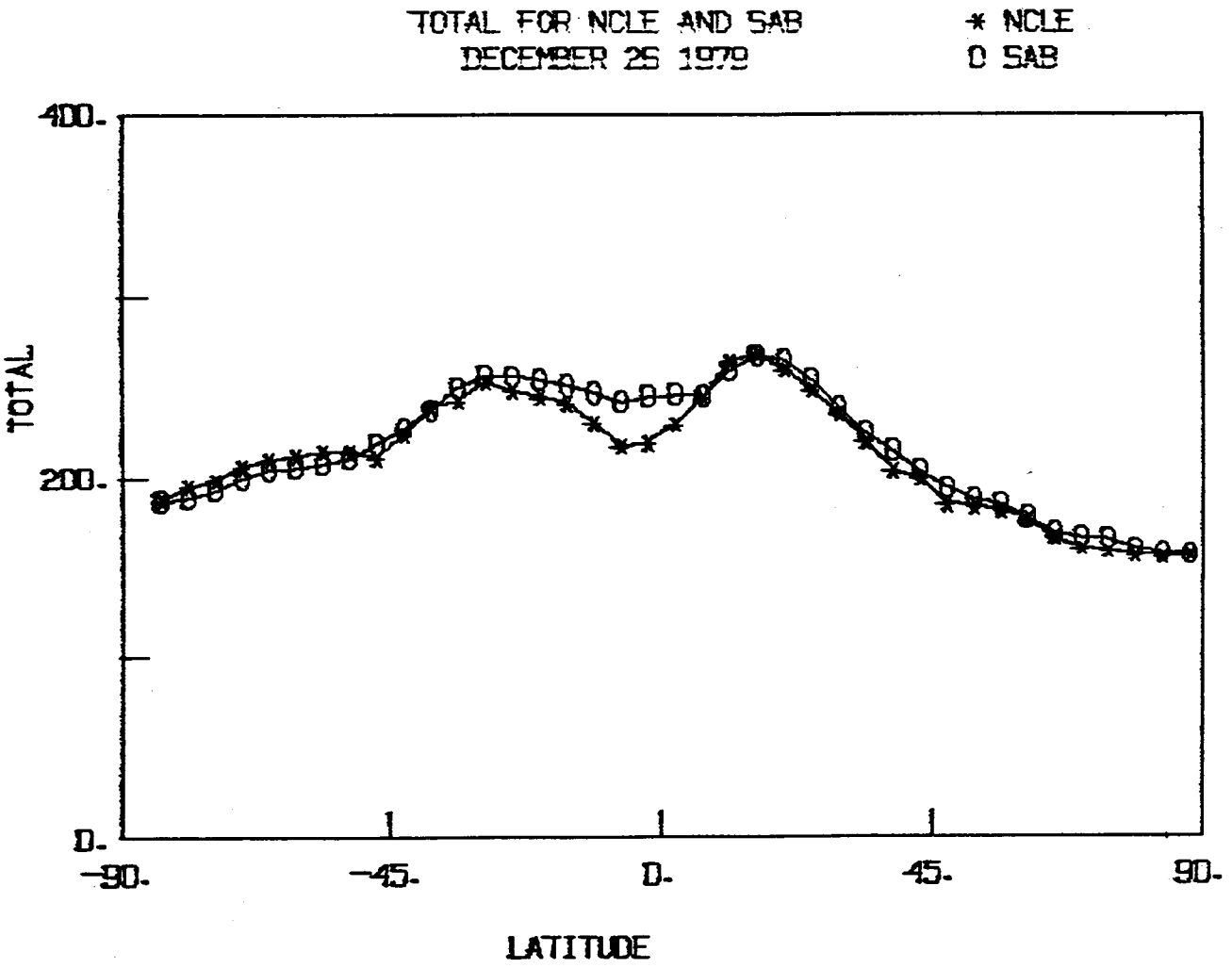

LATITUDE	NCLE	SAB
-87.75	0.0000	185.8000
-83.25	187.5601	187.0000
-78.75	194.9456	188.8000
-74.25	198.7158	193.0000
-69.75	206.1997	199.2000
-65.25	209.9572	204.5000
-60.75	212.1175	206.0000
-56.25	214.3695	207.7000
-51.75	213.9315	211.0000
-47.25	211.0967	218.2000
-42.75	223.6109	226.7000
-38.25	239.1287	237.3000
-33.75	242.5770	249.2000
-29.25	252.4596	256.0000
-24.75	247.9706	255.2000
-20.25	244.4796	253.7000
-15.75	241.1911	250.6000
-11.25	230.2955	246.6000
-6.75	217.3831	241.7000
-2.25	219.1583	244.9000
2.25	229.4076	246.0000
6.75	244.0994	244.7000
11.25	264.1121	258.8000
15.75	268.8342	267.3000
20.25	259.5857	264.6001
24.75	248.5991	254.0000
29.25	235.5629	238.5000
33.75	219.6382	225.0000
38.25	203.9977	214.9000
42.75	199.8177	203.9000
47.25	185.2717	194.1000
51.75	183.6678	187.6000
56.25	181.7597	184.9000
60.75	177.3848	178.0000
65.25	166.9197	169.5000
69.75	160.5637	166.9000
74.25	158.7287	165.9000
78.75	156.2992	160.2000
83.25	155.1654	157.5000
87.75	156.8603	156.6000

FIGURE 7.2 Total (day-night average) longwave flux zonal means using SAB and MLE-NCLE methods.

also listed. Values for the daytime and nighttime longwave flux from the SAB are not available. A comparison between those cannot be made at this point. Also to be noted is that the MLE results are for December 26, 1979. A full length comparison and analysis should be made after the complete SAB dataset is developed.

SECTION 8

PERPENDICULAR BISECTOR ALGORITHM

A statistical approach simpler than the MLE method is the use of a perpendicular bisector algorithm. This is based upon the distance of the observed point in the visible-IR radiance space from the radiance means for the appropriate bins. This is accomplished by replacing the ellipses by circles of equal radius for all scene types, viz., land, partly cloudy over land, mostly cloudy over land, and overcast, for example. The standard deviations for all the bins are accordingly set to a uniform value of 100. The value is independent of the viewing angle combination and also independent of the underlying scene type.

The MLE algorithm uses the standard deviations in the visible and IR. When these values are equal to each other, the ellipse representing the ensemble of observations becomes a circle in the visible-IR radiance space. The correlation coefficient is therefore set equal to zero. For the purposes of this study, three distinct cases are considered.

Case 1: $\sigma_{SW}, \sigma_{LW} = 100$; COR = 0.0

Case 2: $\sigma_{SW}, \sigma_{LW} = 100$

Case 3: $\sigma_{SW}, \sigma_{LW} = 1000.$

8.1 GLOBAL MEAN PARAMETERS

The effect of using a perpendicular bisector to classify the scene type on the radiation budget parameters is investigated for four days in the month

of June 1979. The days analyzed are June 1, June 10, June 20, and June 30. The comparison is performed with the results of NCLE. Table 8.1 presents the global mean results for the three cases outlined in section 8, along with the NCLE case. It is apparent that the global means are not very sensitive to the changes in the standard deviation. At the global scale, the perpendicular bisector method yields results which are essentially identical to the use of MLE method. Results for the other days (June 10, 20, and 30) are computed for cases 2 and 3 only and are also shown in the table.

8.2 ZONAL AVERAGES

Zonal means of instantaneous albedo, daytime, nighttime, and total longwave fluxes are computed for the three cases mentioned above. Differences in the zonal means between these cases and the NCLE case are shown in a series of figures. Figure 8.1a, b and c shows the instantaneous albedo differences for case 1, case 2 and case 3 respectively. COL100, LW100, and LW1000 on the ordinate refer to case 1, case 2, and case 3. In case 1, the albedo differences are very small, indicating that use of the appropriate standard deviation for each bin and the corresponding correlation coefficient has not significantly changed the zonal mean instantaneous albedo values. In cases 2 and 3, where the actual correlation coefficients are used, the albedo differences are higher. Also, note that the larger the standard deviation used (σ_{SW}, σ_{LW} = 100 or 1000), the larger are the differences. In the neighborhood of the North Pole, both of them show a negative value for the difference. This is the region where the scene

TABLE 8.1 Global Mean Instantaneous Albedo and LW Fluxes for the Three Cases Mentioned in Section 8. Case 1 corresponds to the perpendicular bisector algorithm and results are shown for June 1.

	NCLE	CASE 1	CASE 2	CASE 3
June 1, 1979				
Ins. Albedo	0.2838	0.2832	0.2821	0.2810
LW Flux (Day)	237.7320	237.7133	237.6419	237.6387
LW Flux (Night)	222.8179	222.8435	222.8428	222.8470
LW Flux (Total)	230.0783	230.0834	230.0467	230.0432
June 10, 1979				
Ins. Albedo	0.2821		0.2807	0.2791
LW Flux (Day)	240.4142		240.3161	240.3104
LW Flux (Night)	224.9382		224.9677	224.9707
LW Flux (Total)	232.8567		232.8140	232.8060
June 20, 1979				
Ins. Albedo	0.2879		0.2861	0.2856
LW Flux (Day)	239.5011		239.3913	239.3816
LW Flux (Night)	224.3380		224.3946	224.3981
LW Flux (Total)	232.7540		232.7252	232.7138
June 30, 1979				
Ins. Albedo	0.2808		0.2795	0.2790
LW Flux (Day)	240.7985		240.6920	240.6922
LW Flux (Night)	225.5027		225.5554	225.5583
LW Flux (Total)	232.8135		232.7892	232.7894

C-2

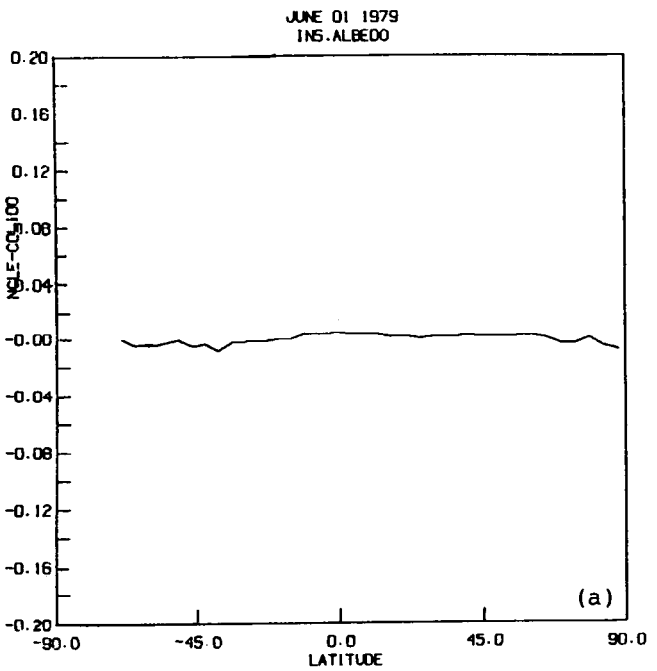

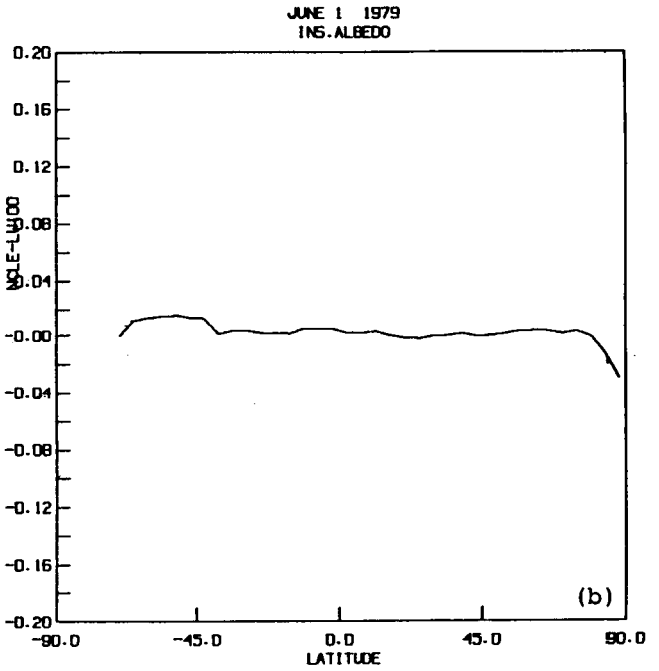

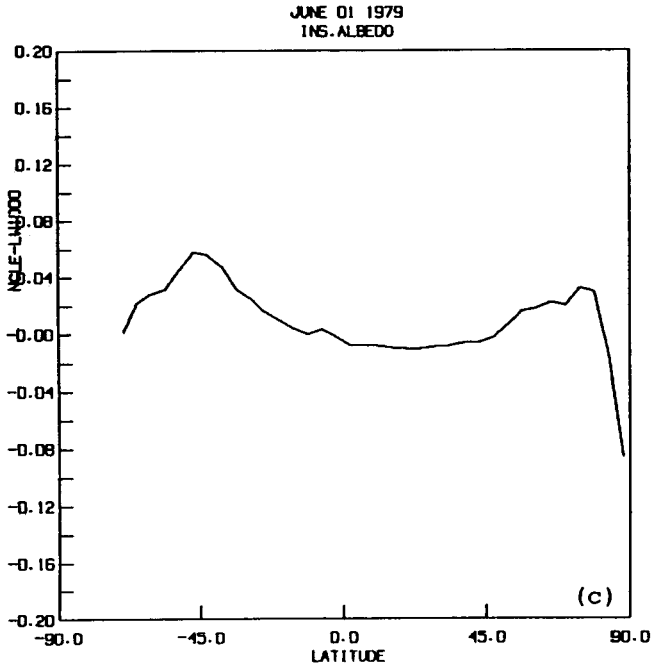

FIGURE 8.1 Zonally averaged instantaneous albedo differences between MLE-NCLE case and (a) the perpendicular bisector algorithm case (case 1), (b) modified algorithms (case 2), and (c) case 3.

selection is based upon shortwave only radiances and the value of correlation coefficient is not relevant to this case. Apparently, the magnitude of the standard deviation does have an effect on the scene and thus the albedo.

Daytime longwave fluxes are shown in Figure 8.2a,b,c for the three cases. The mean difference in 8.2,a is near 0.1 W/m^2 consistent with the values in Table 8.1. When the condition on correlation coefficient is removed the longwave flux differences during daytime are larger; but in all cases, the differences do are most of the time smaller than 1.0 W/m^2. Figure 8.3a,b,c shows the nighttime longwave flux differences. These values range between -0.2 and +0.2 W/m^2 except near the South Pole, where the difference is about 0.8 W/m^2. In this region, all the plots show identical differences, indicating that the scene selection here using longwave only is not sensitive to the value of the standard deviation. This is in contrast to the albedo difference variation near the North Pole discussed earlier. The results for the total longwave flux differences are shown in Figure 8.4a,b,c. For case 1, the differences are of the order of 0.1 W/m^2 while for cases 2 and 3, the values are larger, but the maximum difference is of the order of 1 W/m^2.

8.3 TARGET AREA COMPARISONS

The instantaneous albedo values for case 1 and the NCLE run are compared in Figure 8.5a. The parameters of the linear regression are shown in the figure. The correlation coefficient R is extremely high (0.999) and the RMS difference is 0.0081. The daytime, nighttime and total longwave flux comparisons are shown in Figure 8.5b,c,d, and indicate extremely high correlation between the results with the perpendicular bisector algorithm and

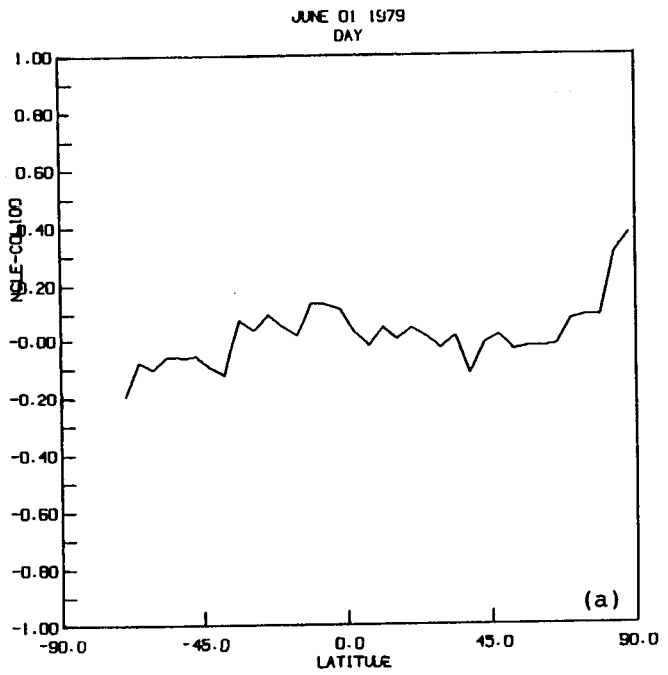

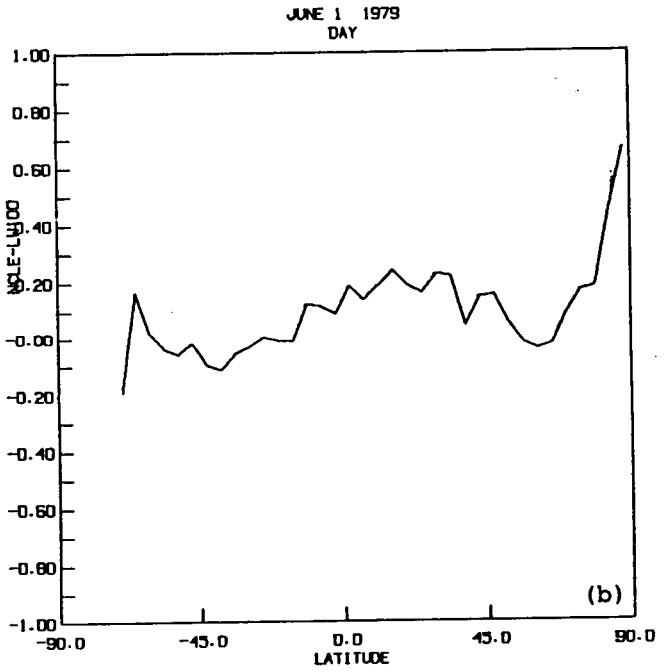

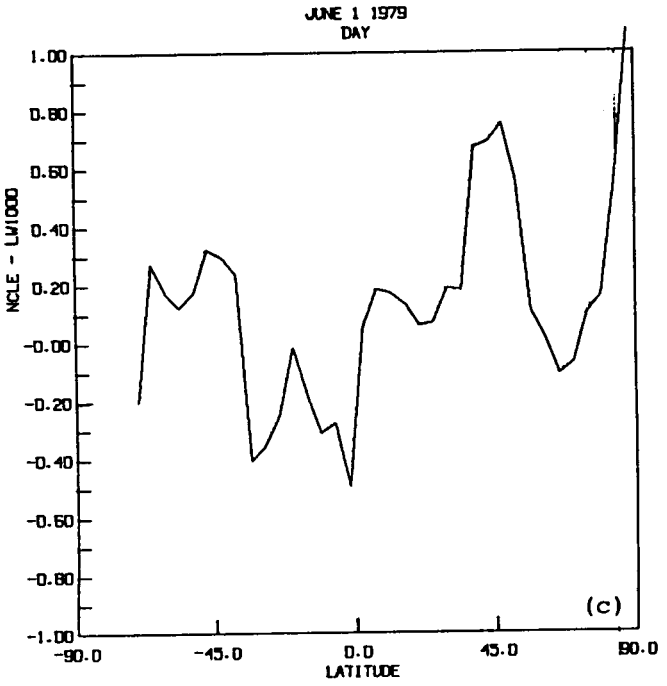

FIGURE 8.2 Zonally averaged daytime longwave flux differences between MLE-NCLE case and (a) the perpendicular bisector algorithm case (case 1), (b) modified algorithms (case 2), and (c) case 3.

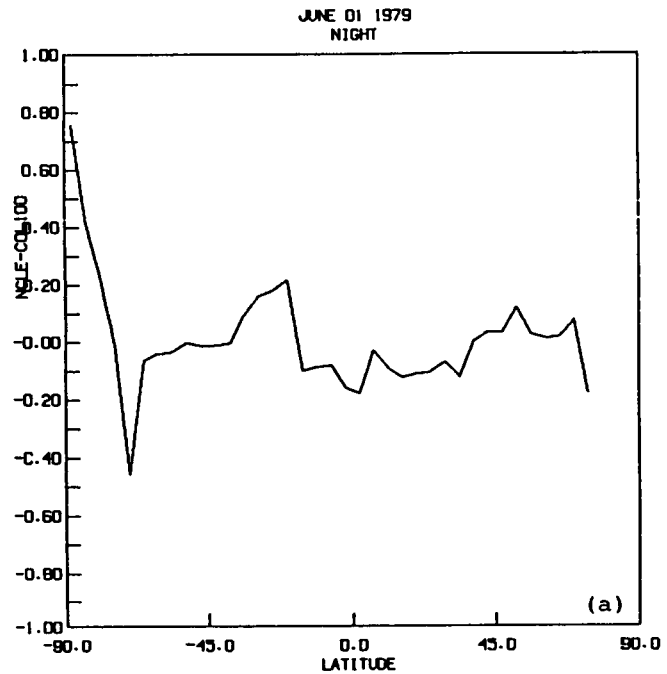

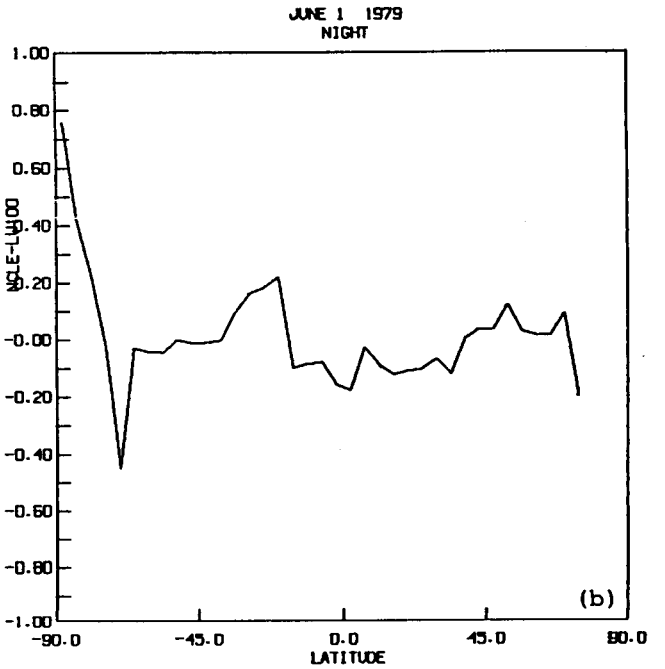

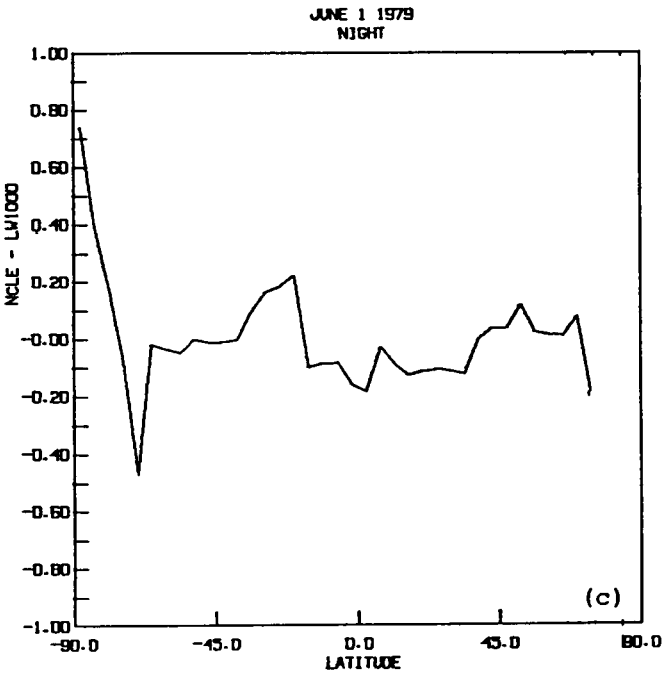

FIGURE 8.3 Zonally averaged nighttime longwave flux differences between MLE-NCLE case and (a) the perpendicular bisector algorithm case (case 1), (b) modified algorithms (case 2), and (c) case 3.

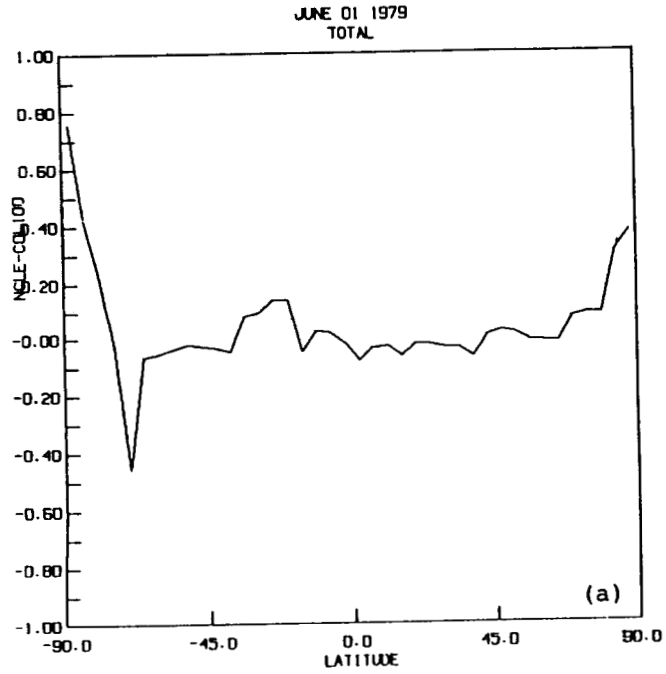

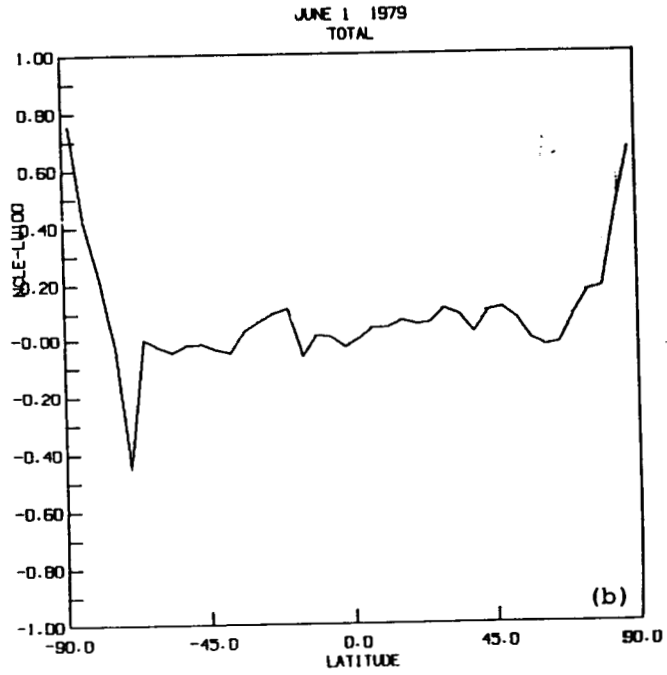

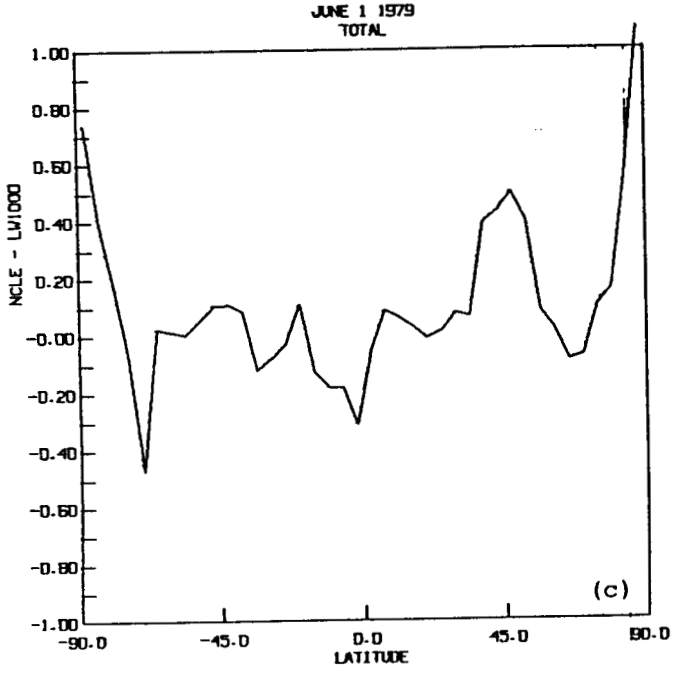

FIGURE 8.4 Zonally averaged day, night average (total) longwave flux differences between MLE-NCLE case and (a) the perpendicular bisector algorithm case (case 1), (b) modified algorithms (case 2), and (c) case 3.

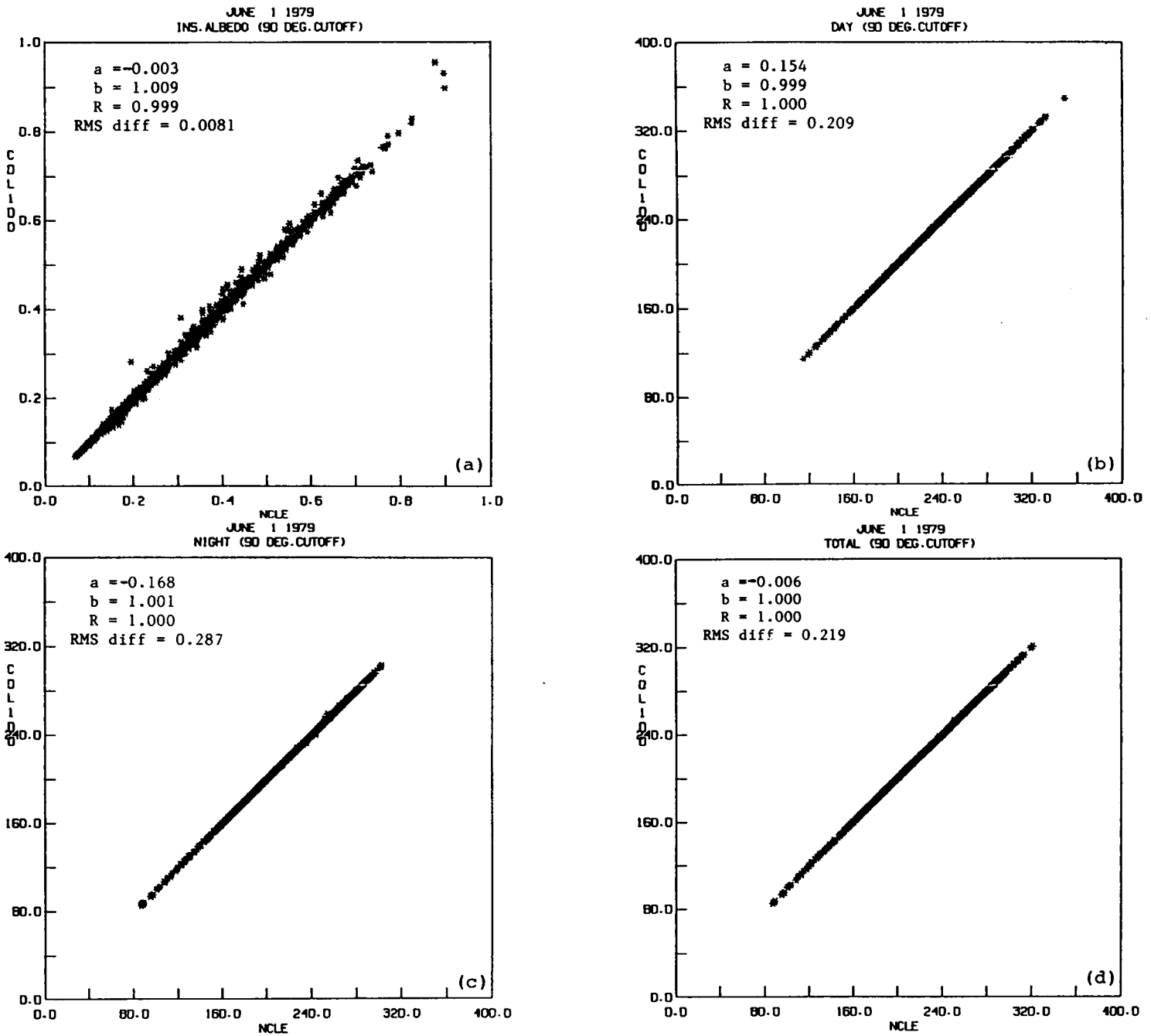

FIGURE 8.5 Linear regression plot of (a) instantaneous albedo using case 1 with MLE-NCLE case, (b) daytime longwave flux, (c) nighttime longwave flux, and (d) total longwave flux.

the MLE method. The RMS differences in this case are of the order of 0.2 to 0.3 W/m^2.

All the above results indicate very little effect, if any, on the computed radiation budget parameters due to the use of perpendicular bisector algorithms instead of the MLE method. The TA means tend to be nearly the same. Figure 8.6,a shows the differences in the individual reflected flux values for the ocean TA 662 with about 100 observations. The fractional change in instantaneous albedo is shown in Figure 8.6,b. Many of the higher albedo estimates with the perpendicular bisector method (CORCCOL100) are of the order of 20% to 30%. The 150% increase for one flux value using case 1 is apparently because of the choice of a more cloudy scene.

Results for a land and a desert TA are shown in Figure 8.7 and 8.8. TA 889, with land as the underlying surface, experienced decreases in instantaneous albedo up to 0.05 (Fig. 8.7,a). Fractional increases in the computed albedo are shown in Figure 8.7b. The decreases in instantaneous albedo are as high as 20% to 25% compared to the NCLE case. We also note that ocean generally experienced an increase, while land shows a decrease. The results for the desert TA 1418 show (Fig. 8.8,a) that several of the individual albedos are larger when case 1 is used, thus indicating an increase in desert albedo with the new method. The increases, however, do not exceed 0.03 or about 11% of the NCLE values. Fractional changes for desert are shown in Figure 8.8b.

Results for the emitted flux are shown in Figure 8.9 for a snow TA 25 and for ocean TA 662 in Figure 8.10. For TA 25, the changes in the emitted

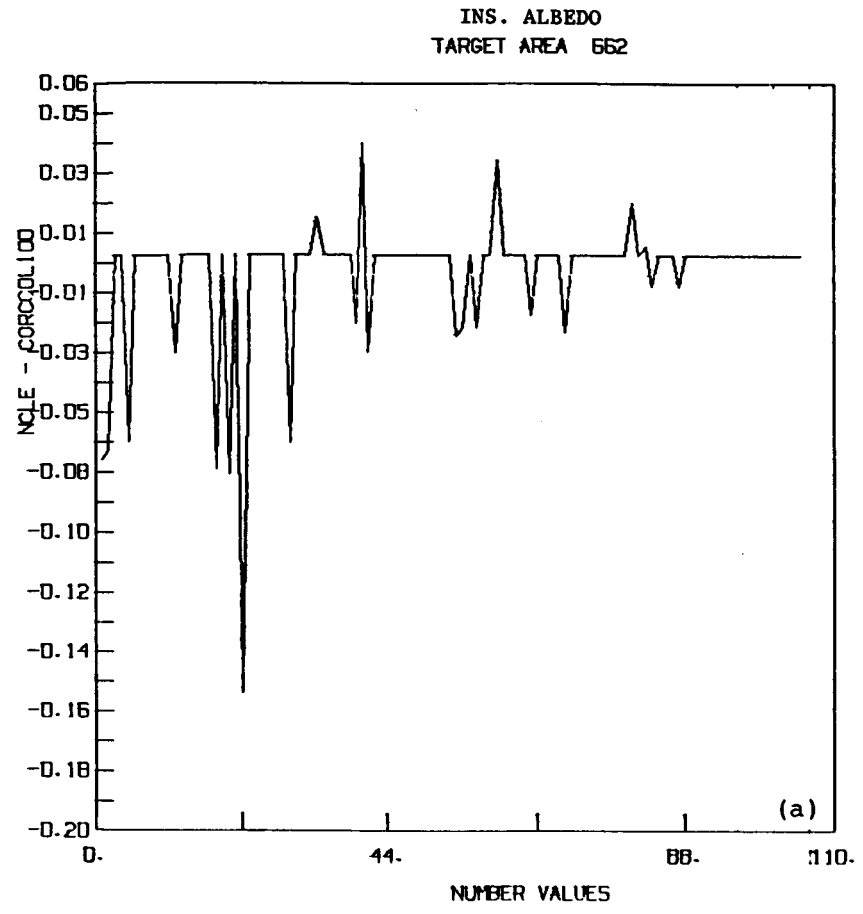

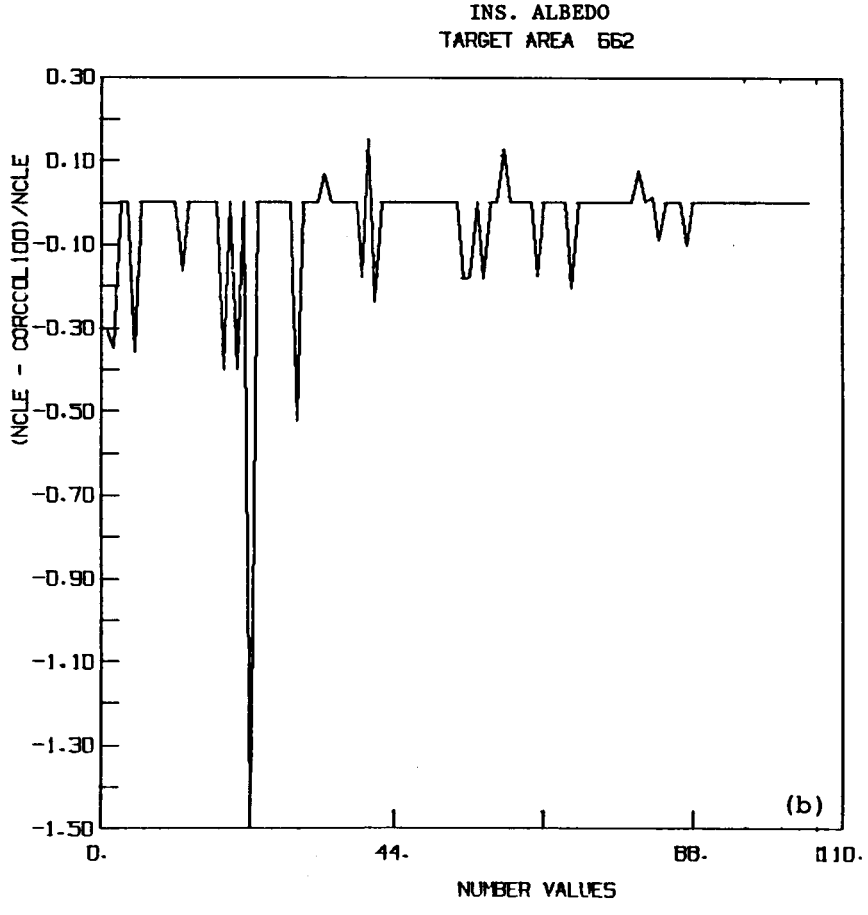

FIGURE 8.6 Differences in individual estimates of instantaneous albedo from radiance observations for TA 662 using MLE-NCLE and case 1. (a) Instantaneous albedo differences; (b) normalized differences.

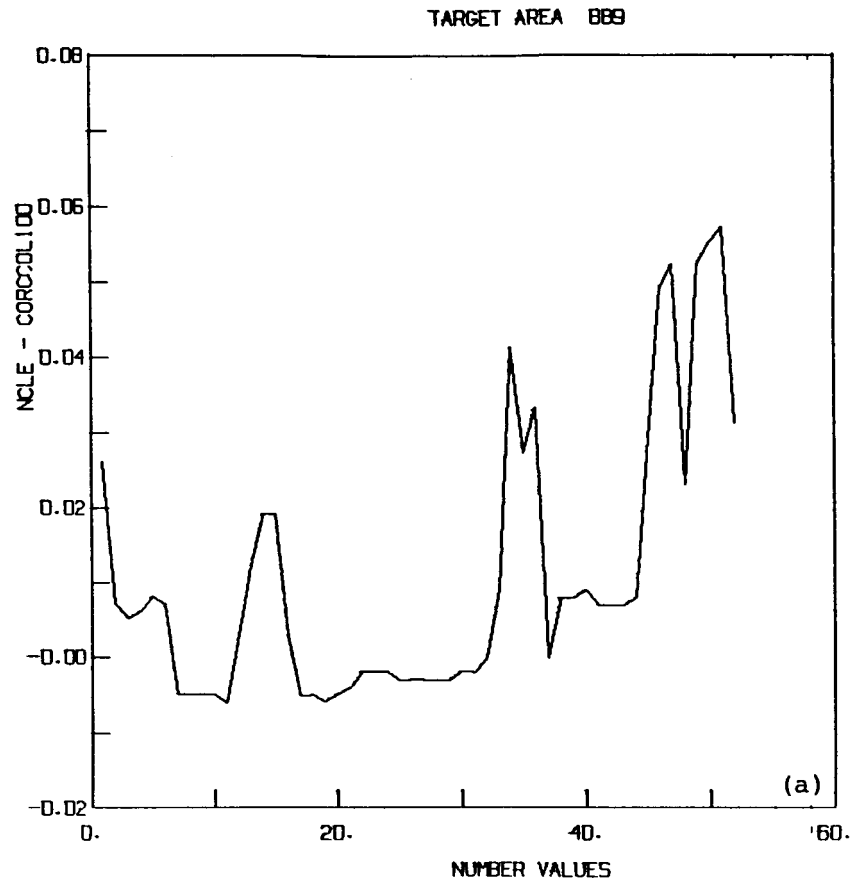

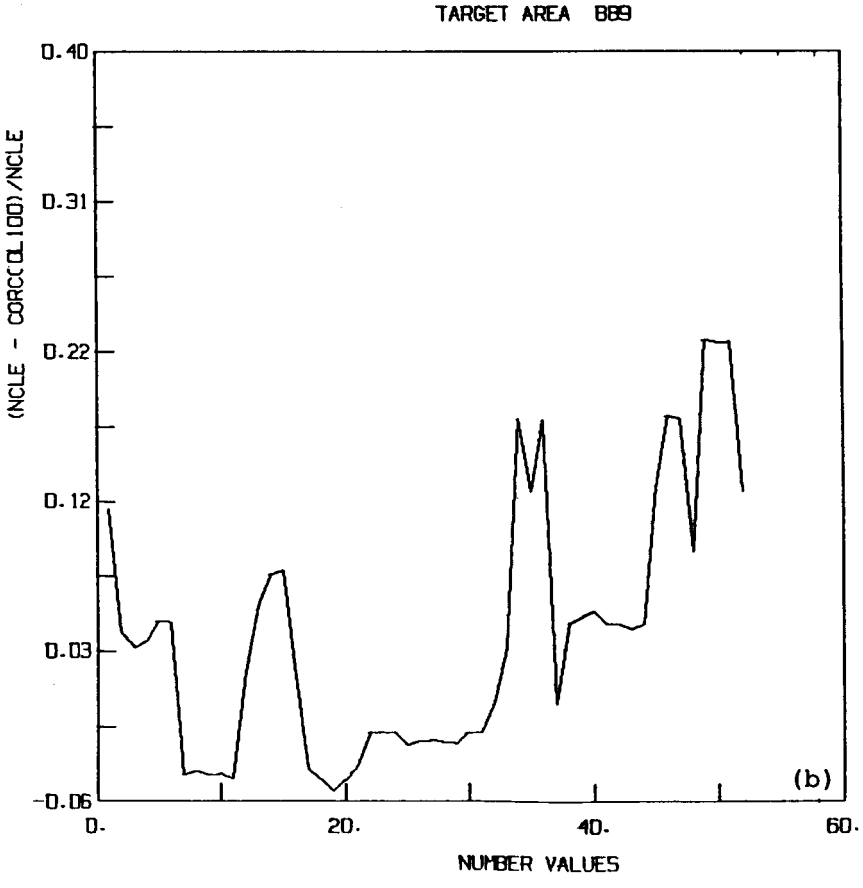

FIGURE 8.7 Differences in individual estimates of instantaneous albedo from radiance observations for TA 889 using MLE-NCLE and case 1. (a) Instanteous albedo differences; (b) normalized differences.

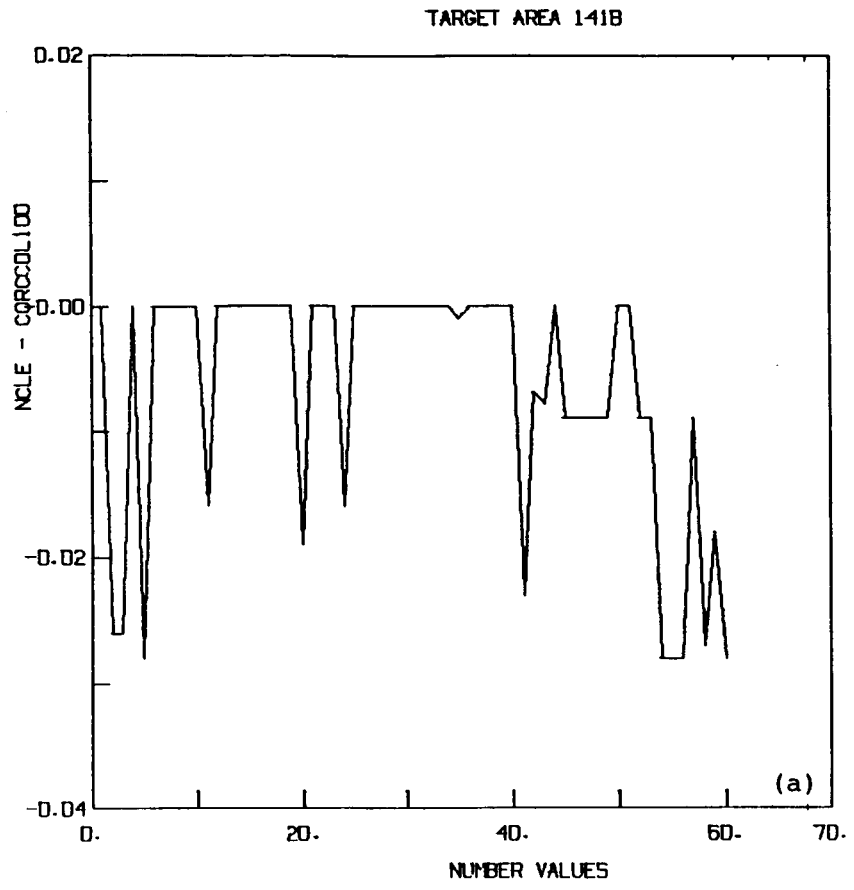

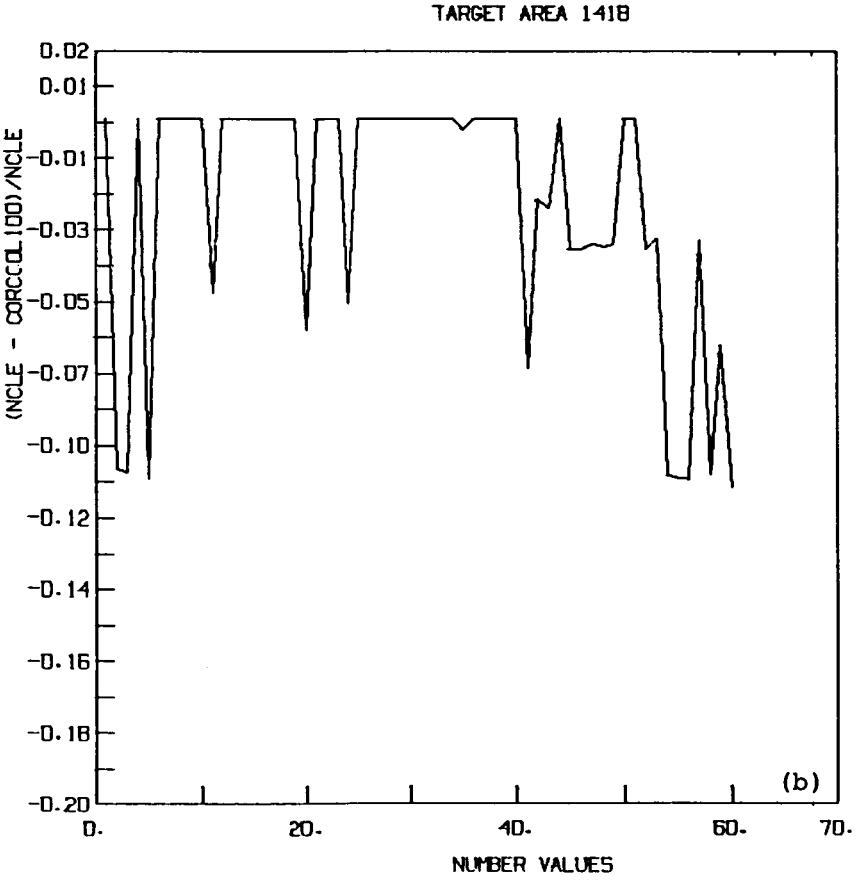

FIGURE 8.8 Differences in individual estimates of instantaneous albedo from radiance observations for TA 1418 using MLE-NCLE and case 1. (a) Instantaneous albedo differences; (b) normalized differences.

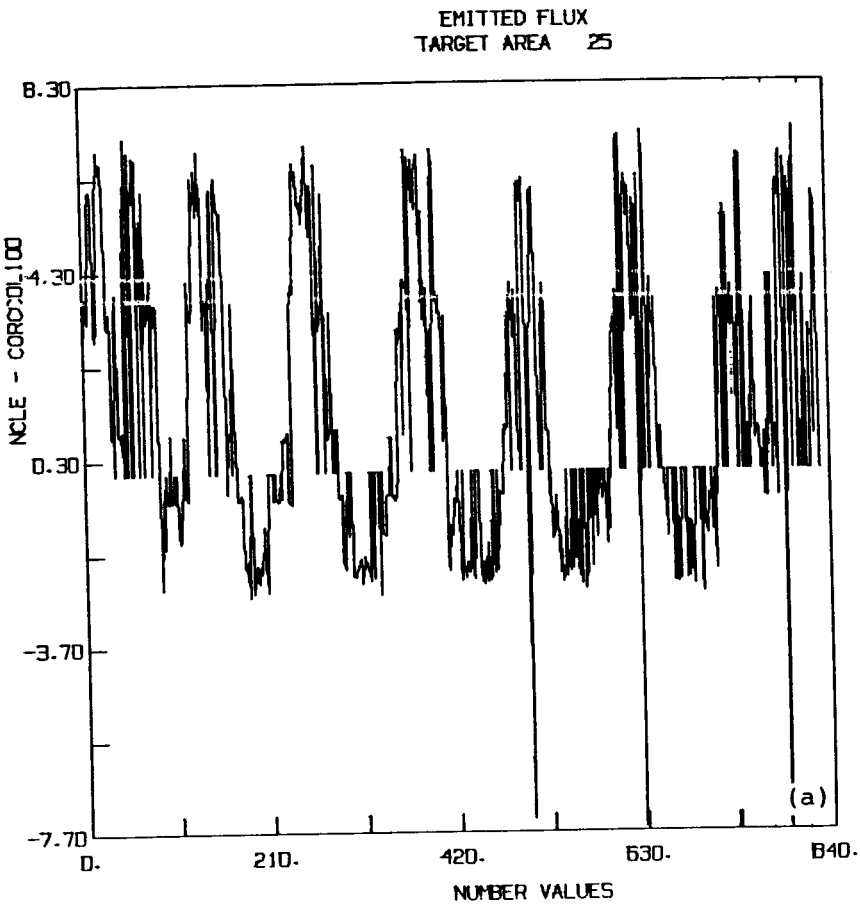

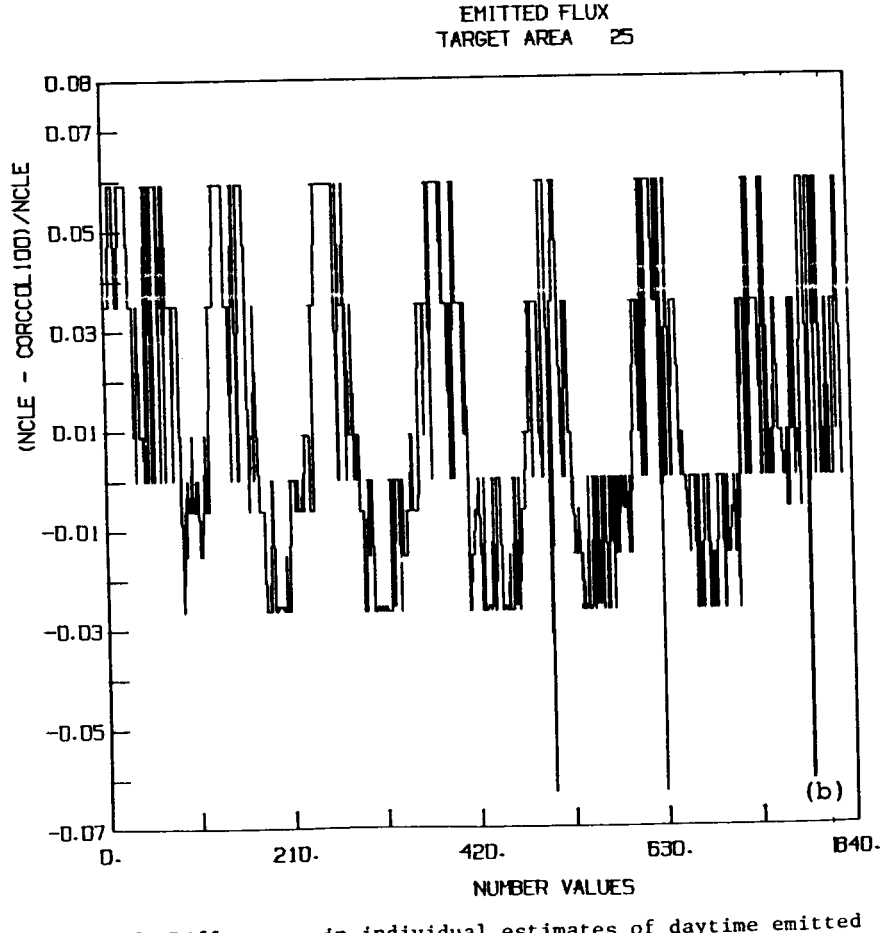

FIGURE 8.9 Differences in individual estimates of daytime emitted longwave flux from radiance observations for TA 25 using MLE-NCLE and case 1. (a) Longwave flux differences; (b) normalized longwave flux differences.

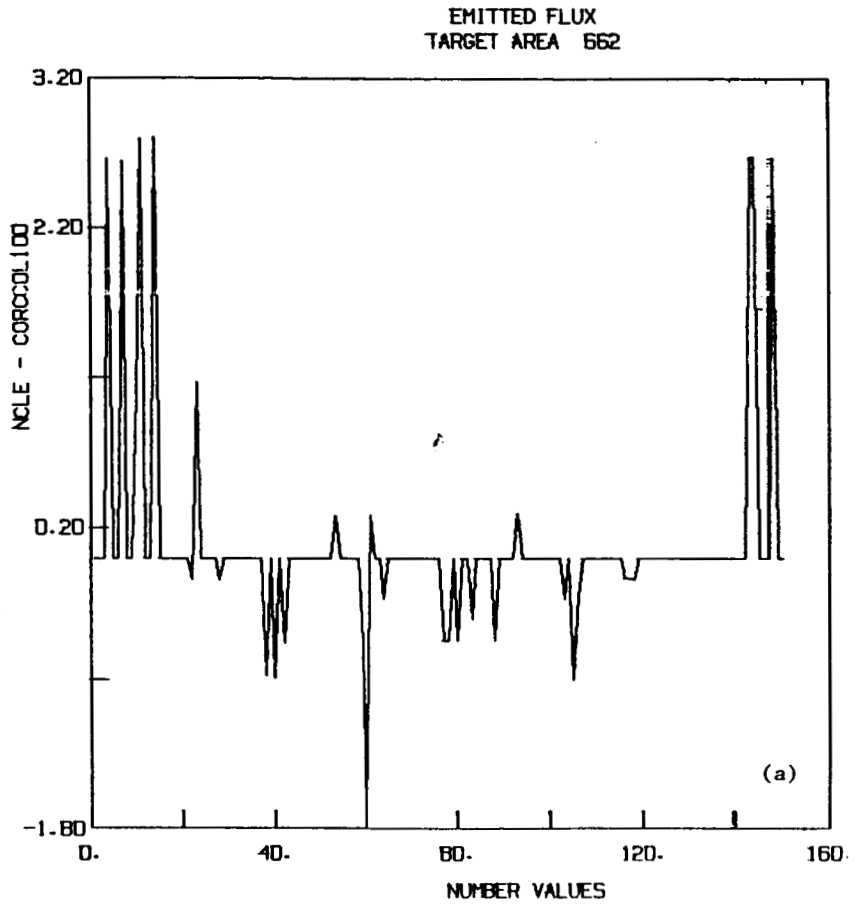

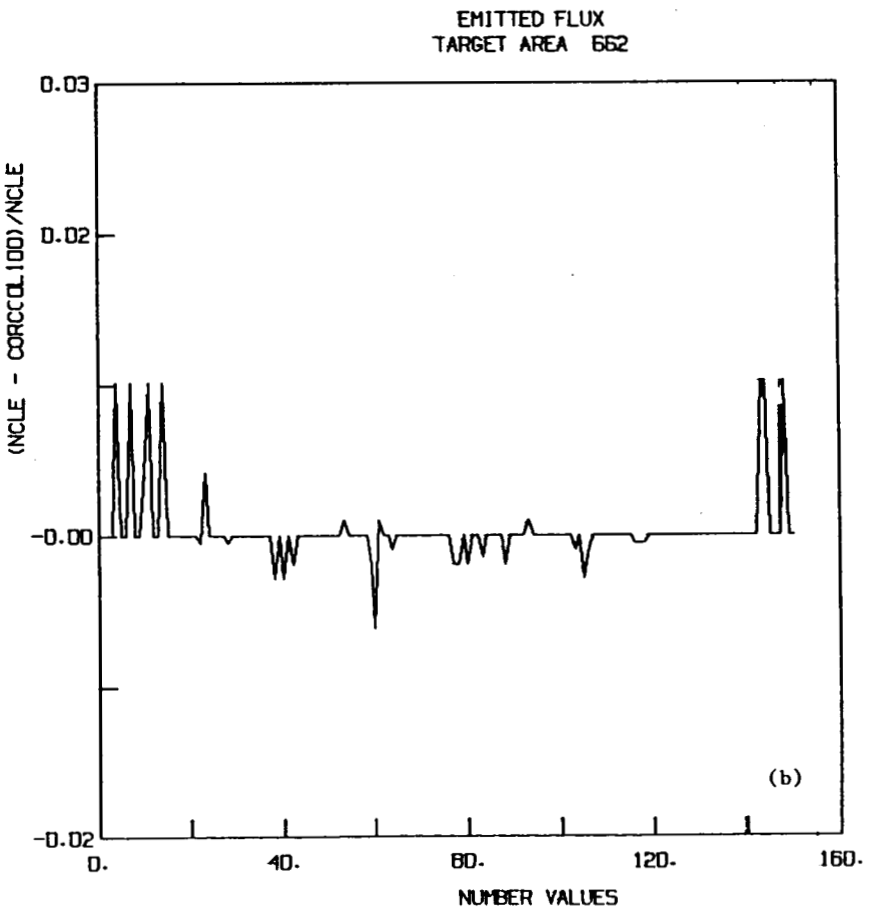

FIGURE 8.10 Difference in individual estimates of daytime emitted longwave flux from radiance observations for TA 662 using MLE-NCLE and case 1. (a) Longwave flux differences; (b) normalized longwave flux differences.

flux are of the order of about 5 to 6 W/m^2 and correspond to differences of at the most 6% (Fig. 8.9,b). Over the ocean (TA 662), emitted flux differences are 3 W/m^2 or less (Fig. 8.10,a) corresponding to about 1% difference from the NCLE case (Fig. 8.10,b).

8.4 CONCLUSIONS

The use of perpendicular bisector algorithm has not significantly altered the radiation budget parameters, when it is done consistently. Instantaneous albedo and longwave flux values experience very minor changes at the global, zonal, and even TA spatial scales. The differences in scene identification are apparent only when considering the individual flux estimates for a TA from radiance values. At that sampling level, some significant differences appear and also some biases depending upon the underlying surface being land, ocean, desert, etc.

SECTION 9

VALIDATION OF SCENE SELECTION

Proper identification of scene using radiance measurements from satellites is a crucial aspect in the estimation of Earth radiation budget parameters. Since the underlying scene (geography) at the surface is known, this determination is primarily to pick out the presence of cloud and its amount in the path of the radiances. A large number of techniques are presently used for this cloud identification. An intercomparison of six methods, two from each of three groups, viz., threshold methods, radiative transfer methods and data clustering methods, is presented in Rossow et al. (1985) as part of a continuing program on cloud analysis techniques under the auspices of the international satellite cloud climatology program (ISCCP). In the present work, our attempt is to validate the cloud amounts retrieved using scanner observations from the Earth Radiation Budget instrument on Nimbus-7, with other available cloud datasets for the same period. While the cloud amounts derived from ERB agree very well with those from THIR, we note an interesting agreement between the cloud fields derived from ERB using shortwave radiances only with those derived from longwave channels from HIRS2/MSU.

9.1 BRIEF DESCRIPTION OF THE METHOD

The Earth Radiation Budget experiment aboard the Nimbus-7 satellite included three separate groups of sensors. One group consisted of ten sensors to monitor the solar flux and a second group of four sensors was

intended to monitor the earth flux as seen at the satellite. The third group which is of interest here consisted of the narrow-field of view (NFOV) sensors with four telescopes to view the radiation emerging from the top of the atmosphere and to measure the shortwave (0.2 - 4.8 μm) and the longwave (4.5 - 50.0 μm) radiances by using spectral filters (Jacobowitz et al., 1984). Each radiance pair measured by the telescopes is compared with clear sky radiances and based upon empirical models of bidirectional reflectance, and is classified as clear (0-5% cloudiness), partly cloudy (5-50% cloudiness), mostly cloudy (50-95% cloudiness), or overcast (95% and above cloudiness). The method of maximum likelihood estimation (MLE) is used for this classification (Smith et al., 1986). It is based upon determining the probability density function for each of the four cloud cover categories from the measured radiance pair and assigning the cloud cover with the maximum probability density function. During daytime both the shortwave and longwave radiances are used, while at night, only longwave radiance is used. The cloud amount derived this way is referred to as the CSL cloud amount. When only longwave radiance is used both day and night, the cloud amount is called the CL cloud amount. Shortwave radiances only may be used leading to the CS cloud amount but this is only determined during daytime.

9.2 COMPARISON OF RESULTS

ERB measured radiances for the month of June 1979 have been used to derive cloud amounts with the three methods, viz., LW only, SW only and LW and SW together. The cloud amounts obtained with the longwave and shortwave together show very good agreement with the cloud amounts derived from THIR

(Figures 9.1 and 9.2). The THIR cloud amounts used in the present comparisons are the ones which are improved using the ultraviolet reflectances from total ozone mapping spectrometer (TOMS) on Nimbus-7 (Stowe et al., 1986). The zonal mean cloudinesses for June 20 are shown in Figure 9.3. The three figures show the very good agreement between the cloud amounts derived from ERB using the shortwave and longwave and the THIR/TOMS cloud amount values.

The effect of decreasing cloud amounts using shortwave only (CS), longwave only (CL) and shortwave and longwave together (CSL) is shown in Figure 9.4. The solid line represents the CSL cloud amount, the dashed and dotted lines represent the CS and CL amounts respectively. The CL and CSL cases follow close together with CL giving slightly higher values in the intertropical convergence zone (ITCZ). The CS cloud amount differs significantly from the other two, with the largest differences (80% versus 55%) in the ITCZ. Both the cloud amount and the spatial extent of the ITCZ are smaller in the CS picture.

The cloud amount derived from HIRS2/MSU (Susskind et al., 1986) for the same month are shown in Figure 9.5. Also shown are the cloud amount for ERB (CSL) and THIR/TOMS. HIRS2/MSU values show a systematic difference relative to the other two. The derived cloud amount near the ITCZ is nearly half of the cloud amount value from the other two. In spite of the differences, these two cloud amount values show much better agreement than those with CSL, CL or THIR.

HIRS2/MSU cloud amounts are the effective cloud amount values (Susskind et al., 1986) and as such incorporate the cloud emissivity ε. In the presence

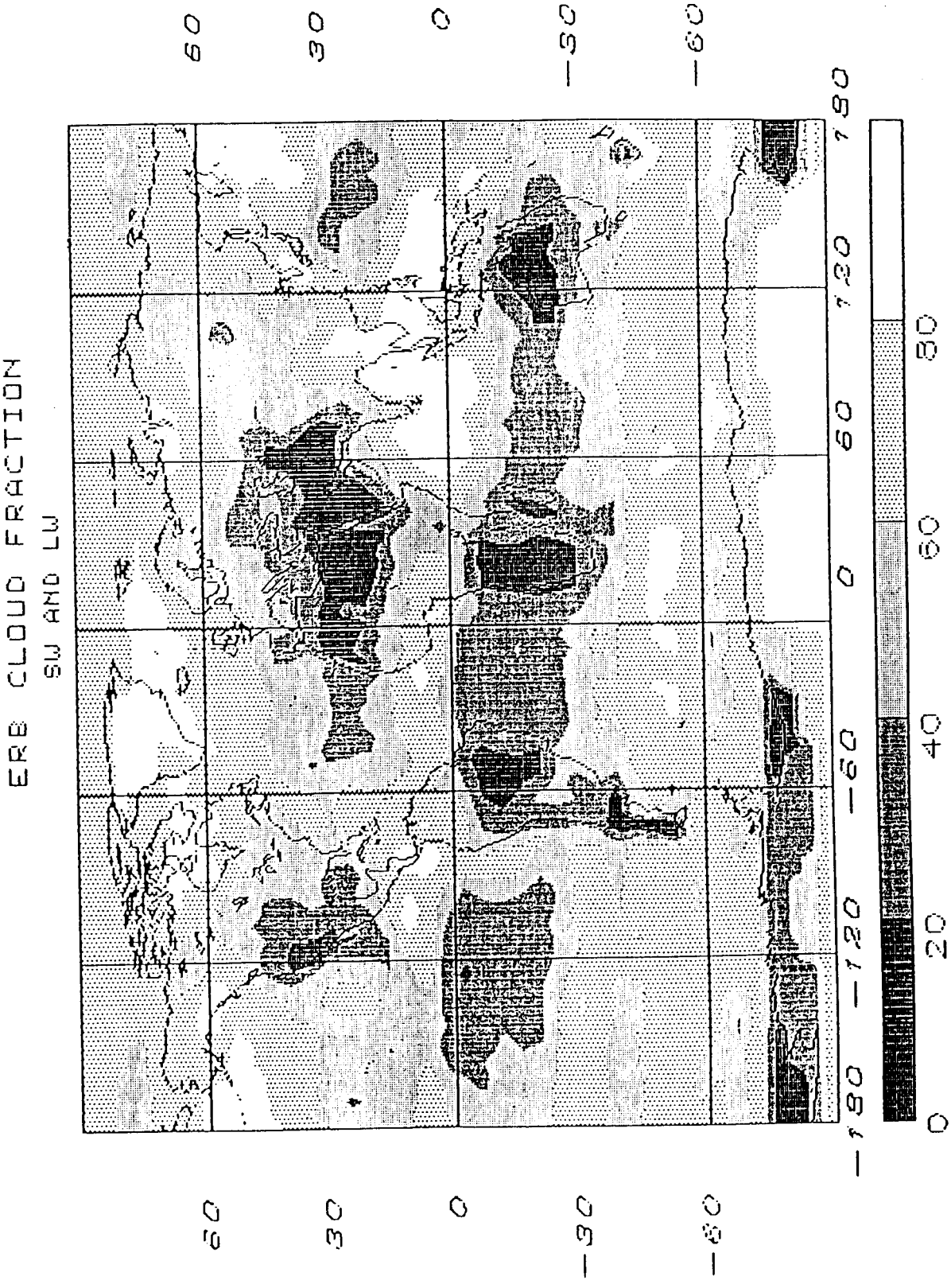

FIGURE 9.1 Global distribution of monthly mean daytime cloud fractions derived using Nimbus-7 ERB scanner observations for June 1979. This is referred to as CSL cloud amount in the text. Both shortwave and longwave radiances are used. The color code is shown at the bottom.

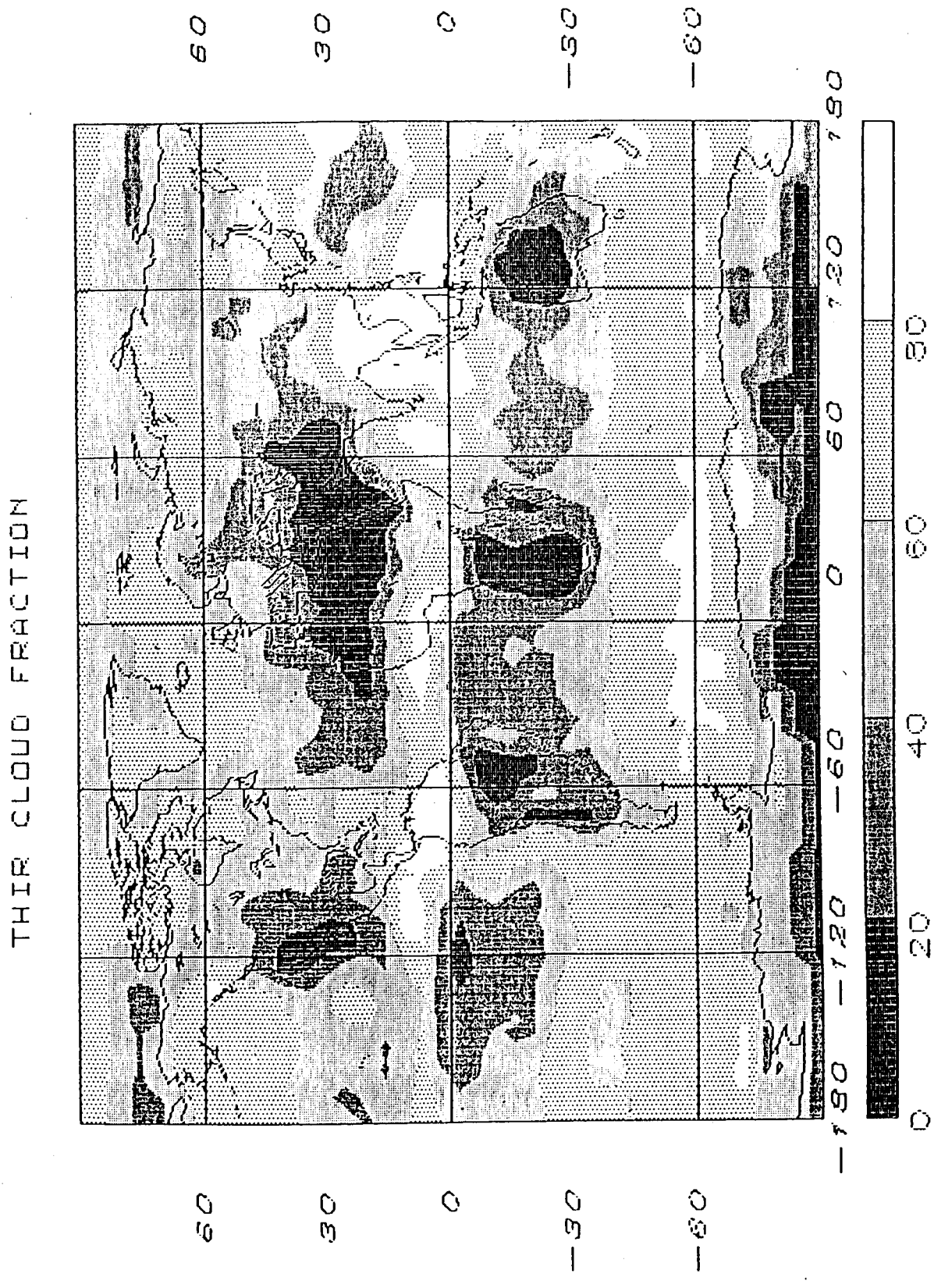

FIGURE 9.2 Global distribution of monthly mean daytime cloud fractions from THIR for June 1979. Improvements due to inclusion of ultra-violet reflectances due to TOMS are included. Data kindly provided by P. Hwang.

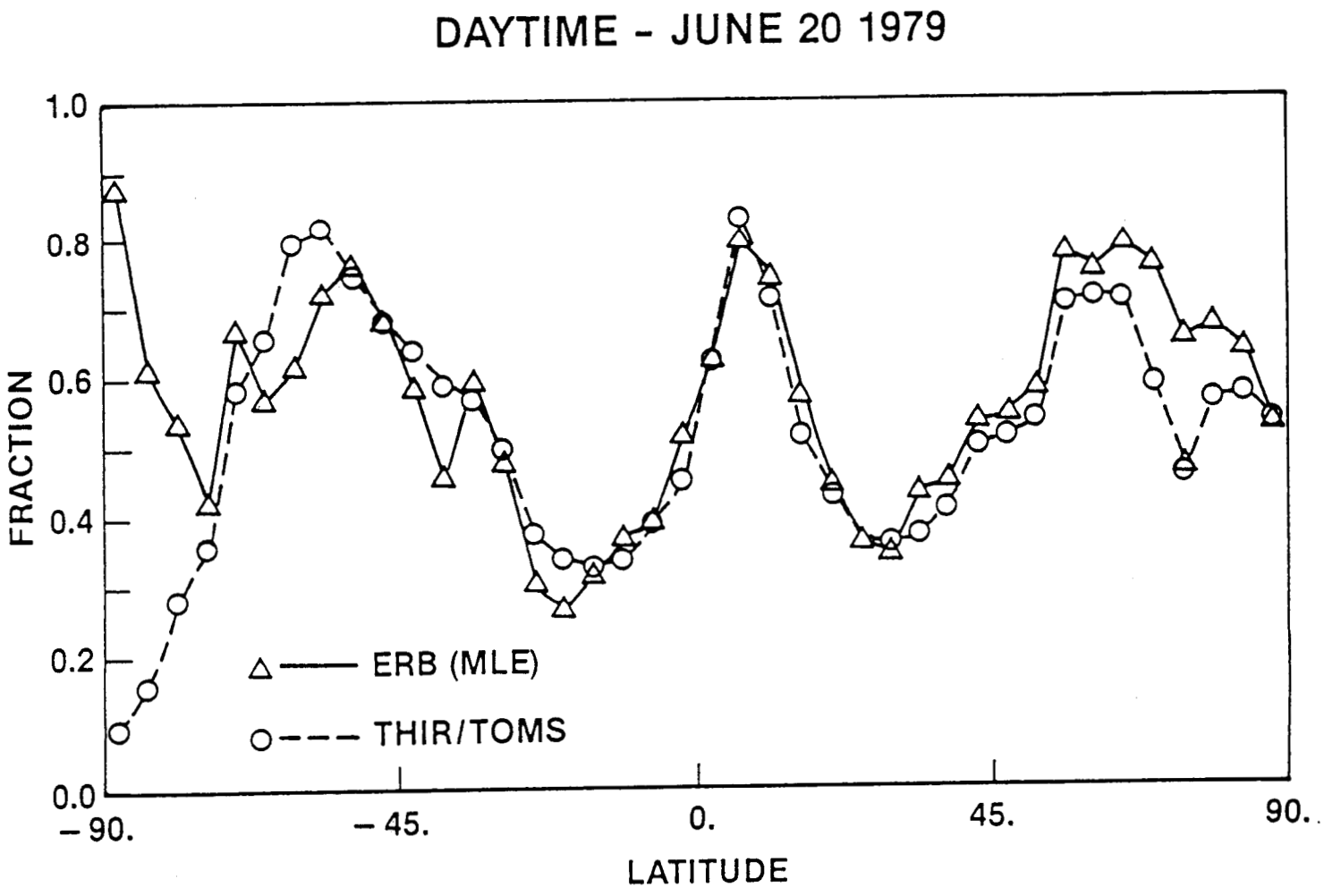

FIGURE 9.3 Zonal mean cloud statistics for June 20, 1979 from Nimbus-7 ERB scanners and from THIR. The sudden jumps and discontinuities in the southrn hemisphere in the ERB values are due to clear sky longwave flux fields and are discussed in the text.

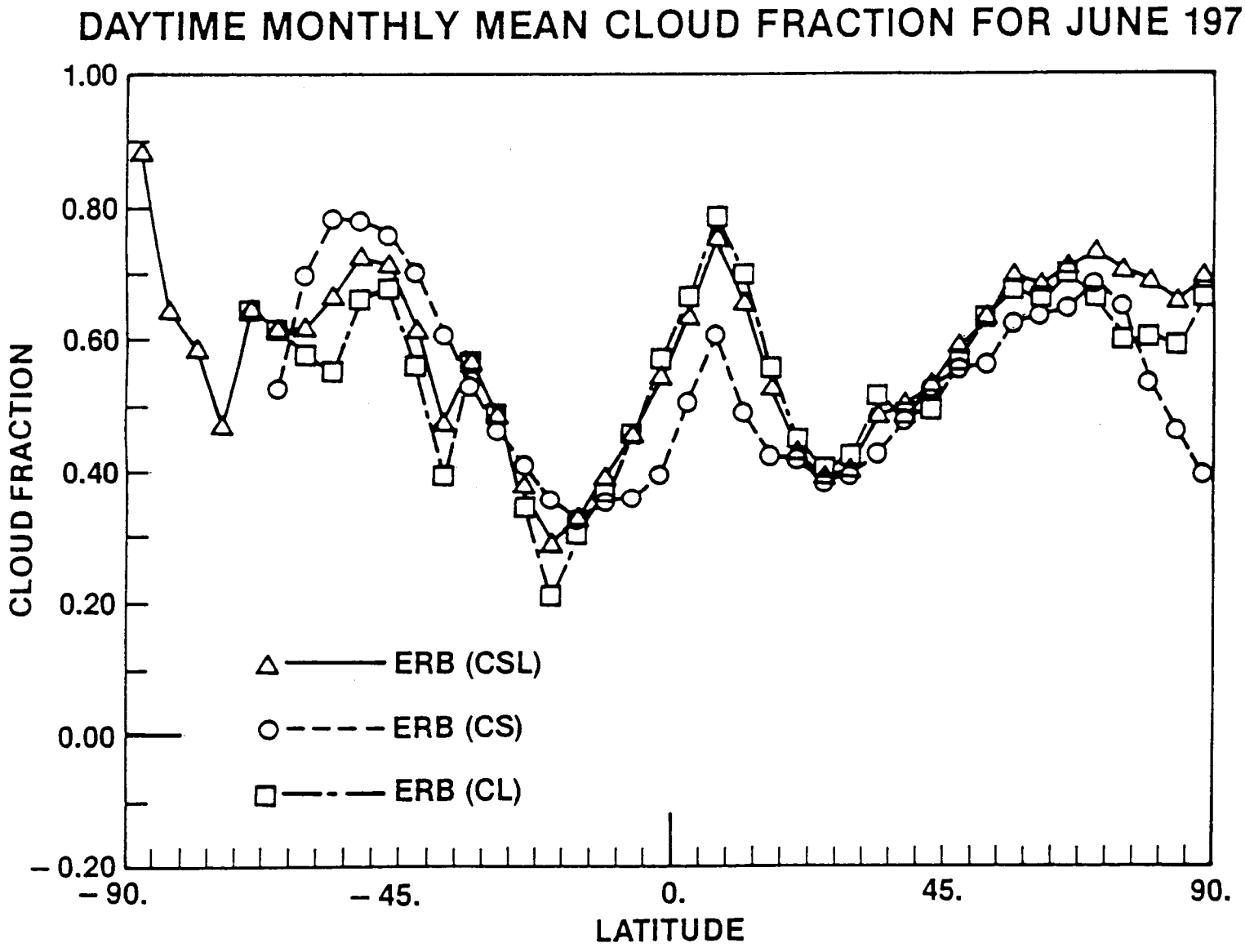

FIGURE 9.4 Zonal mean cloud amounts from ERB derived using shortwave and longwave together (CSL), SW only (CS), and longwave only (CL) cases. Monthly mean daytime cloud amounts only are shown.

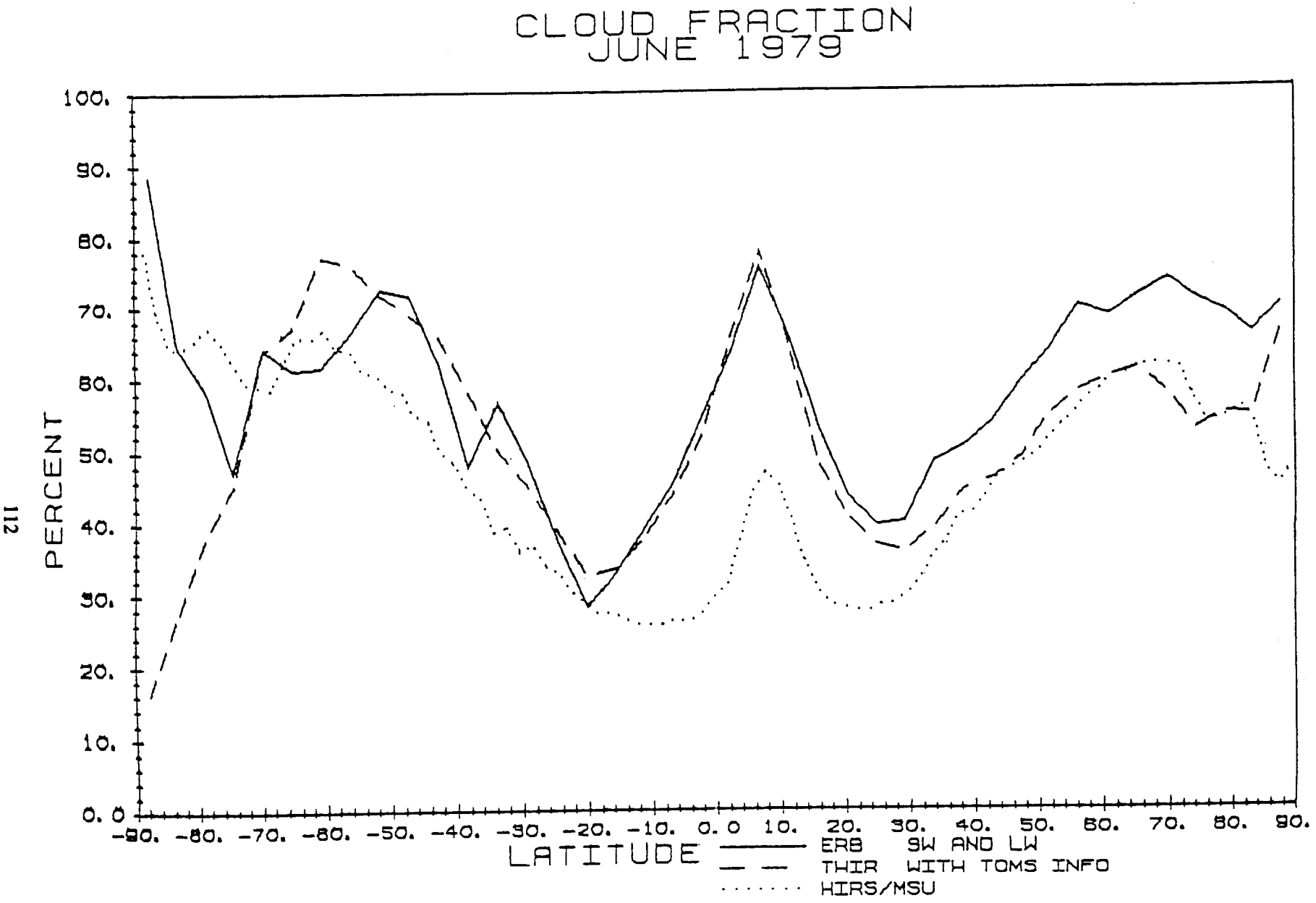

FIGURE 9.5 Zonal mean cloud amounts for June 1979 using ERB CSL (solid line), THIR/TOMS (dashed line), and HIRS2/MSU (dots). Daytime values only are shown.

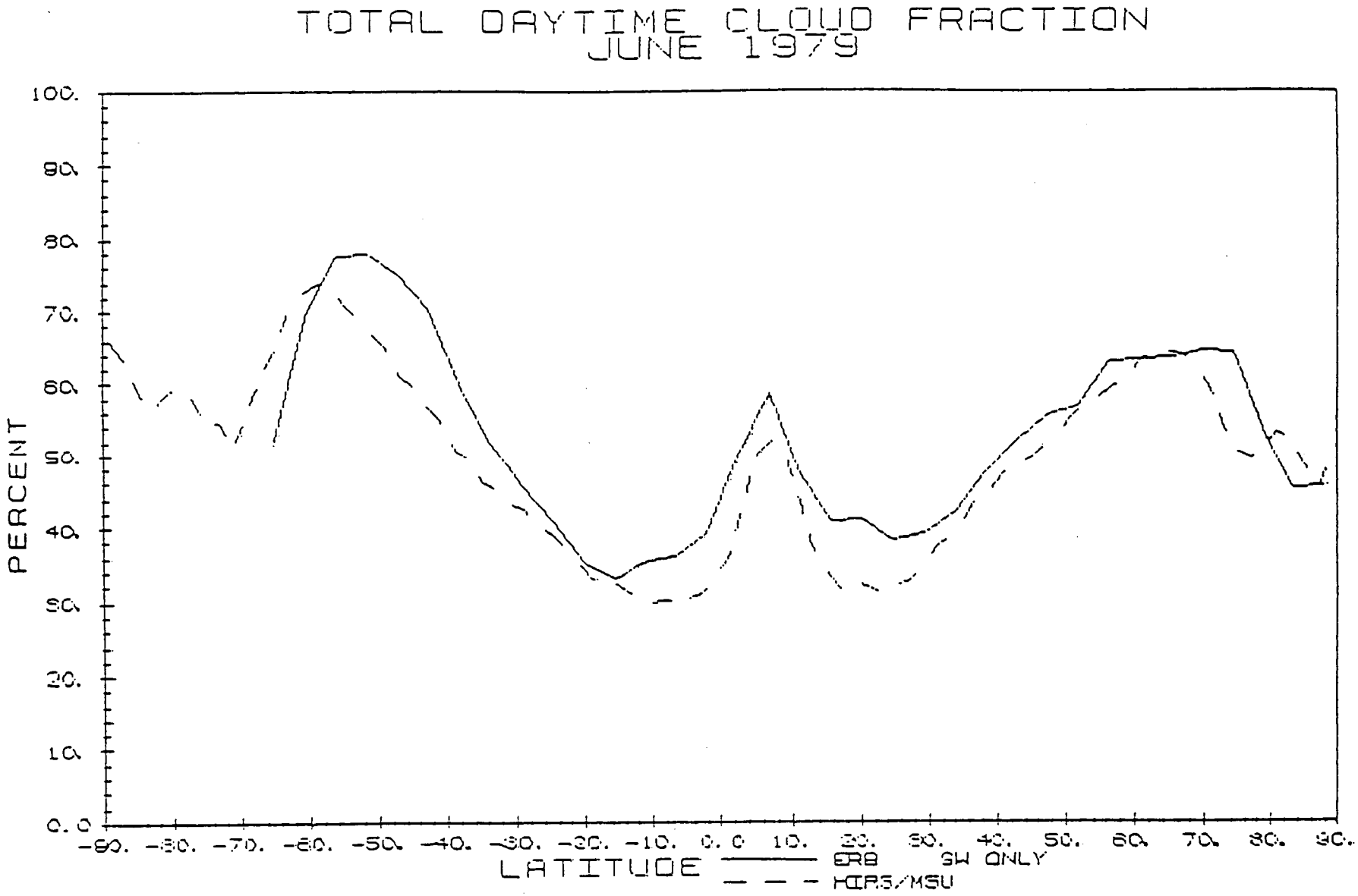

FIGURE 9.6 Zonally averaged monthly mean cloud amounts from ERB CS and HIRS2/MSU for June 1979.

of cirrus for example, the estimated cloud amount is considerably smaller due to the smaller emissivity of cirrus. The smaller cloud amounts noted in the tropics are predominantly due to cirrus. A similar reduction in the cloud amount appears in the shortwave only case also. The cloud amount is determined on the basis of the reflected shortwave radiance from top of the cloud. This radiance value is dependent on the reflectance of the cloud and its optical thickness. Thus the lower cloud amounts with the CS case are due to the presence of clouds of low optical thickness.

9.3 CONCLUSIONS

The present results indicate that the maximum likelihood estimation (MLE) method using shortwave and longwave radiances from ERB leads to cloud amounts in good agreements with THIR/TOMS values.

There are systematic regional differences in the cloud amounts derived using shortwave only relative to those obtained from longwave only or longwave and shortwave together.

The cloud amounts derived from ERB using shortwave only (CS) are similar to the HIRS2/MSU cloud amounts and are smaller than the THIR/TOMS and ERB (CSL) values, particularly in regions where cirrus predominates. The lower values with CS are attributed to clouds with low optical thickness.

SECTION 10

FUTURE WORK

1. Study the effect of season on the agreement between SAB and MLE methods: one month in each season.

2. CLE and NCLE bidirectional model differences and their effects on the regional albedos.

3. Study the effect on budget parameters (for at least one month) due to the nighttime emission models.

4. Sensitivity of ERB parameters to clear sky longwave flux fields derived from ERBE observations.

REFERENCES

Arking, A., and S. Vemury, 1984: NIMBUS-7 ERB Data Set: A Critical Analysis. J. Geophy. Res., 89(D4), 5089-5097.

Jacobowitz, H., H. V. Soule, H. L. Kyle, F. B. House, and the NIMBUS-7 ERB Experiment Team, 1984: The Earth Radiation Budget Derived from the NIMBUS-7 ERB Experiment, J. Geophys. Res., 89, 5021-5038.

Rossow, W. B., F. Mosher, E. Kinsella, A. Arking, M. Desbois, E. Harrison, Minnis, E. Ruprecht, G. Seze, C. Simmer and E. Smith, 1985: ISCCP Cloud Algorithm Intercomparison, J. of Clim. & Appl. Meteor., Vol. 24, No. 9, 877-903.

Smith, G. L., R. N. Green, E. Raschke, L. M. Avis, J. T. Suttles, B. A. Wielicki, and R. Davis, 1986: Inversion methods for satellite studies of the Earth's radiation budget: Development of algorithms for the ERBE mission, Rev. Geophys. and Space Phy., Vol. 24, No. 2, 407-421.

Stowe, L. L., P. P. Pellegrino, P. H. Hwang, P. K. Bhartia, T. G. Eck, C. G. Wellemeyer, M. Yeh, C. S. Long, 1986: NIMBUS-7 Global Cloud Climatology: Algorithm and Validation. (Pre-print).

Susskind, J., D. Reuter, M. T. Chahine, 1986: Cloud Fields Retrieved From Analysis of HIRS2/MSU Sounding Data, Submitted to the Special Issue of J. G. R. on IAMAP/IAPSO.

Vemury, S. K., L. L. Stowe and H. Jacobowitz, 1984: Sample Size and Scene Identification (Cloud): Effect on Albedo, J. Geophy. Res., 89(D4), 5345-5353.

Vemury, S. K., 1985: Validation of the ERBE Scanner Scene Identification Methodology: Analysis with NIMBUS-7 ERB Data, NASA Contractor Report 172596.

Vemury, S. K., B. Wielicki, and J. T. Suttles, 1985: Scene Identification using Maximum Likelihood Estimation, EOS Transactions, American Geophysical Union, Vol. 66, No. 18, 240-241.

Standard Bibliographic Page

1. Report No.	2. Government Accession No.	3. Recipient's Catalog No.
NASA CR-178243		

4. Title and Subtitle	5. Report Date
Evaluation of the ERBE Scene Identification Algorithm	March 1987
	6. Performing Organization Code

7. Author(s)	8. Performing Organization Report No.
S.K. Vemury	STC-2122

9. Performing Organization Name and Address	10. Work Unit No.
Science and Technology Corporation 101 Research Drive Hampton, VA 23666	11. Contract or Grant No. NAS1-18166

12. Sponsoring Agency Name and Address	13. Type of Report and Period Covered
National Aeronautics and Space Administration Washington, DC 20546	Contractor Report
	14. Sponsoring Agency Code 665-45-30-01

15. Supplementary Notes

NASA Langley Research Center Technical Representative: J. T. Suttles

Final Report

16. Abstract

All the studies presented in this report are intended to evaluate the sensitivity of the radiation budget parameters and the scene selection process to different factors. The use of ERB-7 'CLE' models provides instantaneous albedo and longwave flux values which are in essential agreement in the 70° cutoff case with those from the SAB method. The increase in albedo with increasing satellite zenith angle cutoff is not apparent at the target area level for different surface types. 'GOES' models seem to show an increase in instantaneous albedo at the global level with satellite zenith angle of the same nature as the ERB-7 models investigated in a previous report and are, therefore, probably not an improvement. The use of recently derived 'NCLE' models did not make a noticeable change in the budget parameters; but the cloud classification did show hemispherical differences and caused a day-night readjustment of cloudiness amounts. Preliminary results for an additional month (December 1979) indicate good agreement between the SAB and MLE methods. Additional work is required to establish the agreement for all seasons. Comparison of derived cloud amounts with other data sets such as THIR/TOMS indicates good zonal agreement.

Investigations on sampling adequacy at different temporal averaging intervals with the SAB method, indicate larger uncertainties in small time average cases. For a 6-day averaging period, sampling is very poor with only 23% of the globe contributing toward the global mean albedo.

Effect of modifications to the MLE procedure seem to have little effect on the derived budget quantities in an averaged sense. Significant differences in the flux values due to differences in scene selection are apparent in individual target areas studies. We note that a modification of the MLE procedure to mimic the perpendicular bisector algorithm indicated no effect on the gross radiation budget quantities.

17. Key Words (Suggested by Authors(s))	18. Distribution Statement
ERBE Scene validation Maximum likelihood estimation ERB radiation budget parameters Sensitivity studies	Unclassified-Unlimited Subject Category 47

19. Security Classif.(of this report)	20. Security Classif.(of this page)	21. No. of Pages	22. Price
Unclassified	Unclassified	131	A07

For sale by the National Technical Information Service, Springfield, Virginia 22161